INTERNATIONAL SCHOOL FOR ADVANCED STUDIES

CONDENSED MATTER THEORY SECTOR

ma per seguir virtute e canoscenza

SISSA

PH. D. THESIS.

THEORY AND AB INITIO SIMULATION OF ATOMIC HEAT TRANSPORT.

Author:

Aris MARCOLONGO

Supervisors:

Stefano BARONI

Paolo UMARI

External Referees:

Flavio TOIGO

Nicola MARZARI

DECEMBER, 2014

VIA BONOMEA 265, 34136 TRIESTE- ITALY

Contents

Chapter 1

Introduction

The thermal conductivity coefficient, referred as λ in this thesis, describes the propriety of materials to conduct heat. It provides, through the celebrated Fourier law $\boldsymbol{J} = -\lambda \nabla T$, a constant of proportionality between the energy current $\boldsymbol{J}$ and the local temperature gradient. Its value varies a lot among different materials: Copper for example presents a thermal conductivity of 385 $\frac{W}{mK}$, fused Silica of 1.46 $\frac{W}{mK}$ and water of 0.60 $\frac{W}{mK}$, always at ambient conditions. The high difference between thermal conductivity of water and of Copper is due to the different physical processes active in these two systems. Copper is a metal and therefore heat transfer is mainly due to conduction electrons: if present, this contribution is the prevalent one. In liquid water the lattice contribution to thermal conductivity is the only one present and this explains the high difference between the thermal conductivity of metals and insulators.

The value of this transport coefficient can change dramatically the dynamics of physical systems. For example, experimental results suggest that thermal conductivity of silicates in the earth mantel decreases after the melting therefore impeding heat transport and promoting further melting, with an exponential growth. For technological applications, there is a general interest in engineering materials with a low thermal conductivity. Thermal barriers coatings, fundamental in aero-engine components, are such an example since they must sustain the high temperature gradient present in the system without giving origin to high energy currents and rapid thermalizations. Thermoelectric generators require the development of low thermal conducting materials as well, in order to maximize their efficiency. More recently an interest on the precise control of heat transport at nano and mesoscopic scales, where quantum effects are expected to play a crucial role, has grown. An example is the development of phase change memory, a type of non-volatile random access memory. In these devices,

according to the phase of the cell, changed through an heating element, a bit of 1 or of 0 is memorized. These are only a few examples of the important role played by thermal conductivity in modern applications.

The main goal of modern electronic structure theory is to describe physical properties of materials, given their chemical composition, in order to analyze interesting physical phenomena and aid technological development. Ab initio simulations, based on density functional theory (DFT), have demonstrated a very good predictive power for several properties of interest. Equilibrium structural properties , phonon energies, dielectric functions and absorption spectra can be predicted with an ever increasing accuracy, thanks to the development of new exchange correlation functionals. With the advent of the Car-Parrinello scheme, DFT-based ab initio molecular dynamics calculations could be performed in an efficient way as well, therefore making it possible to access inherently dynamical property, like particle diffusion in liquid systems. Thermal conductivity is one such dynamical properties which however still lacks a proper ab initio scheme for its computation. In this thesis we develop a new technique for computing the value of this coefficient in insulating systems, considering the lattice contribution to thermal conductivity.

The validity of the Boltzmann transport equation, commonly used for lattice thermal conductivity computations, is restricted to solids below their melting temperature, where disorder and anaharmonicities can be treated in a perturbative way. Other approaches are at the moment restricted to classical systems where accurate inter-atomic potentials are at disposal. There is therefore the need for a methodology able to compute thermal conductivity in liquid and highly disordered systems, in an ab initio framework. The approach developed in this thesis is of general validity and is based on the application of the Green Kubo formula, which gives a connection between transport coefficients and spontaneous fluctuations at equilibrium. Till now it was surprisingly thought that such a method was inherently ill defined in an ab initio framework, because it is not possible to uniquely define an energy density in quantum systems. We will show that this indeterminacy does not affect the value given by Green Kubo formula, thus leading to a well defined scheme.

The thesis is organized as follows. In the second chapter we will review the existing methods used for thermal conductivity calculations, thus showing the need for new approaches. In the third chapter we will present the Green Kubo formalism and show that it is suitable for considering quantum effects in thermal conductivity calculations. In the fourth chapter we will apply the Green Kubo formula and develop a well defined methodology for a quantum thermal conductivity computation in a plane wave, pseudo-potential scheme. Finally, in the

fifth chapter, we will provide a first benchmark of the new approach and an interesting application. As a benchmark, we will compute thermal conductivity of Argon DFT, which is known to be described well by classical pair potentials, both with the methodology developed and with a classical formulation, arriving always at comparable results. We will then compute thermal conductivity of heavy water at ambient conditions. An ab initio approach to this problem is of interest because, in such an important liquid, classical potentials are well known to overestimate by 30 % the value of thermal conductivity.

| Chapter | 2 |

Computational methods

As discussed in the introduction, thermal conductivity of dielectric materials is mainly due to atomic contributions. The kinetic theory of lattice vibrations was the first one developed for explaining experimental measurements, providing a celebrated connection with the specific heat at constant volume. Later Green-Kubo relations were found, linking thermal conductivity and equilibrium spontaneous fluctuations of the heat flux. Both theories provide computational methods routinely applied to derive thermal conductivity coefficients from numerical simulations, reviewed in this chapter. The first section is devoted to kinetic theory, put on a computational framework by the phonon Boltzmann equation. In the second section we discuss non-equilibrium methods, a direct application of Fourier law. Then in the third section the Green-Kubo method is discussed and in the fourth we report an interesting methodology which combines equilibrium and non-equilibrium methods, referred as the "synthetic" method. A final discussion points out the main advantages and drawbacks of each technique: it arises the need of a new methodology, able to compute quantum contributions to the thermal conductivity of liquids and disordered systems.

2.1   The Phonon Boltzmann Equation

An appealing physical picture, providing a qualitative description of thermal transport in solids, is given by kinetic theory, as embodied in the phonon Boltzmann equation (PBE) [1]. The PBE applies to periodic solids far from the melting point, where anharmonic and disorder effects, while essential for providing a finite value of thermal conductivity, can be treated in a perturbation way. Phonons are treated as semi-classical quasi-particles, characterized by well defined values of position $\mathbf{r}$, momentum $\mathbf{k}$, and energy $\epsilon_{\mathbf{k}}$. The uncertainty principle,

2. Computational methods

$|\Delta \mathbf{x}||\Delta \mathbf{k}| \geq 1$, is disregarded in a coarse grained picture using phonon wave-packets with a well defined group velocity $\mathbf{v_k}$. We consider here for simplicity the single band case and the semi-classical equations of motion read:

$$\dot{\mathbf{r}} = \mathbf{v_k} = \frac{1}{\hbar} \frac{\partial \epsilon_{\mathbf{k}}}{\partial \mathbf{k}}, \tag{2.1}$$

$$\hbar \dot{\mathbf{k}} = \mathbf{F}_{ext}, \tag{2.2}$$

where $\epsilon_{\mathbf{k}}$ is the phonon dispersion relation and $\mathbf{F}_{ext}$ accounts for external fields and finite lifetimes due to scattering events. A central object of the theory is the distribution function $f(\mathbf{k}, \mathbf{r})$ which measures the number of carriers with momentum $\mathbf{k}$ at position $\mathbf{r}$. The flux of energy, essential for computing thermal conductivity as discussed in the introduction, is given by the equation:

$$\mathbf{J}(\mathbf{r}) = \int d\mathbf{k} f(\mathbf{k}, \mathbf{r}) \epsilon_{\mathbf{k}} \mathbf{v_k}, \tag{2.3}$$

thus identifying the phonon quasi-particles as "energy-carriers". No such simple single particle description, to our knowledge, has yet been found for liquids. From this point of view, the theories of transport in liquids and solids are qualitatively different.

The PBE is an evolution equation for the phonon distribution function $f(\mathbf{k}, \mathbf{r})$. The power of this technique resides in the simple semi-classical form of the evolution equation. When macroscopic external fields are absent it can be written:

$$\dot{f}(\mathbf{k}, \mathbf{r}) = \dot{f}(\mathbf{k}, \mathbf{r})\big|_{\text{diff}} + \dot{f}(\mathbf{k}, \mathbf{r})\big|_{\text{scatt}} =$$
$$= -\mathbf{v}_k \frac{\partial f(\mathbf{k}, \mathbf{r})}{\partial \mathbf{r}} + \dot{f}(\mathbf{k}, \mathbf{r})\big|_{\text{scatt}} = 0, \tag{2.4}$$

where stationarity has been imposed by equating to zero the total time derivative. The diffusive contribution, $\dot{f}(\mathbf{k}, \mathbf{r})\big|_{\text{diff}}$, describes motion in space in a collisionless regime, due to the phonon group velocity. The second contribution, $\dot{f}(\mathbf{k}, \mathbf{r})\big|_{\text{scatt}}$, takes into account scattering events with other phonons, able to change the phonon momentum. All dynamical effects are included in the scattering coefficients where quantum effects can be incorporated via Fermi golden rule [2].

In the limit of small thermal gradients the non-equilibrium distribution is close to the equilibrium Bose Einstein distribution evaluated at the local temperature: $f(\mathbf{k}, \mathbf{r}) \sim f_0(\epsilon_{\mathbf{k}}, T(\mathbf{r}))$, where $f_0(\epsilon, T) = \left(\exp \left[\frac{\epsilon}{k_B T} \right] - 1 \right)^{-1}$. The simplest approximation to the scattering terms is the so called the relaxation time approximation, which reads:

$$\dot{f}(\mathbf{k}, \mathbf{r})\big|_{\text{scatt}} = -\frac{f(\mathbf{k}, \mathbf{r}) - f_0(\epsilon_{\mathbf{k}}, T(\mathbf{r}))}{\tau_{\mathbf{k}}}. \tag{2.5}$$
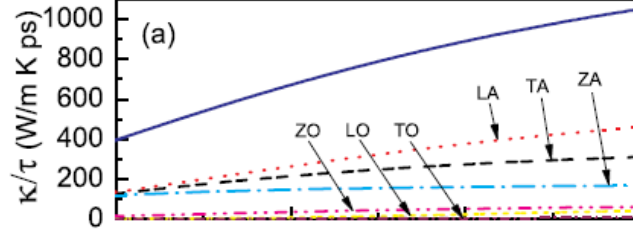
Figure 2.1: Thermal conductivity of mono-layer graphene computed by the Boltzmann transport equation, divided into its mode contributions, along the $\Gamma - M$ direction, from ref [6]

The computation of $\tau_{\mathbf{k}}$ can be performed using either semi-empirical [3] models, or from first principles using density functional (perturbation) theory [2, 4]. The relaxation time is certainly longer than the mean collision time, since it is well known that not all collisions can contribute to thermal current degradation [5]. We need to observe that the relaxation time approximation, although simplifying the task of solving the PBE, can be formally derived from the general PBE only under the assumption of elastic scattering events [1] and is therefore not of general validity. Within this approximation the PBE is easily solved and the resulting thermal current has the expression:

$$J_i = \sum_j \lambda_{i,j} \partial_j T(\mathbf{r}), \tag{2.6}$$

$$\lambda_{i,j} = \sum_{\mathbf{k}} v_{\mathbf{k},i} v_{\mathbf{k},j} \tau_{\mathbf{k}} c_{\mathbf{k}}, \tag{2.7}$$

where $c_{\mathbf{k}}$ is proportional to the contribution of mode $\mathbf{k}$ to the constant volume heat capacity and is given by:

$$c_{\mathbf{k}} = \frac{e^{\frac{\epsilon_{\mathbf{k}}}{k_B T}}}{(e^{\frac{\epsilon_{\mathbf{k}}}{k_B T}} - 1)^2} \frac{\epsilon_{\mathbf{k}}^2}{k_B T^2}. \tag{2.8}$$

Equation (2.6) permits to separate the contribution to the thermal conductivity into individual phonon modes, as illustrated in fig. 2.1.

Expression (2.6) can be easily computed at a DFT level. Phonon frequencies are nowadays routinely computed in a DFT approach by using either DFPT techniques [7] or under the frozen phonon approximation [8]. Both methods also permit to compute the third order terms in the energy expansion, from which one can extract phonon self energies and lifetimes [9], in perturbation theory. An interesting alternative technique to compute phonon lifetimes
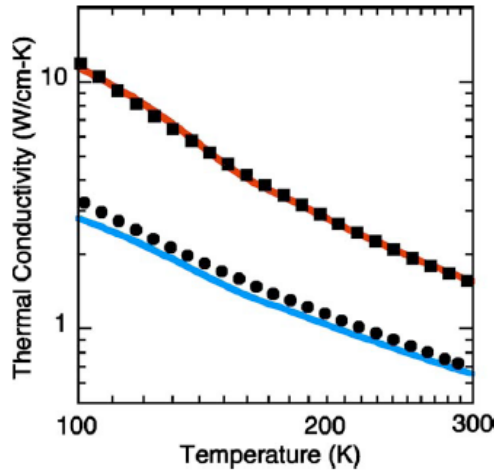
2. Computational methods

Figure 2.2: Lattice thermal conductivity of Silicon (squares) and Germanium (circles) computed using the Boltzmann transport equation, from ref [2]. The lines are experimental values.

non perturbatively has been devised by Koker [10], who suggests to derive phonon lifetimes from the frequency spectrum of the atomic velocity autocorrelation function. The theory of the PBE has been developed much further, both from the computational point of view, for example avoiding the relaxation time approximation [2, 3], and from a fundamental one (see [1] for a discussion).

Assuming that the relaxation times and the modulus of the group velocities do not depend on the phonon momentum, equation (2.6) simplifies to the classical formula [5]:

$$\lambda = \frac{1}{3} C_v v l. \tag{2.9}$$

An expression for l, based on dimensional analisys, has been proposed:

$$l \sim \frac{a_0}{\alpha \gamma T}, \tag{2.10}$$

where a_0 is the lattice parameter, γ is the Gruneisen parameter, α the expansion coefficient and T the temperature. This formula makes it explicit that anharmonic effects, embodied in α and γ, are essential for describing heat transport. The agreement of equation 2.10 with experiment is only qualitative, thus confirming the need of a more qualitative approach to the PBE, for example through equation 2.6. In figure 2.2, we instead report a thermal conductivity computation of Silicon and Germanium, displaying an excellent agreement with experiment.

2.2   Non-equilibrium molecular dynamics

In non-equilibrium molecular dynamics (NEMD) the computation of transport coefficients is tackled directly by simulating a system subject to an external perturbation and by computing the associated conjugate flux. Thermal conductivity is then obtained from Fourier law, in the limit of small thermal gradients. Different techniques can be used to realize the desired steady state: as an example we discuss here the Müller-Plathe [11] method, which is routinely used and shows the typical features of this class of computational methods.

The presence of thermal inhomogeneities requires the division of the system into a number of subsystems that have to be chosen large enough so as to achieve local thermodynamic equilibrium. This is essential in order to define a local temperature and a temperature gradient. The Müller-Plathe method starts by subdividing an orthorhombic simulation cell into slabs perpendicular to the $z-$ axes. During the simulation different temperatures will be evaluated for each slab and a unidimensional temperature gradient is defined by finite differences. A local instantaneous temperature is then defined within each slab through the formula:

$$T_s = \frac{1}{3N_s k_B} \sum_{n \in s-\text{slab}} \frac{1}{2} m v_n^2, \tag{2.11}$$

where every atom is supposed to have the same mass m and N_s is the number of particles inside the s_{th} slab. Two slabs are chosen as the "hot" and the "cold" slab and connected to two thermal reservoirs kept at different temperatures (the analog of the "heater" and the "coolant" in the experimental axial-heat flow method [12]). In order to enforce periodic boundary conditions a "ring" geometry is used, such as depicted in fig. 2.3.

The peculiarity of the Müller-Plathe method is the way in which the reservoirs are modeled. Instead of fixing two external temperatures, an energy flux is driven by suitably changing the velocities of the atoms in the cold slab and the ones in the hot slab. This is achieved by identifying, with a fixed frequency, the hottest atom in the cold slab, the coolest atom in the hot slab, and by swapping their velocities, scaled by the square root of the ratio of the atomic masses to enforce momentum conservation [1]. This procedure will effectively produce a flux of energy across the system provided the hottest atom in the cold slab is hotter than the coolest atom in the cold slab. This is always the case if the temperature gradient is small enough, and the value of the energy flux thus obtained will depend on the swapping frequency (different recipes for creating thermal fluxes in the same geometry have been later proposed [13, 14]).

---

[1]This favors the reaching of a steady state, since only a subspace of the micro-canonical ensemble is spanned during the dynamics.
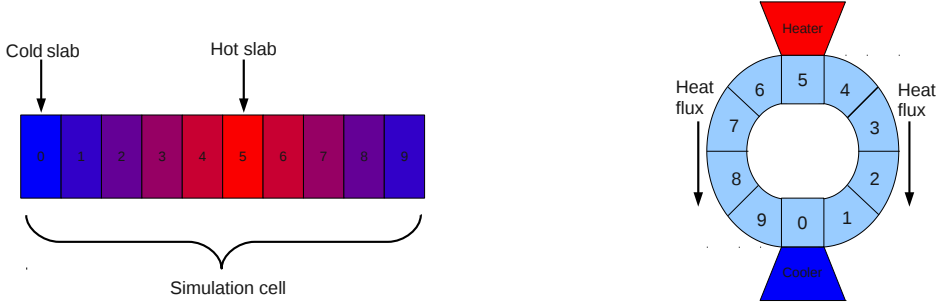
2. Computational methods

Figure 2.3: (left) Example of a slab division of the simulation cell in a Müller-Plathe NEMD computation. Temperature rises going from the $n = 0$ slab to the $n = 5$ slab and then decrease in a continuous way from $n = 5$ to $n = 9$, coming back to the same value at slab $n = 0$. (right) Setup correspondent to the slab division. The geometry of the system permits heat flow from the heater to the cooler along two different (symmetrical) paths.

The energy flux is the ratio of the total kinetic energy transported through the system by the kinetic energy swaps during the simulation time T, and the product between T and the cross-sectional area of the simulation cell. The resulting expression for thermal conductivity, to be computed under steady conditions, is given by Fourier law:

$$\lambda = -\frac{\sum_{transf} \frac{m}{2}\left(v_h^2 - v_c^2\right)}{2TA\langle\frac{\partial T}{\partial z}\rangle}, \tag{2.12}$$

where v_h and v_c are the velocities before being exchanged of the particle in the hot slab and in the cold slab respectively. m is the mass of the particles (we stick here to a mono-atomic fluids), A the cross sectional area of the simulation cell perpendicular to z, $\langle\frac{\partial T}{\partial z}\rangle$ the observed temperature gradient (it is a fluctuating quantity). The transfers considered in the sum are those observed in a simulation of length T. The factor of two is due to the ring geometry chosen.

The rationale behind the Müller-Plathe algorithm is that the heat flux is a quantity characterized by big fluctuations, whereas temperature, being a quantity calculated as an average over many particle, does not fluctuate so wildly. Therefore it is preferable to impose a flux on the system and measuring a temperature rather than imposing a temperature gradient and measuring the resulting flux. A typical temperature profile measured in a NEMD Müller-Plathe computation is reported in figure 2.4.
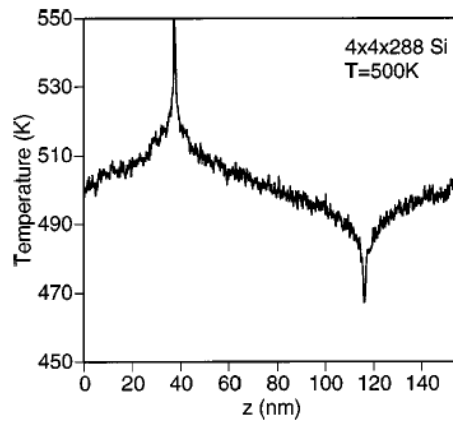
Figure 2.4: Typical temperature profile in a NEMD simulation, from ref. [15]

2.3 Equilibrium molecular dynamics

In equilibrium molecular dynamics (EMD) transport coefficients are evaluated by exploiting the fluctuation dissipation theorem that establishes a relation between non-equilibrium coefficients and spontaneous fluctuations occurring at equilibrium. This theorem is embodied in the so called "Green-Kubo" formulas that will be derived in chapter 3. The same task is performed by the well known formula $C_V = \langle (\Delta E)^2 \rangle_{eq}$ for the specific heat. Such a connection is important because it shows that a complete knowledge of the non-equilibrium distribution function is not essential for the computation of transport coefficients and, from a computational point of view, it permits to simulate equilibrium systems, a much easier task than simulating the non-equilibrium response to macroscopic perturbations, as in NEMD methods. Green-Kubo relations applied to molecular dynamics calculations have the general form:

$$K = \alpha \int_0^{+\infty} \langle A_0(t) A_0(0) \rangle_{eq} dt, \tag{2.13}$$

where K is the transport coefficient of interest (in our case, thermal conductivity), A_0 an observable and α a constant. Precise expressions of A_0 and α depend on the coefficient considered. The derivation of Green-Kubo formulas can be quite different, depending on the macroscopic quantity of interest. In the case of thermal transport, derived explicitly in chapter 3, the Green-Kubo formula establishes a relation between the thermal conductivity and the spontaneous fluctuations of the heat flux:

11

$$\lambda = \frac{1}{3Vk_BT^2} \int_0^{+\infty} \langle \mathbf{J}(t) \cdot \mathbf{J}(0) \rangle_{eq} dt, \tag{2.14}$$

where $\mathbf{J}(t)$ is called the *heat flux*. The precise expression of $\boldsymbol{J}(t)$, depending on ion positions and velocities at time t will be given in next chapter, in the particular case of a two-body potential. In figure 2.5 we see a typical result of a Green-Kubo computation. The autocorrelation function of the heat flux, in the reference called $\mathbf{S}$ instead of $\mathbf{J}$, has to be explicitly computed till its decay and approximated as a sample mean, as in formula 5.1 of chapter 5 . For large t only few estimates are available, therefore eventually the plot of the integral as a function of the upper time of integration, shown in the inset, is dominated by statistical errors. Enough statistics has to be acquired in order to observe a statistically significant plateau.

The time decay of the autocorrelation function varies considerably from system to system. In liquids it can be of the order of one picosecond, while in solids it can be as large as hundreds of picoseconds [16, 17, 18, 19, 20]. The shape can qualitatively vary as well. As an example, in figure 2.6 we compare the heat-flux autocorrelation function for two classical models, flexible and rigid, of water at ambient conditions. The high frequency oscillations in the flexible water model are due to fast intra-molecular modes that are disregarded in the rigid model. Yet the thermal conductivities resulting from the simulations are rather similar. Ref. [18] reports, in units of $W/(mK)$, values of $0.776, 0.806, 0.797, 0.816$ for different rigid models and of $0.854, 0.851, 0.793$ for flexible models, always at ambient conditions. The experimental value reported is $0.6096 W/(mK)$.

2.4   Synthetic methods

Synthetic methods were developed as an alternative way to compute the equilibrium time correlation functions appearing in Green-Kubo relations, avoiding their explicit evaluation as an equilibrium average, which usually converges slowly. They perform this task by realizing particular nonequilibrium settings, associated with mechanical perturbations ad hoc designed, differently from standard NEMD methods. The EMD and NEMD methods described in previous sections are generally preferred in applications because they are much easier to implement. In figure 2.7 the heat current autocorrelation function computed by synthetic methods and by EMD for the same Lennard Jones fluid are shown to agree.

Synthetic methods exploit a formal similarity between the Green-Kubo expressions for bounda-
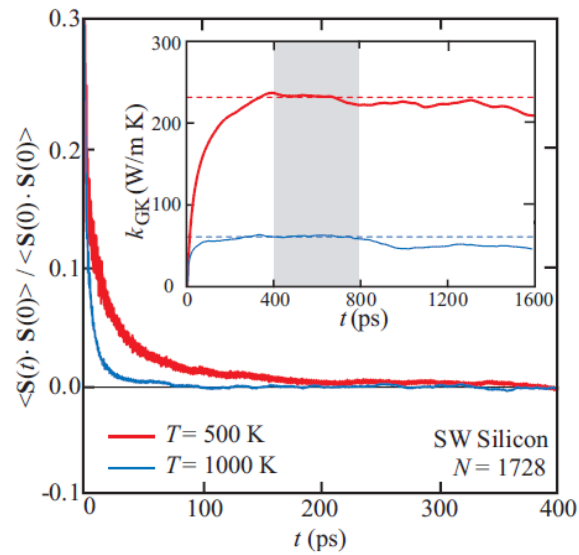
Figure 2.5: Heat current autocorrelation function and its integral (inset) for Stillinger-Weber silicon using EMD, from ref. [21]
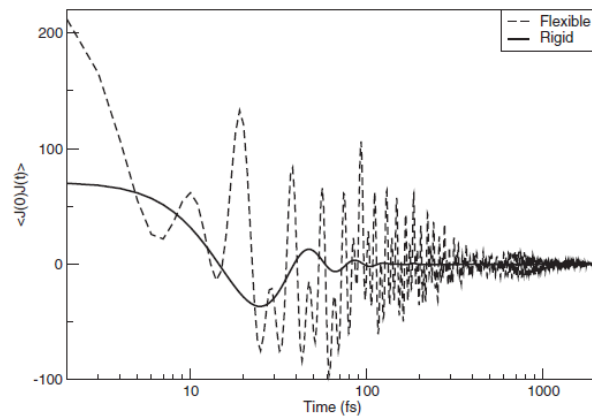

Figure 2.6: Heat current autocorrelation function for classical and rigid water computed by EMD, from ref. [18]

ry-driven transport phenomena (like thermal conductivity) and the ones associated with the linear response to mechanical disturbances, described by perturbative terms in the Hamiltonian of the system (like electrical conductivity). In both cases an expression presenting the time integral of an equilibrium autocorrelation function of a certain flux is derived, as in eq. 2.13. On the other hand, boundary-driven transport phenomena are more difficult to simulate, since there is always the need to model a thermal reservoir or a wall, external to the system of interest and breaking the homogeneity of the system. An additive term in the Hamiltonian, acting homogeneously on every particle of the system, does not suffer from this problem. In synthetic methods a boundary-driven transport phenomenon is simulated by an additional term in the equations of motion [22, 23]:

$$\dot{\mathbf{q}}_i = \frac{\partial H^0}{\partial \mathbf{p}_i} + F(t)\mathbf{C}_i \tag{2.15}$$

$$\dot{\mathbf{p}}_i = -\frac{\partial H^0}{\partial \mathbf{q}_i} + F(t)\mathbf{D}_i, \tag{2.16}$$

where $F(t)$ is a scalar (non dependent on the configuration) giving the time dependence of the perturbation and $\mathbf{C}_i$ and $\mathbf{D}_i$ are coefficients to be fixed. H_0 is the original Hamiltonian in the absence of the perturbation. Non-Hermitian linear response theory permits to compute the response to the perturbation of a generic observable A. The dissipative heat flux is the observable appearing in the final relation:

$$\langle A(t) \rangle = \langle A(0) \rangle + \int_0^t \chi_A^{J_{diss}}(t - t')F(t')dt' \tag{2.17}$$

$$\chi_A^{J_{diss}}(t) = \beta \langle A(t)J_{diss}(0) \rangle_{eq} \tag{2.18}$$

and is linked to the choice of the $\mathbf{C}_i$ and $\mathbf{D}_i$:

$$J_{diss} = \sum_{i=1}^{N} \left[-\mathbf{D}_i \cdot \frac{\mathbf{p}_i}{m} + \mathbf{C}_i \cdot \mathbf{F}_i \right], \tag{2.19}$$

where observables evolve always with the free propagator. Choosing C_i and D_i carefully J_{diss} can be forced to be equal to the J given by Green-Kubo theory for the Lennard Jones system. The mechanical perturbation can be therefore merely used to probe the system in order to compute, through linear response, the selected auto-correlation function and does not have any physical meaning. This explains the adjective "synthetic" attached to these methods. The standard choice for F is $F(t) = F\theta(t)$. This permits to obtain directly the time integral,
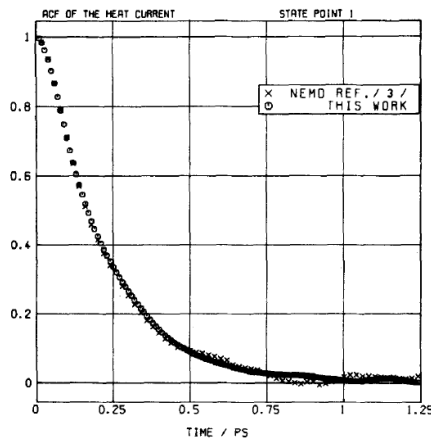
Figure 2.7: Comparison between the heat current autocorrelation function computed with synthetic methods and and by EMD for a Lennard Jones system, from ref. [24]

applying (2.18) with $A = J$:

$$lim_{t\to\infty}\langle J(t)\rangle = \langle J(0)\rangle - \beta F \int_0^{+\infty} \langle J(t')J(0)\rangle_{eq} dt'. \qquad (2.20)$$

The drawback of this choice is that in general the limit on the left does not exist, because for long times the external perturbation heats the system. This is a second order effect and in this condition linear response theory does not apply. For every finite F, no matter how small, there is a time t such that $\langle A(t)\rangle$ is not given anymore by linear response theory. One way to get out of this situation is applying a thermostat that is able to maintain the system in a steady linear regime. One has to check that the transport coefficient obtained is the same independently of the presence of a thermostat. Theoretical results in this sense are given in [23]. Other choices for F are possible in order to compute the whole autocorrelation function, not just its time integral [24].

2.5 Expanding the scope of molecular simulations

The methods described so far have their own, often complementary, advantages and drawbacks. The application of the PBE requires a rather cumbersome workflow since phonon frequencies, velocities and lifetimes need to computed. It becomes even more complicated when the full solution of the PBE, avoiding the relaxation time approximation, is needed. This approach can be implemented in an ab-initio framework based on DFT, and accounts for

quantum effects that may be important at low temperatures but its application is limited to crystals well below the melting point, where phonon dispersions are defined and anharmonic effects small enough to be treated perturbatively. Actually when the solid is highly harmonic this is the method to be chosen. In fact NEMD and EMD methods, even if they do not suffer of such restrictions, are more effective when anharmonic effects lead to short lifetimes. Nevertheless, when dealing with liquids and disordered systems, EMD and NEMD methods are actually the only ones at disposal. NEMD methods, under the Müller-Plathe methodology, have been implemented in an ab-initio framework as well, but scattering of phonons from the thermal reservoirs lead to slow size convergence. To circumvent this problem, an additional modeling is required, in order to fit the results to infinite volume. An other intrinsic source of slow convergence is due to the fact that local thermodynamic equilibrium must be reached in different regions of the simulation cell. Furthermore, the inhomogeneity of the system is associated to high thermal gradients and undesired density variations [25]. EMD methods, based on the Green-Kubo approach do not suffer from these problems and in fact show a much weaker size dependence. They have been implemented, for the moment, only for classical potentials and their validity is therefore limited by the ability of these potentials to simulate the system of interest. An ab initio approach would therefore be desirable. It is actually believed that fundamental problems do not permit application of EMD to quantum systems. We cite from reference [26]:

The widely use Green-Kubo relation does not serve for our purposes, because in first-principles calculations it is impossible to uniquely decompose the total energy into individual contributions from each atom.

This is not right. We will see in chapter 3 that a microscopic definition of the energy current can be provided in a Born-Oppenheimer, adiabatic, framework. The non-uniqueness of the energy decomposition is a problem affecting also classical systems, but does not change the result given by the Green-Kubo formula. This problem is discussed in the third chapter of this thesis.

Chapter 3

Green-Kubo formalism

Green-Kubo formulas relate dissipative transport coefficients to spontaneous, equilibrium fluctuations of the flux responsible for the transport process [27, 28, 29, 30]. The proof of these relations depends on the process considered. Two main families of perturbations can be identified: *mechanical* and *thermal*. Mechanical perturbations can be described by an additive term in the Hamiltonian of the system, such as e.g. an external electric field. Thermal disturbances, such as thermal gradients, cannot be described by any mechanical perturbation and belong to the second family. In both cases the main ingredient required for making a connection between equilibrium and non equilibrium properties is linear response theory (LRT). In the first section of this chapter we will introduce the needed statistical mechanical background and show how LRT can be directly used to treat mechanical perturbations. The second section is devoted instead to the extension of LRT needed for describing thermal transport coefficients and in the third section the celebrated Green-Kubo formula for thermal conductivity is derived via Navier-Stokes equations. Then the Green-Kubo formula is analyzed: in the fourth section its behavior under combination of different thermal transport processes is shown, whereas the next one is devoted to the problem of the energy density indeterminacy, which only apparently prevents application of the Green-Kubo formula in a quantum adiabatic framework. Finally, a different viewpoint on this problem is proposed as an application of Mori's memory function formalism.

3.1 Classical linear response theory

3.1.1 Notation and basic concepts

To fix notations and conventions we summarize here the main ingredients necessary to give a statistical mechanical description of classical systems. The microscopic state of the system is referred to as a phase space point, parametrized by a couple of generalized coordinates (q, p). In a system of N particles q can be taken as the three dimensional positions coordinates $q = (\mathbf{r}_1, ..., \mathbf{r}_N)$ and p their conjugate momenta $p = (m_1 \mathbf{v}_1, .., m_N \mathbf{v}_N)$. The Hamiltonian of the system is a real scalar function of the generalized coordinates $H(q, p)$, which entails all information about the microscopic dynamics of the system. The time evolution of a microscopic state is described by a system of first order differential equations, the Hamilton equations:

$$\dot{q} = \frac{\partial H(q, p)}{\partial t}, \tag{3.1}$$

$$\dot{p} = -\frac{\partial H(q, p)}{\partial t}. \tag{3.2}$$

On the other hand, a statistical ensemble is described by a distribution function $f(q, p, t)$, positive and normalized to unity, that gives the probability for the system to be found at a given space point (q, p). In equilibrium systems, described by the canonical ensemble, the distribution function is the Boltzmann distribution $f_0(q, p) \sim \exp(-\beta H(q, p))$, where $\beta = \frac{1}{k_B T}$ as usual.

Observables are functions of the phase space coordinates $A(q, p)$ (complex values are also allowed), and their expectation value is defined as:

$$\langle A \rangle_f \equiv \int dp \, dq \, f(q, p) A(q, p). \tag{3.3}$$

The distribution function for all purposes can be mathematically considered as a measure in phase space. The Cauchy-Schwarz inequality can therefore be applied to prove that, for two generic observables A and B and any distribution function f:

$$\langle |A(q, p)B(q, p)| \rangle_f^2 \quad \leq \quad \langle |A(q, p)^2| \rangle_f \langle |B(q, p)|^2 \rangle_f. \tag{3.4}$$

When f does not coincide with the equilibrium distribution it may evolve with time, according to the Liouville equation:

$$\frac{\partial f(q, p, t)}{\partial t} = -i\hat{L} f(q, p, t), \tag{3.5}$$

where the Liouville operator $\hat{L}$, also called the *Liouvillean*, is defined in terms of the well known Poisson bracket: :

$$\hat{L}\circ = i\{H,\circ\}_{pb}, \tag{3.6}$$

$$\{A(q,p),B(q,p)\}_{pb} \equiv \frac{\partial A(q,p)}{\partial q}\frac{\partial B(q,p)}{\partial q} - \frac{\partial B(q,p)}{\partial p}\frac{\partial A(q,p)}{\partial q}. \tag{3.7}$$

It is simple to verify that $\hat{L}f_0 = 0$, so that the Boltzmann distribution is stationary with respect to time evolution and the Liouville equation preserves the normalization of the distribution function. The operator $\hat{U}(t)$ is defined as the propagator for the distribution function: $\hat{U}(t)f(q,p,0) = f(q,p,t)$. In the case of a time-independent Hamiltonian and Liouvillean:

$$\hat{U}(t) = e^{-i\hat{L}t}. \tag{3.8}$$

We will use time dependent observable only propagating with time independent Liouvilleans, therefore this equation will always be valid in our calculations. We observe that the Liouville operator is Hermitian with respect to either one of the following two scalar products in the vector space of the observables:

$$(A,B) = \int dq\,dp\,A^*(q,p)B(q,p), \tag{3.9}$$

$$(A,B) = \int dq\,dp\,f^0(q,p)A^*(q,p)B(q,p). \tag{3.10}$$

Therefore the operator U is unitary with respect to both of these scalar products and $U^\dagger(t) = U^{-1}(t)$.

The explicit reference to the time dependent distribution function is reminiscent of the Schrödinger picture in quantum mechanics, since the distribution function evolves, while observables are kept fixed. In analogy to quantum mechanics, one can switch to a classical Heisenberg picture, where distribution functions are kept fixed and observables evolve in time, defining a time dependent observable $A(q,p,t)$: [1]

$$\langle A\rangle_{f(t)} = (f(t),A) = (\hat{U}(t)f(0),A) = \tag{3.11}$$

$$= (f(0),\hat{U}^\dagger(t)A) \equiv (f(0),A(t)) = \langle A(t)\rangle_{f(0)}, \tag{3.12}$$

where the first of the scalar products (3.10) has been considered. $A(t)$, defined as $U^\dagger(t)A$, satisfies the differential problem:

$$\dot{A}(t) = i\hat{L}A(t),$$

$$A(t=0) = A. \tag{3.13}$$

---

[1]For the sake of simplicity, as it is usual in the literature, depending on the number of arguments $A()$ can indicate the time dependent observable or the static one

The time dependent observable $A(q, p, t)$ can be explicitly obtained from $A(q, p)$ by replacing q with $q(t)$ and p with $p(t)$, where $q(t)$ and $p(t)$ are the solutions to the Hamilton equations with initial conditions $q(0) = q$, $p(0) = p$:

$$\hat{U}^+(t)A(q, p) = e^{-t\{H, \circ\}_{pb}}A(q, p) = e^{t\frac{d}{dt}}A(q, p) = A(q(t), p(t)), \tag{3.14}$$

where identities (3.7), (3.8) and the standard relation between Poisson Brackets [31] and time derivatives have been used.

3.1.2 Linear response to mechanical perturbations

We consider a system described by the unperturbed Hamiltonian H_0 and subject to a mechanical perturbation H':

$$H = H_0 + H'(t), \tag{3.15}$$

$$H'(t) = -\lambda(t)V, \tag{3.16}$$

where $V = V(q, p)$ is an observable and the function $\lambda(t)$, phase space independent, fixes the time dependent strength of the perturbation. We suppose that at $t = -\infty$ the system is in thermal equilibrium with respect to the Hamiltonian H_0 and that $\langle V \rangle_{eq} = 0$. In all calculations we write $\langle \rangle_{eq}$ instead of $\langle \rangle_{f_0}$, where $f_0 \sim \exp(-\beta H_0(q, p))$.

The perturbation results in a perturbed Liouvillean operator acting on the distribution function:

$$\hat{L}f = \hat{L}_0 f + \hat{L}'f, \text{where} \tag{3.17}$$

$$\hat{L}'f = -i\lambda\{V, f\}_{pb}. \tag{3.18}$$

In the limit of weak fields we can suppose that the distribution function will be close to the equilibrium $f_0(q, p)$, so that:

$$f(q, p, t) = f_0(q, p) + f'(q, p, t) + O(\lambda^2). \tag{3.19}$$

Plugging this equation into (3.7) and disregarding higher order terms we get the linearized Liouville equation:

$$\frac{\partial f'}{\partial t} = -i\hat{L}_0 f' - \lambda\{V, f_0\}_{pb}. \tag{3.20}$$

This is a first order differential equation, with boundary condition $f(q, p, t = -\infty) = f_0(q, p)$ and therefore admits an explicit integral solution:

$$f' = -\int_{-\infty}^{t} \hat{U}_0(t-s)\{V, f^0\}_{pb} \quad \lambda(s)ds \tag{3.21}$$

$$= -\beta f^0 \int_{-\infty}^{t} \hat{U}_0(t-s)\dot{V}(s)\lambda(s)ds, \tag{3.22}$$

where the propagator $\hat{U}_0$ is the unperturbed Liouvillean propagator, which also defines the Heisenberg picture for time dependent observables. In the last step we used the identity:

$$\{V, f^0\}_{pb} = \beta \dot{V} f^0, \tag{3.23}$$

which can be verified by plugging in the explicit form of the equilibrium distribution.

Fix now an observable A of our system. If the system is in equilibrium the value $\langle A(t) \rangle_{eq}$ does not depend on t and, without loss of generality, we suppose $\langle A(t) \rangle_{eq} = 0$ for every t. The time-dependent response of the observable A to the perturbation H' is obtained in the Schrödinger picture by multiplying eq. (3.22) by $A(q, p)$ and integrating over phase space. The canonical distribution that has arisen in equation (3.22) is fundamental in the calculation:

$$\langle A(t) \rangle = -\beta \int_{-\infty}^{t} \lambda(s)ds \int dq\, dp\, f^0(q, p) A(q, p) \hat{U}_0(t-s)\dot{V}(q, p, s), \tag{3.24}$$

where the time dependence of the operators is determined by the unperturbed Hamiltonian H_0. The latter can be rewritten in the standard form:

$$\langle A(t) \rangle = \int_{-\infty}^{t} \Phi_{AV}(t-s)\lambda(s)ds,$$
$$\Phi_{AV}(t) = \beta \frac{\partial}{\partial t} \langle A(t)V(0) \rangle_{eq}, \tag{3.25}$$

The expectation value on the right-hand side of eq. 3.25 is the time correlation function of the observables A and V, often indicated with the symbol $C_{AV}(t)$:

$$C_{AV}(t) \equiv \langle A(t)V(0) \rangle_{eq} \tag{3.26}$$

and we just proved that the time derivative of $C_{AV}(t)$ is, apart from factors, $\Phi_{AV}(t)$.

Equation (3.25) is the main result of LRT: it manages to express linear (non-equilibrium) response in terms of a correlation function depending entirely on equilibrium quantities.

An alternative expression for $\Phi_{AV}(t)$, usually referred to as the fluctuation-dissipation theorem and closer to the one obtained by quantum linear response theory [32], can be found

when f_0 is the canonical distribution function. Expanding again the Poisson bracket [2]:

$$\Phi_{AV}(t) = -\beta \langle A(t)\{H,V\}_{pb}\rangle_{eq}$$

$$= -\beta \int dqdp f^0 A(t) \left(\frac{\partial H}{\partial q}\frac{\partial V}{\partial p} - \frac{\partial H}{\partial p}\frac{\partial V}{\partial q} \right)$$

$$= \int dqdp A(t) \left(\frac{\partial f^0}{\partial q}\frac{\partial V}{\partial p} - \frac{\partial f_0}{\partial p}\frac{\partial V}{\partial q} \right)$$

$$= -\int dqdp f^0 \left(\frac{\partial}{\partial q}\left(A\frac{\partial V}{\partial p} \right) - \frac{\partial}{\partial p}\left(A\frac{\partial V}{\partial q} \right) \right) = \langle\{A(t),V(0)\}_{pb}\rangle_{eq}, \tag{3.27}$$

where we used partial integration to move the derivative from f_0 to A and commutation of partial derivatives to simplify the resulting expression. Comparing equations (3.25) and (3.27) we deduce:

$$\beta\frac{\partial}{\partial t}C_{AV}(t) = \langle\{A(t),V(0)\}_{pb}\rangle_{eq}. \tag{3.28}$$

Green-Kubo relations for mechanical perturbations follow as a direct application of the formulas developed. As an example we compute the response of the electric current due to a weak macroscopic uniform electric field, i.e. the electric conductivity. We consider a a classical, isotropic system of N interacting particles with charge z_i. The perturbation H' and the resulting electric current $\mathbf{J}_E$ are:

$$H' = -\left(\sum_{i=1}^N z_i e\mathbf{r}_i \right) \cdot \mathbf{E}(t), \tag{3.29}$$

$$\mathbf{J}_E = \sum_{i=1}^N z_i e\mathbf{v}_i, \tag{3.30}$$

where as before $\mathbf{r}_i$ and $\mathbf{v}_i$ are the particle's positions and velocities, whereas $\mathbf{E}(t)$ is the strength of the external electric field. Formula (3.25) gives (the components of the electric field $\boldsymbol{E}(t)$ play the role of variable λ):

$$\Phi_{\mathbf{JE}}(t) = \frac{\beta}{3}\langle \mathbf{J}_E(t) \cdot \mathbf{J}_E(0)\rangle_{eq}. \tag{3.31}$$

The zero frequency component describes the response σ to static electric fields:

$$\sigma = \frac{\beta}{3V}\int_{-\infty}^{+\infty} \langle \mathbf{J}_E(t) \cdot \mathbf{J}_E(0)\rangle_{eq}dt. \tag{3.32}$$

---

[2]The algebra of time correlation functions permits to switch time derivatives, so that $\langle \dot{A}(t)B(0)\rangle = -\langle A(t)\dot{B}(0)\rangle$

It is immediate to see that if all the particles are equally charged, $z_i = z$, than conservation of momentum imposes $\sigma = 0$.

3.2 Green-Kubo relations for thermal disturbances

We now describe how Green-Kubo relations can be obtained for thermal disturbances. We will follow a simple example, deriving explicitly a Green-Kubo relation associated to a particular diffusion process, leaving application to thermal conductivity for the next sections. The discussion will closely follow ref. [33, 34, 35]. Useful discussions can also be found in ref. [36, 37].

3.2.1 Phenomenological descriptions

We begin with a brief discussion of how phenomenological descriptions arise from microscopic theories. These descriptions are based on the concept of local thermal equilibrium (LTE), which makes it possible to define space-dependent thermodynamic variables varying on length scales that are long with respect to the typical inter-atomic distances and that fluctuate, in the absence of external perturbations, around the global, position-independent value, on time scales that are long with respect to the typical molecular relaxation times. These variables are usually called *hydrodynamic variables* and phenomenological differential equations give a dynamical description of their time evolution. The dynamics of the other "fast" variables is treated instead on a statistical mechanical base, thanks to the hypothesis of LTE.
The main example of hydrodynamic variables consists in locally conserved quantities, which satisfy an evolution equation of the type:

$$\dot{f}(\mathbf{r}, t) = -\nabla \cdot \mathbf{J}_f(\mathbf{r}, t). \tag{3.33}$$

A locally conserved quantity plays a special role because the decaying time of its long wavelength components diverges when very small wavelengths are considered, that is in the macroscopic limit. In fact the correlation function $\langle f(q, t) f(-q, 0) \rangle$ when $q = 0$ is exactly constant and not subject to any decay: as a consequence, $\tau(q) \to \infty$ when $q \to 0$. Non conserved observables relax to equilibrium much faster, on molecular time scales: there is therefore a dynamical decoupling of the conserved variables from all the others, which permits to consider the hydrodynamic variables as describing LTE. This decoupling is practically performed and the phenomenological equations form a closed system if we are able to write, in the

macroscopic limit, all currents entering the conservation equations as a function of the hydrodynamic variables. The coefficients entering these relations are exactly what remains in the evolution equations after the decoupling procedure and constitutive relations, a consequence of LTE, can play a role.

This general framework will be now be clarified through the definition of a simple "thermal" transport coefficient. We consider a system of $2N$ interacting particles and assign a certain "charge" $z_i = +1$ to half of the particles and $z_i = -1$ to the remaining. This defines a microscopic conserved density:

$$\rho(\mathbf{r}) = \sum_i \delta(\mathbf{r} - \mathbf{r}_i) z_i \tag{3.34}$$

and a current, in reciprocal space:

$$\mathbf{J}(\mathbf{q}) = \sum_i e^{-i\mathbf{q}\mathbf{r}} \mathbf{v}_i z_i,$$

$$\dot{\rho}(\mathbf{q}) = -i\mathbf{q} \cdot \mathbf{J}(\mathbf{q}). \tag{3.35}$$

In the macroscopic limit, the relaxation of the density ρ becomes very slow, because of the conservation equation it respects. Thanks to the way in which we defined ρ, not relating it to any property of the system, we can suppose that its dynamics is decoupled from all the other conserved quantities. A hydrodynamic theory describes the evolution equations for the small wavelength, small frequency components of $\rho(\mathbf{r})$: from now on we will therefore switch to coarse grained quantities. Microscopic and coarse grained variables coincide, in reciprocal space, for small $\mathbf{q}$.

The next step consists in understanding which can be the relation between the (macroscopic) current $\mathbf{J}$ and the conserved density. This point can be tricky to understand and it constitutes the main difficulty when building phenomenological descriptions of many body systems. In this simple case we expect that the current will be proportional to the unbalance between particles with charge $z_i = +1$ and charge $z_i = -1$. Therefore in the linear regime we expect the following expression to hold:

$$\langle \mathbf{J}(\mathbf{r}) \rangle = -D \langle \nabla \rho(\mathbf{r}) \rangle. \tag{3.36}$$

Equation (3.36) is the phenomenological equation defining the diffusion coefficient D. We can combine this equation and the conservation property to obtain:

$$\langle \rho(\mathbf{q}, z) \rangle = \frac{\langle \rho(\mathbf{q}, t = 0) \rangle}{iz - Dq^2}. \tag{3.37}$$

This equation describes the time evolution of the slow variable ρ in terms of the transport coefficient. It is interesting to note that, to describe the time evolution of the slow variable,

details of the complicated many body interactions have been hidden behind a single scalar coefficient. The same evolution can be described by LRT, as explained in the next section. We will then use these results to derive a recipe to compute D, i.e. a Green-Kubo relation.

3.2.2 Slow processes described by linear response theory

In this section A will be a generic slow observable of the system, defining a hydrodynamic variable in the sense of the previous paragraph. We suppose that at a certain time t_0 it presents a non equilibrium value $\langle A(t_0) \rangle \neq 0$. For $t > t_0$ the system will continue its free evolution. Linear response theory is able to describe the evolution of the slow variable and the description will be used to obtain Green-Kubo relations for the second family of transport coefficients described in the introduction.

One starts by creating, starting from a global equilibrium condition and using formally in equation (3.16) the same observable A as a perturbing field, the initial non equilibrium state. The choice of λ is made:

$$\lambda(t) = \lambda_0 e^{\epsilon t} \quad \text{for} \quad t\langle 0,$$
$$\lambda(t) = 0 \quad \text{for} \quad t > 0, \tag{3.38}$$

where ϵ is a small infinitesimal parameter put to switch on smoothly the perturbation. At $t = 0$ a non-equilibrium state is realized. During the process, since A is a slow variable, the system will always respect LTE and remain in the linear regime. Using then equation (3.25) we obtain:

$$\langle A(t) \rangle = \int_{-\infty}^{t} \Phi_{AA}(t-s)\lambda(s)ds. \tag{3.39}$$

Plugging $t = 0$ and using the explicit time dependence of the perturbation:

$$\langle A(t=0) \rangle = \chi_{AA}\lambda_0. \tag{3.40}$$

This permits to identify χ_{AA}, whose definition has been given in appendix A, eq. A.11, with a static susceptibility. Now we turn to relaxation. Since the external field is zero when $t > 0$, deriving both terms of equation (3.39):

$$\langle \dot{A}(t) \rangle = \lambda_0 \Phi_{AA}(t) \quad t > 0. \tag{3.41}$$

It is easy to Fourier-Laplace transform this identity and using the static result (3.40) we obtain:

$$\langle A(z) \rangle = \frac{1}{iz}\left(1 - \chi_{AA}(z)\chi_{AA}^{-1}\right)\langle A(t=0) \rangle, \tag{3.42}$$

25

where $\chi_{AA}(z)$ is the dynamical susceptibility of appendix A. This equation gives the time evolution for $t > 0$ of the slow variable in terms of the response function which standard LRT is able to write as an equilibrium autocorrelation function, as shown in equations 3.25 and A.4. We can also rewrite, using relation A.13:

$$\langle A(z) \rangle = \beta \left[C_{AA}(z) \chi_{AA}^{-1} \right] \langle A(t = 0) \rangle, \tag{3.43}$$

where C is defined as before:

$$C_{AA}(t) = \langle A(t) A(0) \rangle_{eq}. \tag{3.44}$$

What we actually found is a connection between the slow time evolution of macroscopic, non equilibrium values of $\langle A \rangle$, with equilibrium fluctuations of the same variable. Onsager in his celebrated works used such a connection as an hypothesis [38, 39]. Of course, as a consequence of 3.43, the decay time of $C_{AA}(t)$ will be of the same order of the typical time scale on which the non-equilibrium, slow variable, varies and therefore much longer than the typical molecular relaxation times.

3.2.3 Equating the descriptions

The descriptions of the previous two sections are equivalent in the linear regime and in the macroscopic limit. We rewrite (3.43) applied to our case:

$$\langle \rho(\mathbf{q}, z) \rangle = \beta \left[C_{\rho\rho}(\mathbf{q}, z) \chi_{\rho\rho}^{-1}(\mathbf{q}) \right] \langle \rho(\mathbf{q}, t = 0) \rangle. \tag{3.45}$$

By comparing the latter and 3.37 we find for small q:

$$C_{\rho\rho}(\mathbf{q}, z) = \frac{\beta^{-1} \chi_{\rho\rho}}{iz - Dq^2}, \tag{3.46}$$

where we defined the static correlation:

$$\lim_{q \to 0} \chi_{\rho\rho}(\mathbf{q}) = \chi_{\rho\rho}. \tag{3.47}$$

Finally, using equation (A.15) we get a Green-Kubo relation for this coefficient:

$$D = \lim_{\omega \to 0} \lim_{q \to 0} \frac{1}{\chi_{\rho\rho}} \frac{\omega}{q^2} \chi_{\rho\rho}''(q, \omega). \tag{3.48}$$

With the help of the equation (A.10) and of the main linear response theory result (3.25) this equation can be written in a way ready to be implemented in a computer program:

$$D = \frac{\beta}{6V\chi_{\rho\rho}} \int_0^{+\infty} \langle \mathbf{J}_0(t) \cdot \mathbf{J}_0(0) \rangle_{eq} dt \tag{3.49}$$

$$\mathbf{J}_0 = \sum_{i=1}^N z_i \mathbf{v}_i. \tag{3.50}$$

, which is a Green-Kubo relation for the macroscopic transport coefficient D.

We summarize the practical procedure followed for defining the diffusion coefficient D and obtaining the Green-Kubo relation for the second family of transport coefficients:

1. Conserved, slow variables, were identified;

2. An expression for the currents in terms of the hydrodynamic variables, that is, a phenomenological description, must be found by some argument (in general symmetry properties of the system under consideration). Use must be made of constitutive relations, which describe LTE;

3. The evolution equations, now a closed system, are solved and relaxation is described in terms of phenomenological coefficients;

4. A comparison with the description of relaxation provided by LRT permits to identify transport coefficients with correlation functions of equilibrium fluctuations, thus leading to the Green-Kubo relations;

The entire procedure is also a test of validity of the phenomenological equations. For example if application of (3.50) in computer simulations does not lead to converged results, this means that the description was not correct.

3.3 Relaxation of simple fluids: the Navier-Stokes equations

We now apply the outlined procedure in order to obtain the Green-Kubo expression for thermal conductivity in one component, atomic or molecular isotropic fluids [3]. Navier-Stokes equations describe time evolution in these systems and are valid at time and at length scales over which LTE can be realized. Therefore in this section all variables are subject to a coarse graining procedure. We will consider only small departures from a global equilibrium state and distinguish the fluctuating parameters from the number of arguments: an expression like $T(\mathbf{r})$ for example will refer to the local fluctuating temperature, whereas T to the equilibrium ,position independent, one.

We report here (see [23] for a derivation) the Navier-Stokes equations, which are a consequence of particle number, momentum and energy conservation. Denoting with $n(\mathbf{r})$,$g(\mathbf{r})$

---

[3]two component fluids require different treatments because of the presence of more conserved variables [40].

and $\epsilon(\mathbf{r})$ the respective densities:

$$
\begin{cases}
\dfrac{\partial \langle n(\mathbf{r},t) \rangle}{\partial t} = -\dfrac{\partial}{\partial r_a} Q_a(\mathbf{r},t) \\[2ex]
\dfrac{\partial \langle g_a(\mathbf{r},t) \rangle}{\partial t} = -\dfrac{\partial}{\partial r_b} P_{a,b}(\mathbf{r},t) \, , \\[2ex]
\dfrac{\partial \langle \epsilon(\mathbf{r},t) \rangle}{\partial t} = -\dfrac{\partial}{\partial r_a} J_a(\mathbf{r},t)
\end{cases}
\tag{3.51}
$$

where m is the mass of an atom/molecule and a suitable current has been defined for every conserved quantity.

The currents appearing in equations 3.51 can actually be written as a function of the hydrodynamics variables, at the cost of introducing additional transport coefficients and constitutive relations. First of all we must define the streaming velocity $\mathbf{v}(\mathbf{r})$:

$$
v_a(\mathbf{r},t) \equiv \frac{\langle g_a(\mathbf{r},t) \rangle}{m \langle n(\mathbf{r},t) \rangle}.
\tag{3.52}
$$

In terms of the streaming velocity the currents read [23]:

$$
\begin{cases}
Q_a = \langle g_a(\mathbf{r},t) \rangle \\[3ex]
P_{a,b}(\mathbf{r},t) = p(\mathbf{r},t)\delta_{a,b} - 2\eta \left(\dfrac{\partial_a v_b(\mathbf{r},t) + \partial_b v_a(\mathbf{r},t)}{2} - \dfrac{1}{3} \partial_a v_a(\mathbf{r},t) \right) \\[2ex]
\quad - \zeta \partial_a v_a(\mathbf{r},t)\delta_{a,b} \\[3ex]
J_a(\mathbf{r},t) = (\epsilon + p) v_a(\mathbf{r},t) - \lambda \partial_a T(\mathbf{r},t)
\end{cases}
\tag{3.53}
$$

where η and ζ are the shear and bulk viscosity respectively and $p(\mathbf{r},t)$ the local pressure. We observe that, taken as independent variables, energy and number density describe completely the local equilibrium state. This means that temperature, pressure and all thermodynamic variables can be taken as a function of these two fluctuating variables and that the system of differential equations is closed.

Plugging the expression of the currents (3.53) into (3.51) the evolution equations are made

explicit as:

$$\begin{cases} \partial_t \langle \delta n(\mathbf{r},t) \rangle = -\frac{1}{mn} \partial_a \langle \delta g_a(\mathbf{r},t) \rangle \\[2em] \partial_t \langle \delta g_a(\mathbf{r},t) \rangle = -\partial_a \delta p(\mathbf{r},t) + \frac{\zeta + \frac{\eta}{3}}{mn} \partial_a \partial_b \langle \delta g_b(\mathbf{r},t) \rangle \\[0.5em] \qquad\qquad + \frac{\eta}{mn} \partial_b \partial_b \langle \delta g_a(\mathbf{r},t) \rangle \\[2em] \partial_t \langle \delta \epsilon(\mathbf{r},t) \rangle = -(\epsilon + p) \frac{1}{mn} \partial_a \langle \delta g_a(\mathbf{r},t) \rangle + \lambda \partial_b \partial_b \delta T(\mathbf{r}) \end{cases} , \qquad (3.54)$$

where Einstein summation convention has been used. Every fluctuating variable has been replaced in (3.54) with its fluctuation with respect to the mean value, denoted here with a δ. This is possible because the system at equilibrium is uniform. The main difficulty in solving these equations is that $\delta p(\mathbf{r},t)$ and $\delta T(\mathbf{r},t)$ must be rewritten in terms of a complete independent set of hydrodynamic variables. After some manipulations, described in appendix B , one is able to recover an expression formally equal to the one obtained by linear response theory. We define the new variables:

$$A_1(\mathbf{k},t) = \delta n(\mathbf{k},t)$$

$$A_2(\mathbf{k},t) = \delta g^l(\mathbf{k},t)$$

$$A_3(\mathbf{k},t) = \delta q(\mathbf{k},t) = \delta \epsilon(\mathbf{k},t) - \frac{\epsilon + p}{n} \delta n(\mathbf{k},t)$$

and the matrix, depending only on the modulus of $\mathbf{k}$:

$$M(k) = \begin{pmatrix} z & -\frac{k}{m} & 0 \\ -kmc^2 & z + ik^2 D_l & -\frac{\beta_V}{nc_v} k \\ ik^2 \lambda \frac{\beta_V T}{n^2 c_v} & 0 & z + i \frac{k^2 \lambda}{c_v} \end{pmatrix}, \qquad (3.55)$$

where c_v is the specific heat per particle at constant volume, β_V the isothermal compressibility and c^2 the adiabatic speed of sound. The final result gets the form:

$$M_{ij}(k) \langle A_j(\mathbf{k},z) \rangle = \langle A_i(\mathbf{k},t=0) \rangle, \qquad (3.56)$$

where $M_{ij}(k)$ is called the hydrodynamic matrix [41].

3.3.1 Green-Kubo formula for thermal conductivity

Equation (3.43) can be generalized to the case of several space-dependent variables $A_i(\mathbf{r})$ in the matrix form:

$$\langle A_i(\mathbf{k},z) \rangle = \beta \left[C(\mathbf{k},z) \chi^{-1}(\mathbf{k}) \right]_{ij} \langle A_j(\mathbf{k},t=0) \rangle \qquad (3.57)$$

with the correlation matrix:

$$C_{ij}(\mathbf{k}, t) = \frac{1}{V} \langle A_i(\mathbf{k}, t) A_j(-\mathbf{k}, 0) \rangle. \tag{3.58}$$

By comparison with (3.56) we obtain:

$$C(k, z) = iM(k)^{-1} C(k, t = 0), \tag{3.59}$$

which is already a "Green-Kubo" relation, since it involves the matrix M, containing transport coefficients, and the equilibrium correlation function matrix C.

To extract information about thermal conductivity the focus here goes to the element $C_{qq}(k, z)$ in equation (3.59). We need for this purpose to perform an expansion for small k and the matrix product on the right member. The needed values of the matrix $C(k = 0, t = 0)$ can be computed using thermodynamic fluctuation theory and the results needed are derived in appendix C:

$$C_{qn}(t = 0) = \beta^{-1} T \left(\frac{\partial n}{\partial T} \right)_p \tag{3.60}$$

$$C_{qg}(t = 0) = 0 \tag{3.61}$$

$$C_{qq}(t = 0) = \beta^{-1} n c_p T, \tag{3.62}$$

where c_p is the specific heat per particle, at constant pressure.

To perform the matrix inversion in equation 3.59 the eigenvalues of $M(\mathbf{k})$ up to second order in k, derived in appendix B, are needed:

$$z_0 = -ik^2 D_T$$

$$z_1 = ck - ik^2 \Gamma \quad z_2 = -ck - ik^2 \Gamma,$$

where: $D_T = \frac{\lambda}{n c_p}$ is the thermal diffusivity and Γ the sound diffusion attenuation coefficient. From the explicit expression for the inverse of the matrix M it is evident that, for fixed k and as a function of z, $C_{qq}(k, z)$ will have three poles, one for each eigenvalue. Up to regular terms, for finite k, one can extract the singular behavior considering pole contributions:

$$C_{qq}(k, z) \sim \sum_{i=1}^{3} \frac{A_i(k)}{z - z_i(k)} \tag{3.63}$$

$$A_i(k) = \lim_{z \to z_i} C_{qq}(k, z)(z - z_i). \tag{3.64}$$

From figure 3.1, we see that in the limit $k \to 0$ only a singularity in $z = 0$ can arise, where the poles merge. After performing the calculation and summing the residues, in the small k
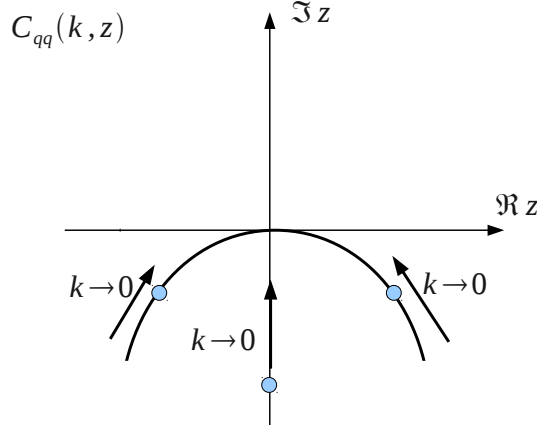
Figure 3.1: Pole structure of $C_{qq}(k,z)$ for finite k. The arrows indicate where poles merge as $z \to 0$.

limit one out of the three poles develops a singularity near $z = 0$, with a resulting asymptotic behavior:

$$C_{qq}(k,z) \sim \frac{i\beta^{-1}nc_p}{z + ik^2 D_T},$$
(3.65)

up to regular terms regular in z for small k.

Using equation (A.15) we obtain:

$$\chi''_{qq}(k,\omega) = Tnc_p \frac{k^2\omega D_T}{\omega^2 + (k^2 D_T)^2},$$
(3.66)

and inserting the definition of the thermal diffusivity D_T:

$$\lambda = \frac{1}{T} \lim_{\omega \to 0} \lim_{k \to 0} \frac{\omega}{k^2} \chi''_{q,q}(k,\omega).$$
(3.67)

This is finally one form of the Green-Kubo formula for thermal conductivity, which can be rewritten, using the fluctuation dissipation theorem:

$$\lambda = \frac{1}{2k_B T^2} \lim_{\omega \to 0} \lim_{k \to 0} \frac{\omega^2}{k^2} \tilde{C}_{q,q}(k,\omega) = \frac{1}{2k_B T^2} \lim_{\omega \to 0} \lim_{k \to 0} \frac{\tilde{C}_{\dot{q},\dot{q}}(k,\omega)}{k^2}.$$
(3.68)

These equations can be further simplified. It will be shown in section 3.4 that, under the following hypothesis:

$$\lim_{\omega \to 0} \lim_{k \to 0} \frac{\tilde{C}_{\dot{n},\dot{n}}(k,\omega)}{k^2} = 0,$$
(3.69)

we can conclude:

$$\lim_{\omega \to 0} \lim_{k \to 0} \frac{\tilde{C}_{\dot{q}+\alpha\dot{n},\dot{q}+\alpha\dot{n}}(k,\omega)}{k^2} = \lim_{\omega \to 0} \lim_{k \to 0} \frac{\tilde{C}_{\dot{q},\dot{q}}(k,\omega)}{k^2}$$
(3.70)

31

for every α. Choosing $\alpha = \frac{\epsilon + p}{n}$ the standard Green-Kubo result is obtained:

$$\lambda = \frac{1}{2k_B T^2} \lim_{\omega \to 0} \lim_{k \to 0} \frac{\tilde{C}_{\dot{\epsilon}, \dot{\epsilon}}(k, \omega)}{k^2}. \tag{3.71}$$

Property (3.69) holds because:

$$\omega^2 \lim_{k \to 0} \frac{\tilde{C}_{\dot{n}, \dot{n}}(k, \omega)}{k^2} = \omega^2 \lim_{k \to 0} \tilde{C}_{g^l, g^l}(k, \omega) = \tag{3.72}$$

$$= \lim_{k \to 0} \tilde{C}_{\dot{g}^l, \dot{g}^l}(k, \omega) = \lim_{k \to 0} k^2 \tilde{C}_{P_{zz}, P_{zz}}(k, \omega) = 0, \tag{3.73}$$

where we have chosen in the last step to make the limit in the zeta direction.

3.3.2 The heat flux

The heat flux, already introduced in section 2.3, is fundamental for application of the Green-Kubo formalism [42]. For the derivation, we first of all rewrite (3.71) in a more explicit way:

$$\lambda = \int_0^{+\infty} dt \lim_{q \to 0} \frac{\langle \dot{\epsilon}(\mathbf{q}, t) \dot{\epsilon}(-\mathbf{q}, 0) \rangle}{V q^2} \tag{3.74}$$

From now on we will consider $k_B T^2 = 1$ in order to simplify notations. We will nevertheless leave explicitly the volume dependence in order to emphasize the thermodynamic limit: this means that the computation of physical quantities requires a limit over big cells.

The limit for small q is never explicitly numerically performed. The derivative of the energy density can be replaced by the energy current, defined by the conservation relation:

$$\dot{\epsilon}(\mathbf{r}, t) = -\nabla \cdot \mathbf{j}(\mathbf{r}, t) \tag{3.75}$$

Exploiting the latter relation, in reciprocal space, and isotropy, equation 3.74 becomes:

$$\lambda = \int_0^{+\infty} dt \lim_{q \to 0} \frac{\langle \dot{\epsilon}(\mathbf{q}, t) \dot{\epsilon}(-\mathbf{q}, 0) \rangle}{V q^2} = \int_0^{+\infty} dt \lim_{q \to 0} \frac{q_i q_j}{V q^2} \langle j_i(\mathbf{q}, t) j_j(-\mathbf{q}, 0) \rangle =$$

$$= \frac{1}{3V} \int_0^{+\infty} dt \langle \mathbf{J}(t) \mathbf{J}(0) \rangle, \tag{3.76}$$

, where Einstein summation convention over Cartesian coordinates has been considered and the heat flux $\mathbf{J}(t)$ is defined as:

$$\mathbf{J}(t) \equiv \int d\mathbf{r}\, \mathbf{j}(\mathbf{r}, t). \tag{3.77}$$

When a heat flux $\mathbf{J}(t)$ is computed from an energy density $\epsilon(\mathbf{r}, t)$, we say that $\mathbf{J}(t)$ and $\epsilon(\mathbf{r}, t)$ are associated. We note that this expression is equal, apart from surface contributions, to:

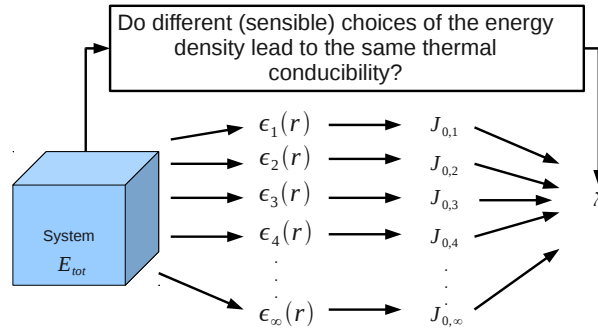$$\mathbf{J}(t) = \int d\mathbf{r}\, \dot{\epsilon}(\mathbf{r}, t) \mathbf{r} \tag{3.78}$$

Figure 3.2

This can be readily verified multiplying by **r** the conservation equation 3.75 and integrating by parts. As a result of the integration by parts, the integrand of this expression is not well defined under periodic boundary conditions. Nevertheless this is the expression taken as a starting point for deriving a heat flux and for applying Green-Kubo formula to thermal conductivity calculations. The scheme proceeds like this:

1. The total energy E of the system under consideration is identified;

2. From the total energy E one derives an energy density $\epsilon(\mathbf{r}, t)$;

3. The energy density $\epsilon(\mathbf{r}, t)$ is inserted into equation (3.78);

4. Using integration by parts, or neglecting surface terms, one recovers an expression well defined under periodic boundary conditions and therefore ready to be implemented on a computer program;

We will follow exactly this scheme in the next chapter when defining an ab-initio heat flux in Born-Oppenheimer systems. The second step of the procedure is quite arbitrary and this indeterminacy problem is pictorially described in figure 3.2. It is exactly the problem that prevented, till now, application of the Green-Kubo formalism in a quantum, DFT, framework, as it was pointed out in the last section of chapter 2. It will be thoroughly discussed, to confirm the correctness of the methodology, in section 3.5. The last step of the procedure is harmless as well, because surface contributions do not affect the value of the Green-Kubo relation: they do not possess the right volume scaling to survive the thermodynamic limit implicit in equation (3.76).

3.4 Combination of thermal transport processes

We defined in the previous paragraph the heat flux as the zero $\mathbf{q}$ component of the energy current density. We indicate with $\lambda(\mathbf{J})$ the thermal conductivity coefficient associated with a heat flux $\mathbf{J}$ and ask ourselves how the thermal conductivity coefficient associated to the sum of two different heat fluxes $\mathbf{J}_1$ and $\mathbf{J}_2$ is related to the individual values $\lambda(\mathbf{J}_1)$ and $\lambda(\mathbf{J}_2)$. We will show that:

$$\lambda(\mathbf{J}_1 + \mathbf{J}_2) = \lambda(\mathbf{J}_1) + \lambda(\mathbf{J}_2) + \Delta_{12}$$
$$|\Delta_{12}| \leq 2\sqrt{\lambda(\mathbf{J}_1)\lambda(\mathbf{J}_2)}. \tag{3.79}$$

As a consequence we have that, if $\lambda(\mathbf{J}_2)$ is zero, than Δ_{12} is zero and $\lambda(\mathbf{J}_1 + \mathbf{J}_2) = \lambda(\mathbf{J}_1)$. Told another way, we can add to the heat flux $\mathbf{J}_1$ another heat flux $\mathbf{J}_2$, without changing the thermal conductivity coefficient, provided that the conductivity associated to the added heat flux is zero. This property will be a useful tool in the next sections.

To prove (3.79) we first divide equation (3.76) into different contributions, using the parity under time reversal of the correlation function:

$$\lambda(\mathbf{J}_1 + \mathbf{J}_2) = \frac{1}{6V}\int_{-\infty}^{+\infty} dt \langle (\mathbf{J}_1 + \mathbf{J}_2)(t) \cdot (\mathbf{J}_1 + \mathbf{J}_2)(0) \rangle = \tag{3.80}$$

$$= \frac{1}{6V}\int_{-\infty}^{+\infty} dt \langle \mathbf{J}_1(t) \cdot \mathbf{J}_1(0) \rangle + \frac{1}{6V}\int_{-\infty}^{+\infty} dt \langle \mathbf{J}_2(t) \cdot \mathbf{J}_2(0) \rangle + \tag{3.81}$$

$$+ \frac{1}{3V}\int_{-\infty}^{+\infty} dt \langle \mathbf{J}_1(t) \cdot \mathbf{J}_2(0) \rangle \tag{3.82}$$

and this defines:

$$\Delta_{12} = \frac{1}{3V}\int_{-\infty}^{+\infty} dt \langle \mathbf{J}_1(t) \cdot \mathbf{J}_2(0) \rangle \tag{3.83}$$

It remains to prove the bound on Δ_{12}. This is a consequence of a generalized Einstein relation [43], usually applied in the case of particle diffusion. Defining:

$$\mathbf{Q}_i(t) = \int_0^t \mathbf{J}_i(t')dt' \quad i = 1,2 \tag{3.84}$$

one gets the identity (we observe that $\mathbf{Q}_i(0) = \mathbf{0}$) :

$$\langle \mathbf{Q}_1(t) \cdot \mathbf{Q}_2(t) \rangle =$$
$$= t \int_0^t dt' \left(\langle \mathbf{J}_1(t') \cdot \mathbf{J}_2(0) \rangle + \langle \mathbf{J}_2(t') \cdot \mathbf{J}_1(0) \rangle \right) \left(1 - \frac{t'}{t} \right) \tag{3.85}$$

and the relations:

$$\lambda(\mathbf{J}_i) = \lim_{t \to \infty} \frac{\langle |\mathbf{Q}_i(t)|^2 \rangle}{6Vt}, i = 1,2. \tag{3.86}$$

34

We can apply these results. Thanks to the Cauchy-Scharwz inequality we have:

$$|\langle \mathbf{Q}_1(t)\mathbf{Q}_2(t)\rangle| \leq \sqrt{\langle \mathbf{Q}_1(t)^2\rangle\langle \mathbf{Q}_2(t)^2\rangle}. \tag{3.87}$$

Therefore:

$$\lim_{t\to\infty} \frac{|\langle \mathbf{Q}_1(t) \cdot \mathbf{Q}_2(t)\rangle|}{6t} \leq \lim_{t\to\infty} \sqrt{\frac{\langle \mathbf{Q}_1(t)^2\rangle}{6t}\frac{\langle \mathbf{Q}_2(t)^2\rangle}{6t}} =$$
$$= \sqrt{\lambda(\mathbf{J}_1)\lambda(\mathbf{J}_2)}. \tag{3.88}$$

Now dividing equation (3.85) by $6t$ and making the limit:

$$\frac{|\Delta_{12}|}{2} = \frac{1}{6V}|\int_{-\infty}^{+\infty} dt' \langle \mathbf{J}_1(t') \cdot \mathbf{J}_2(0)\rangle| \leq \sqrt{\lambda(\mathbf{J}_1)\lambda(\mathbf{J}_2)}, \tag{3.89}$$

which is the desired bound on Δ_{12}.

Finally, we observe that equations (3.79) imply:

$$\sqrt{\lambda(\mathbf{J}_1 + \mathbf{J}_2)} \leq \sqrt{\lambda(\mathbf{J}_1)} + \sqrt{\lambda(\mathbf{J}_2)}. \tag{3.90}$$

This last expression generalizes easily to a finite sum of heat fluxes:

$$\sqrt{\sum_{i=1}^{n} \lambda(\mathbf{J}_i)} \leq \sum_{i=1}^{n} \sqrt{\lambda(\mathbf{J}_i)}. \tag{3.91}$$

3.5 The microscopic energy density indeterminacy

The problem of the energy density indeterminacy has been introduced in section 3.3.2. It reflects the fact that a microscopic energy density is inherently ill defined. Actually thermodynamics provides us with a well defined thermodynamic local energy density $\epsilon^{th}(\mathbf{r}, t)$ as the energy per unit volume (a well defined thermodynamic property) of subsystems surrounding point $\mathbf{r}$:

$$\epsilon^{th}(\mathbf{r}, t) = \frac{E(V)}{V} \tag{3.92}$$

and there must be a range such that the right member is not dependent on the particular volume chosen.

Every definition of a microscopic energy density $\epsilon(\mathbf{r}, t)$ is good as long as it defines, through the relation:

$$\bar{\epsilon}(\mathbf{r}, t) = \frac{\int_V \epsilon(\mathbf{r}, t)d\mathbf{r}}{V} \tag{3.93}$$

the same thermodynamic energy density, that is the microscopic $\epsilon(\mathbf{r}, t)$ must respect $\bar{\epsilon}(\mathbf{r}, t) = \epsilon^{th}(\mathbf{r}, t)$. Eventually, the only condition that we can require for a reasonable energy density

is that its integral coincides with the well defined total energy apart from surface contributions. Nevertheless two macroscopically equivalent but microscopically inequivalent energy densities $\epsilon_1(\mathbf{r}, t)$ and $\epsilon_2(\mathbf{r}, t)$ lead to the same thermal conductivity, when plugged into the Green-Kubo formula, as we are going to verify. We can focus on the associated heat fluxes $\mathbf{J}_1(t)$ and $\mathbf{J}_2(t)$ and what we want to prove in the next sections can be rewritten in the formalism introduced as $\lambda(\mathbf{J}_1) = \lambda(\mathbf{J}_2)$.

As a consequence of the linear relation between heat flux and energy density the heat flux $\mathbf{J}_{12}(t) \equiv \mathbf{J}_1(t) - \mathbf{J}_2(t)$ is associated to the energy difference $\epsilon_{12}(\mathbf{r}, t) \equiv \epsilon_1(\mathbf{r}, t) - \epsilon_2(\mathbf{r}, t)$ and for our purposes, it is sufficient to prove that $\lambda(\mathbf{J}_{12}) = 0$ thanks to the previous section. To understand better the nature of $\mathbf{J}_{12}(t)$ we study a definite example.

3.5.1 Classical two-body potentials

Argon is well described by classical molecular dynamics using a two-body, isotropic, interaction potential. We will use this model in order to understand in which way the energy density indeterminacy can affect the heat flux definition.

To fix notations, we consider N point particles, of mass m, positions $\mathbf{r}_i$, velocities $\mathbf{v}_i$ and a total energy:

$$E = \sum_i \frac{mv_i^2}{2} + \frac{1}{2} \sum_{i,j \neq i} f(|\mathbf{r}_i - \mathbf{r}_j|), \tag{3.94}$$

where the interaction potential $f(x)$ is considered to be short range. To lighten notations, we do not explicitly write in this section the time dependence of atomic quantities, like particle positions and velocities. As a first step we need to define, starting from the total energy expression, an energy density $\epsilon(\mathbf{r}, t)$. The natural choice consists in defining for an atom with index i an atomic energy ϵ_i, coming up with an energy density of the type:

$$\epsilon(\mathbf{r}, t) = \sum_i \delta(\mathbf{r} - \mathbf{r}_i)\epsilon_i. \tag{3.95}$$

Applying equation (3.78) to this particular case we then find:

$$\mathbf{J}(t) = \frac{\partial}{\partial t} \int \epsilon(\mathbf{r}, t)\mathbf{r}d\mathbf{r} = \frac{d}{dt} \sum_i \epsilon_i \mathbf{r}_i. \tag{3.96}$$

The atomic energies ϵ_i must respect $\sum_i \epsilon_i = E$ and the standard choice consists in dividing into two the interaction energy $f(|\mathbf{r}_i - \mathbf{r}_j|)$ between the two atoms with indexes i and j and assigning one half of the interaction to ϵ_i and the other half to ϵ_j. The total atomic energy
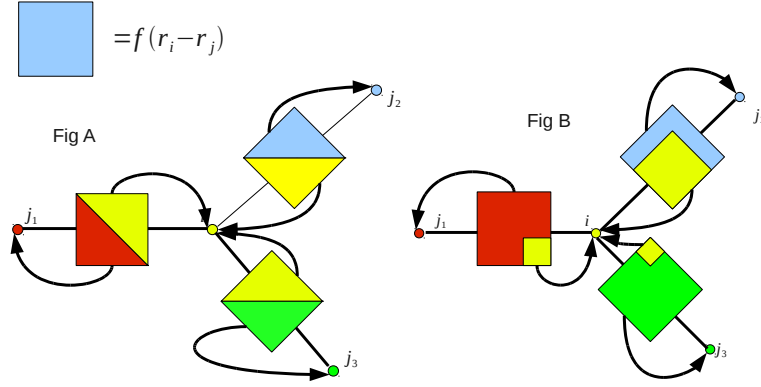
Figure 3.3: Here we pictorially represent the interaction energy between two atoms as a square. To every atom is assigned a color and the amount of interaction energy assigned to the atomic energy of each atom is proportional to the area of the square colored in the same way. Figure *A* reflects the isotropic choice, whereas figure *B* the asymmetric one, described in the text by a matrix μ.

becomes:

$$\epsilon_i = \frac{1}{2}mv_i^2 + \frac{1}{2}\sum_{j\neq i}f(|\mathbf{r}_i - \mathbf{r}_j|). \tag{3.97}$$

A more general situation can be considered, in which the interaction energy is not divided in the same way between to fixed atoms *i* and *j* but favoring one atom over the other. This situation can be realized defining a matrix μ_{ij}. When dividing the interaction energy between two atoms *i* and *j* we will assign $\frac{\mu_{ij}}{2}f(|\mathbf{r}_i - \mathbf{r}_j|)$ to ϵ_i and $\frac{\mu_{ji}}{2}f(|\mathbf{r}_i - \mathbf{r}_j|)$ to ϵ_j. The matrix needs to satisfy the relation $\mu_{ij} + \mu_{ji} = 2$ and the atomic energy now takes the form:

$$\epsilon_i^\gamma = \frac{1}{2}mv_i^2 + \frac{1}{2}\sum_{j\neq i}f(|\mathbf{r}_i - \mathbf{r}_j|)(1 + \gamma_{i,j}), \tag{3.98}$$

where, instead of μ, we defined the matrix $\gamma = 1 + \mu$. This matrix is easier for the purpose of the calculation and turns out to be an antisymmetric matrix. Indeed a partitioning of the total energy has been performed and one can easily verify that the relation $\sum_i \epsilon_i^\gamma = E$ is satisfied. We recover the standard decomposition if $\gamma = 0$.

The two decompositions differ only locally because short range interactions are considered. Nevertheless, they do not lead to the same heat flux. In fact, performing the time derivative

in equation (3.96) we obtain:

$$\mathbf{J}(t) = \sum_i \epsilon_i \mathbf{v}_i + \sum_i [(\mathbf{v}_i \cdot \mathbf{F}_i)\mathbf{r}_i + \frac{1}{2}\sum_{j \neq i} \mu_{i,j} \frac{d}{dt}f(|\mathbf{r}_i - \mathbf{r}_j|)\mathbf{r}_i] \tag{3.99}$$

and the last term can be rewritten:

$$\frac{d}{dt}f(|\mathbf{r}_i - \mathbf{r}_j|) = -\mathbf{F}_{i,j}(\mathbf{v}_i - \mathbf{v}_j). \tag{3.100}$$

Using the relation $\mathbf{F}_i = \sum_{j \neq i} \mathbf{F}_{i,j}$ and the identity:

$$-\frac{1}{2}\sum_{i,j \neq i}[\lambda_{i,j}\mathbf{F}_{i,j} \cdot (\mathbf{v}_i - \mathbf{v}_j)\mathbf{r}_i] = -\frac{1}{2}\sum_{i,j \neq i}[(\mathbf{F}_{i,j} \cdot \mathbf{v}_i)(\lambda_{i,j}\mathbf{r}_i + \lambda_{j,i}\mathbf{r}_j)] \tag{3.101}$$

one obtains the expression:

$$\mathbf{J}(t) = \sum_i \epsilon_i \mathbf{v}_i + \sum_{i,j \neq i}\left[(\mathbf{v}_i \cdot \mathbf{F}_{i,j})\left(\mathbf{r}_i - \frac{\lambda_{i,j}\mathbf{r}_i + \lambda_{j,i}\mathbf{r}_j}{2}\right)\right]. \tag{3.102}$$

This can be rewritten, in order to emphasize how much this result is different from the isotropic one:

$$\mathbf{J}(t) = \mathbf{J}_0(t) + \mathbf{J}_\gamma(t) \tag{3.103}$$

$$\mathbf{J}_0(t) = \sum_i \frac{1}{2}mv_i^2 + \frac{1}{2}\sum_{i,j \neq i}f(|\mathbf{r}_i - \mathbf{r}_j|)\mathbf{v}_i + \sum_{i,j \neq i}\left[(\mathbf{v}_i \cdot \mathbf{F}_{i,j})\frac{(\mathbf{r}_i - \mathbf{r}_j)}{2}\right] \tag{3.104}$$

$$\mathbf{J}_\gamma(t) = \frac{1}{2}\sum_{i,j \neq i}f(|\mathbf{r}_i - \mathbf{r}_j|)\gamma_{i,j}\mathbf{v}_i + \sum_{i,j \neq i}\left[\gamma_{j,i}(\mathbf{v}_i \cdot \mathbf{F}_{i,j})\frac{(\mathbf{r}_i - \mathbf{r}_j)}{2}\right]. \tag{3.105}$$

The first expression $\mathbf{J}_0$ is exactly the one routinely used in Argon simulations, whereas the current $\mathbf{J}_\gamma$ is an additional current intuitively describing a flow of energy due merely to our asymmetric choice of partitioning the interaction energy. Having a closer look at $\mathbf{J}_\gamma(t)$, using the antisymmetric property of the matrix γ, one can recognize that the additional current is a total derivative:

$$\mathbf{J}_\gamma(t) = \dot{\mathbf{P}}(t),$$

$$\mathbf{P}(t) = \frac{1}{4}\left(\sum_{i,j \neq i}f(|\mathbf{r}_i - \mathbf{r}_j|)\gamma_{i,j}(\mathbf{r}_i - \mathbf{r}_j)\right). \tag{3.106}$$

The vector $\mathbf{P}(t)$ has this properties:

1. it is well defined under periodic boundary conditions;

2. it is an extensive quantity and therefore $\frac{\mathbf{P}(t)}{V}$ is bounded;

These are two ways to look at the same property, which deserve some discussion. We say that an observable is well defined under periodic boundary conditions when there is a continuous, global definition, of this observable on the entire phase space given by the simulation cell, to which we apply periodic boundary conditions. This property does not hold for example for the "coordinate" variable x: when reaching the border of the simulation cell, this variable must change discontinuously. This is why, when computing the diffusion of a particle, even in periodic boundary conditions, one can associate arbitrary displacements (even bigger than the simulation cell). The vector $\mathbf{P}$, on the other side, being well defined on the entire phase space is in a way "geometrically limited" and cannot assume arbitrary values: it is limited by a constant. The fact that the vector $\mathbf{P}$ is extensive implies that this constant scales linearly with the volume and therefore $\frac{\mathbf{P}}{V}$ is bounded by the same constant for any dimension of the simulation cell.

As a consequence we have that $\lambda(\mathbf{J}_\gamma) = 0$, as we are going to check in two different ways. In the first method we use that $\mathbf{P}$ is well defined under periodic boundary conditions in order to take out derivatives from the ensemble mean:

$$\lambda(\mathbf{J}_\gamma) = \frac{1}{2V} \int_{-\infty}^{+\infty} dt \langle \dot{\mathbf{P}}(t)\dot{\mathbf{P}}(0)\rangle = \frac{1}{2V} \int_{-\infty}^{+\infty} dt \frac{\partial}{\partial t} \langle \mathbf{P}(t)\dot{\mathbf{P}}(0)\rangle = \tag{3.107}$$

$$= \frac{1}{2V} \langle \mathbf{P}(t)\dot{\mathbf{P}}(0)\rangle \big|_{-\infty}^{+\infty} = \frac{1}{2V}\langle \mathbf{P}\rangle\langle \dot{\mathbf{P}}\rangle - \frac{1}{2V}\langle \mathbf{P}\rangle\langle \dot{\mathbf{P}}\rangle = 0. \tag{3.108}$$

At the same conclusion we arrive applying Einstein identity:

$$\int_0^t \frac{1}{V} \langle \dot{\mathbf{P}}(t)\dot{\mathbf{P}}(0)\rangle \left(1 - \frac{t'}{t}\right) = \frac{1}{t} \frac{\langle (\mathbf{P}(t) - \mathbf{P}(0))^2\rangle}{V}. \tag{3.109}$$

Taking the limit as $t \to \infty$, one sees that, since $\frac{\langle (\mathbf{P}(t)-\mathbf{P}(0))^2\rangle}{V}$ is bounded, the integral is zero. We get also the right volume scaling since the correlation function $\langle AB\rangle$ built from the product of two extensive quantities A and B is extensive as well.

3.5.2 General picture

We have studied for the moment a particular situation. In this section we want to clarify that the features found reflect indeed a general framework and that the Green-Kubo formula is not subject to the energy density indeterminacy problem. It is therefore suitable for applications in a quantum DFT framework.

In the previous section we have shown, by furnishing a direct example, that considering two microscopically inequivalent energy densities $\epsilon_1(\mathbf{r}, t)$ and $\epsilon_2(\mathbf{r}, t)$:

- the associated heat fluxes $\mathbf{J}_1(t)$ and $\mathbf{J}_2(t)$ can be different;

- the correlation functions $\langle \mathbf{J}_1(t)\mathbf{J}_1(0)\rangle$ and $\langle \mathbf{J}_2(t)\mathbf{J}_2(0)\rangle$ can differ as well;

What permitted to verify the equality of the thermal conductivities associated to the different heat fluxes was the fact that they differed by a total derivative vector $\mathbf{P}$, extensive, and limited by a constant scaling linearly with the volume. This is not a coincidence but it is a general property. We know that the two microscopically equivalent energy densities differ only by surface terms. This implies that there must exists a vector $\mathbf{p}(\mathbf{r}, t)$ such that:

$$\epsilon_{12}(\mathbf{r}, t) \equiv \epsilon_2(\mathbf{r}, t) - \epsilon_1(\mathbf{r}, t) = -\nabla \cdot \mathbf{p}(\mathbf{r}, t), \tag{3.110}$$

which can be considered as a relation defining the vector $\mathbf{p}(\mathbf{r}, t)$. Indeed, by Gauss theorem, only surface terms affect the integral of $\epsilon_2(\mathbf{r}, t) - \epsilon_1(\mathbf{r}, t)$ inside a volume V, making the energy per unit volume well defined:

$$\int_V \epsilon_{12}(\mathbf{r}, t) = -\oint \mathbf{p}(\mathbf{r}, t) \cdot d\mathbf{S}. \tag{3.111}$$

From the latter we conclude that the vector $\mathbf{p}(\mathbf{r}, t)$ must fluctuate remaining limited during the dynamics, in order to describe, after application of Gauss theorem, a real surface contribution. Deriving with respect to time equation 3.110 we recognize that $\dot{\mathbf{p}}(\mathbf{r}, t)$ is the current density associated to the energy difference $\epsilon_{12}(\mathbf{r}, t)$:

$$\dot{\epsilon}_{12}(\mathbf{r}, t) = -\nabla \cdot \dot{\mathbf{p}}(\mathbf{r}, t) = -\nabla \cdot \mathbf{j}_{12}(\mathbf{r}, t). \tag{3.112}$$

Relation (3.110) is much similar to the local energy conservation equation, but is has a completely different physical meaning. The total energy difference ΔE_{12} passing across a surface σ in the time interval from 0 to t is:

$$\Delta E_{12} = -\oint_\sigma \left(\int_0^t \mathbf{j}_{12}(\mathbf{r}, t')dt' \right) \cdot d\mathbf{S} \tag{3.113}$$

$$= -\oint_\sigma \left(\mathbf{p}(\mathbf{r}, t) - \mathbf{p}(\mathbf{r}, 0) \right) \cdot d\mathbf{S}. \tag{3.114}$$

Therefore the flux of energy is limited by the maximum fluctuations of the vector $\mathbf{p}$, forcing $\mathbf{j}_{12}(\mathbf{r}, t)$ to change rapidly direction: energy goes back and forth and there is no net flux. The Green-Kubo formula is aware of this fact. When we insert the energy density ϵ_{12} into equation (3.78) we find:

$$\mathbf{J}(t) = \dot{\mathbf{P}}(t) \tag{3.115}$$

$$\mathbf{P}(t) = \int_V \mathbf{p}(\mathbf{r}, t)d\mathbf{r} \tag{3.116}$$

and as a consequence these processes cannot lead to thermal conduction, following exactly the same calculations of the previous paragraph. This is what we needed to confirm that the Green-Kubo formula is not subject to the microscopic energy density indeterminacy problem.

3.5.3 A different viewpoint: Mori's memory function formalism

We now propose a different proof of the independence of the thermal conductivity coefficient given by Green-Kubo formula upon the microscopic choice of the energy density, using the memory function formalism. This proof is less transparent then the one we have previously presented because it deals only with reciprocal space quantities and relies upon a more sophisticated theory [40] but it leads to the same conclusions. Our analysis will be inspired by the study of the magnetization autocorrelation function as described in [34], to which we refer for details and notations of this section.

We consider in this section $\epsilon = \epsilon_{12}$, the energy density difference between two macroscopically equivalent energy densities. It is sufficient to prove that this energy density does not lead to thermal conductivity phenomena (section 3.4).

According to the memory function formalism the equation of motion for the energy autocorrelation function can be written:

$$C_{\epsilon\epsilon}(\mathbf{k}, z) = \frac{i}{z + i\frac{\sigma(\mathbf{k},z)}{\langle\epsilon(\mathbf{k})|\epsilon(\mathbf{k}k)\rangle}}\langle\epsilon(\mathbf{k})|\epsilon(\mathbf{k})\rangle, \tag{3.117}$$

where the brackets, as it is common in Mori's memory function formalism, stand for the second scalar product introduced with formulas 3.10. The self energy sigma $\sigma(\mathbf{k}, z)$ is so defined:

$$\sigma(\mathbf{k}, z) = \langle\dot{\epsilon}(\mathbf{k})|Q\frac{i}{z - QLQ}Q|\dot{\epsilon}(\mathbf{k})\rangle \tag{3.118}$$

$Q = 1 - P$ is a projector in the Hilbert space of observables. It is built from the elementary projectors $P(\mathbf{k})$:

$$P(\mathbf{k}) = \frac{|\epsilon(\mathbf{k})\rangle\langle\epsilon(\mathbf{k})|}{\langle\epsilon(\mathbf{k})|\epsilon(\mathbf{k})\rangle} \tag{3.119}$$

in this way:

$$P = \frac{V}{(2\pi)^3}\int d\mathbf{k}P(\mathbf{k}) \tag{3.120}$$

(these are the exact analogous of the projectors considered in the study of magnetization in [34]). Till now no hypothesis has been done, apart from isotropy. Two ingredients must be still considered. The first one is energy conservation, which has a consequence on the analytical behavior of the self energy:

$$\sigma(\mathbf{k}, z) = k_i k_j d_{ij}(\mathbf{k}, z)$$

$$d_{ij}(\mathbf{k}, z) = \langle j_i(\mathbf{k})|Q\frac{i}{z - QLQ}Q|j_j(\mathbf{k})\rangle \tag{3.121}$$

Using isotropy as well $\sigma(\mathbf{k}, z) = \frac{k^2}{3} Tr(d(\mathbf{k}, z))$. Now, since the current $\mathbf{j}$ is not a conserved quantity, a discussion exactly analogous to the one for the autocorrelation function of the magnetization [34] permits to conclude that d is regular as $\mathbf{k} \to 0$ and as $z \to 0$.

The second ingredient is applying condition (3.110). We find in an isotropic system like the one we are considering now:

$$\langle \epsilon(\mathbf{k}) | \epsilon(\mathbf{k}) \rangle = \frac{k^2}{3} \langle \mathbf{p}(\mathbf{k}) | \mathbf{p}(\mathbf{k}) \rangle \tag{3.122}$$

with $\langle \mathbf{p}(\mathbf{k}) | \mathbf{p}(\mathbf{k}) \rangle$ regular in $k = 0$.

Substituting these two ingredients one obtains:

$$C_{\epsilon\epsilon}(\mathbf{k}, z) \sim \frac{ik^2 P}{z + i\frac{D}{P}} \tag{3.123}$$

where it was defined:

$$D = \lim_{z \to 0} \frac{1}{3} Tr(d(\mathbf{k}, z)) \tag{3.124}$$

$$P = \lim_{k \to 0} \frac{1}{3} \langle \mathbf{p}(\mathbf{k}) | \mathbf{p}(\mathbf{k}) \rangle \tag{3.125}$$

Now applying equation (A.15):

$$\chi''_{\epsilon\epsilon}(\mathbf{k}, \omega) = \frac{k^2 \omega D}{\omega^2 + \frac{D^2}{P^2}} \tag{3.126}$$

and taking the limit:

$$\lim_{\omega \to 0} \lim_{k \to 0} \frac{\omega}{k^2} \chi''_{\epsilon\epsilon}(\mathbf{k}, \omega) = \lim_{\omega \to 0} \lim_{k \to 0} \frac{\omega}{k^2} \frac{k^2 \omega D}{\left(\omega^2 + \frac{D^2}{P^2}\right)} = 0 \tag{3.127}$$

That is what we wanted to prove.

Heat transport in Density-Functional theory

The Green-Kubo formalism developed in the previous chapter can be applied to the computation of lattice thermal conductivity under the Born-Oppenheimer approximation [44]. According to this approximation, ions are considered as classical particles subject to a complicated many body potential $E(\boldsymbol{R})$:

$$E(\boldsymbol{R}) = \min_{\phi} \langle \phi | H_{BO}(\boldsymbol{R}) | \phi \rangle \tag{4.1}$$

$$H_{BO}(\boldsymbol{R}) = -\frac{\hbar^2}{2m} \sum_i \frac{\partial}{\partial^2 \boldsymbol{r}_i} + \frac{e^2}{2} \sum_{i \neq j} \frac{1}{|\boldsymbol{r}_i - \boldsymbol{r}_j|} + \frac{e^2}{2} \sum_{I \neq J} \frac{1}{|\boldsymbol{R}_I - \boldsymbol{R}_J|} - \sum_{i,I} \frac{Z_i e^2}{|\boldsymbol{r}_I - \boldsymbol{R}_i|}, \tag{4.2}$$

where $\boldsymbol{R}_I$ are ions positions, $\boldsymbol{r}_i$ electronic coordinates and e is the electron charge. The minimum is computed over all normalized electronic wavefunctions . Electrons are therefore forced to follow ion motion adiabatically, remaining always in their ground state, at zero temperature. This approximation applies well in the case of insulators, in which we are interested, where a finite gap separates the valence band from excited states.

Density functional theory (DFT), introduced by Hohenbergy and Kohn [45] and solved under the Kohn-Sham scheme [46], provides an efficient way to compute the Born Oppenheimer energy surface $E(\boldsymbol{R})$, once an approximation for the exchange correlation functional, able to describe the physics of the system, is provided. In the first section of this chapter we derive in detail, from the explicit expression of the DFT total energy in terms of Kohn-Sham orbitals, a DFT energy density and an ab-initio adiabatic energy current, well defined under periodic boundary conditions (PBC). It is the exact analog, for energy transport phenomena, of the adiabatic particle current derived by D.J. Thouless [47]. In the second section the implementation

methods needed for computer simulations are discussed.

4.1   Derivation

We outlined in section 3.3.2 of the previous chapter the procedure that needs to be followed in order to derive an explicit expression for an adiabatic heat flux current. We start with the standard DFT expression of the total energy in terms of the Kohn-Sham eigenfunctions and density [48]:

$$E_{DFT} = \frac{1}{2} \sum_I M_I V_I^2 + \frac{1}{2} \sum_{I \neq J} \frac{e^2 Z_I Z_J}{|\mathbf{R}_I - \mathbf{R}_J|}$$
$$+ \sum_n \varepsilon_n - \frac{1}{2} \int \frac{n(\mathbf{r}) n(\mathbf{r}')}{|\mathbf{r} - \mathbf{r}'|} d\mathbf{r} d\mathbf{r}' + \int \left(\epsilon_{XC}[n](\mathbf{r}) - \mu_{XC}[n](\mathbf{r}) \right) n(\mathbf{r}) d\mathbf{r}, \quad (4.3)$$

,where:

$$\int \epsilon_{XC}[n](\mathbf{r}) n(\mathbf{r}) d\mathbf{r} \doteq E_{XC}[n], \quad (4.4)$$

$$\mu_{XC}(\mathbf{r}) \doteq \frac{\delta E_{XC}}{\delta n(\mathbf{r})}$$

$$= \epsilon_{XC}(\mathbf{r}) + \int \frac{\delta \epsilon_{XC}(\mathbf{r}')}{\delta n(\mathbf{r})} n(\mathbf{r}') d\mathbf{r}'. \quad (4.5)$$

The expression of the functional $\epsilon_{XC}[n](\mathbf{r})$ depends on the actual form of the exchange correlation potential used. We derive formulas for the local density approximation (LDA) and the generalized gradient approximation (GGA).

The total energy can be readily written as the integral of a DFT energy density [49]:

$$E_{DFT} = \int e_{DFT}(\mathbf{r}) d\mathbf{r}, \quad (4.6)$$

$$e_{DFT}(\mathbf{r}) = e_{el}(\mathbf{r}) + e_n(\mathbf{r}), \quad (4.7)$$

where:

$$e_{el}(\mathbf{r}) = \sum_n \phi_n^*(\mathbf{r}) \left(\hat{H}_{KS} \phi_n(\mathbf{r}) \right) - \frac{1}{2} n(\mathbf{r}) v_H(\mathbf{r}) + \left(\epsilon_{XC}(\mathbf{r}) - \mu_{XC}(\mathbf{r}) \right) n(\mathbf{r}),$$

$$e_n(\mathbf{r}) = \sum_I \delta(\mathbf{r} - \mathbf{R}_I) \left(\frac{1}{2} M_I V_I^2 + w_I \right),$$

$$w_I = \frac{1}{2} \sum_{J, J \neq I} \frac{e^2 Z_I Z_J}{|\mathbf{R}_I - \mathbf{R}_J|}. \quad (4.8)$$

To perform the computation we replaced ε_n with $\langle \phi_n | H_{KS} | \phi_n \rangle$, where H_{KS} is the self consistent Kohn-Sham Hamiltonian.

As discussed in chapter 2, the energy density $e_{DFT}(\mathbf{r})$ is not uniquely defined. Nevertheless the final result, when used in combination with the Green-Kubo formula, does not depend on the particular density chosen as long as it defines through its spatial integral a good thermodynamic energy density.

In order to apply the Green-Kubo formula, as discussed in section 3.3.2, we need to obtain explicit formulas for the zero wavelength component of the energy current. The remaining calculations are entirely devoted to this task.

Before proceeding we make two important comments:

1. We observe that equations (4.8) do not contain information about the fact that the energy density is a conserved quantity or, in other words, that it satisfies a local continuity equation. This is a dynamical information, as is concerned about time derivatives of the degrees of freedom of the system. Eventually, these derivatives are ruled by Hamilton equations and this is why we expect them to play a fundamental role;

2. We proceed by plugging formally the time derivative of the energy density into the fundamental equation derived in section 3.3.2. which we report here for reference:

$$\mathbf{J}(t) = \int_\Omega \dot{e}(\mathbf{r}, t)\mathbf{r}d\mathbf{r} \tag{4.9}$$

,where Ω is the volume of the system. It coincides in our calculations with the volume of the supercell and therefore we will refer to it with symbol Ω rather than with the more common V. In order to simplify formulas, we will not write any longer the time dependence of the densities and of the currents, as we did in equation 4.9. This explicit equation for the zero wavevector component of the energy current is not well defined in PBC, essentially for the same reason that polarization is not a well defined quantity [50]. Therefore surface, cell dependent, terms need to be taken out during the calculation. Actually, surface contributions,even when not cell dependent, give no contribution to the heat current thanks to the thermodynamic limit entering the Green-Kubo relation and can be freely taken out during the computation.

Again local energy conservation plays a role in formula (4.9). It is only because of the conservation equation that we will be able to obtain an heat current scaling like the volume Ω and not like $\Omega^{\frac{4}{3}}$ as a naive analysis of equation (4.9) would suggest.
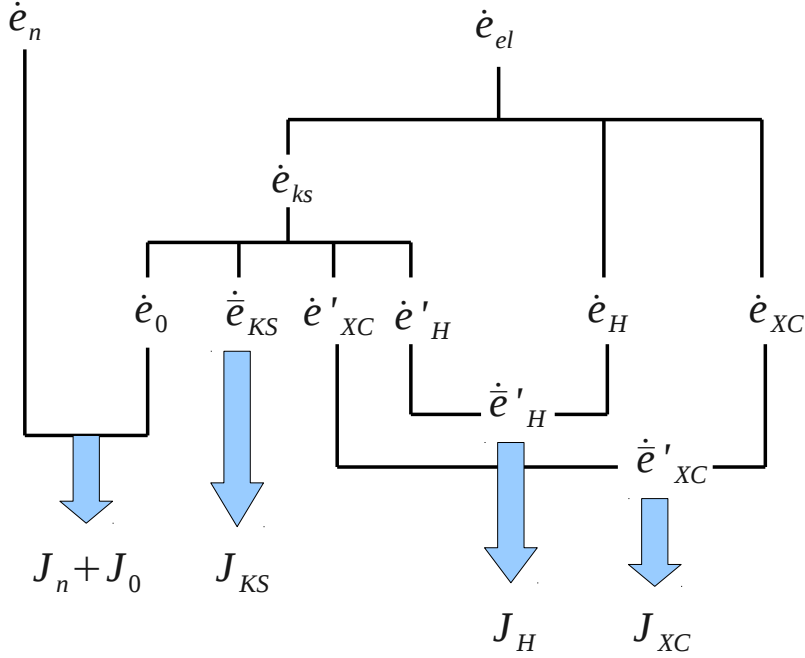
Figure 4.1: Evolution of the flow of the calculation

While feeding the evolution equations into the description we will as a first step explicit the time derivative of the energy density and divide it into several contributions. As a second step, we will combine these contributions and associate to them distinct energy currents. The flow of the computation can be followed through figure 4.1, where the decomposition is made explicit. The final heat flux will be built from the sum of five partial currents.

We begin performing the time derivative of the electronic energy density $e_{el}(\mathbf{r})$ and define explicitly the first terms present in figure 4.1:

$$\dot{e}_{el}(\mathbf{r}) = \dot{e}_{KS}(\mathbf{r}) + \dot{e}_H(\mathbf{r}) + \dot{e}_{XC}(\mathbf{r}), \tag{4.10}$$

where $\dot{e}_H$ and $\dot{e}_{XC}$ are the time derivatives of the last two terms in the first of equations (4.8):

$$\dot{e}_H(\mathbf{r}) = -\frac{1}{2}\left(n(\mathbf{r})\dot{v}_H(\mathbf{r}) + \dot{n}(\mathbf{r})v_H(\mathbf{r})\right) \tag{4.11}$$

$$\dot{e}_{XC}(\mathbf{r}) = \left(\epsilon_{XC}(\mathbf{r}) - \mu_{XC}(\mathbf{r})\right)\dot{n}(\mathbf{r}) + \left(\dot{\epsilon}_{XC}(\mathbf{r}) - \dot{\mu}_{XC}(\mathbf{r})\right)n(\mathbf{r}). \tag{4.12}$$

$\dot{e}_{KS}$ the derivative of the first,

$$\dot{e}_{KS}(\mathbf{r}) = \frac{d}{dt} \sum_n \left(\phi_n^*(\mathbf{r}) \hat{H}_{KS} \phi_n(\mathbf{r}) + \phi_n^*(\mathbf{r}) \hat{H}_{KS} \phi_n(\mathbf{r}) \right)$$
$$= \sum_n \left(\dot{\phi}_n^*(\mathbf{r}) \hat{H}_{KS} \phi_n(\mathbf{r}) + \phi_n^*(\mathbf{r}) \hat{H}_{KS} \dot{\phi}_n(\mathbf{r}) \right) + \sum_n \left(\phi_n^*(\mathbf{r}) \dot{\hat{H}}_{KS} \phi_n(\mathbf{r}) \right)$$
$$= \ddot{e}_{KS}(\mathbf{r}) + \dot{e}_0(\mathbf{r}) + \dot{e}_H'(\mathbf{r}) + \dot{e}_{XC}'(\mathbf{r}). \tag{4.13}$$

The first term in the above equation is defined as:

$$\ddot{e}_{KS}(\mathbf{r}) = \sum_n \left(\dot{\phi}_n^*(\mathbf{r}) \hat{H}_{KS} \phi_n(\mathbf{r}) + \phi_n^*(\mathbf{r}) \hat{H}_{KS} \dot{\phi}_n(\mathbf{r}) \right), \tag{4.14}$$

whereas the last three come from the time derivative of the KS Hamiltonian in eq. (4.13):

$$\dot{e}_0(\mathbf{r}) = \sum_n \phi_n^*(\mathbf{r}) \left(\dot{\hat{v}}_0 \phi_n(\mathbf{r}) \right) \tag{4.15}$$

$$\dot{e}_H'(\mathbf{r}) = \dot{v}_H(\mathbf{r}) n(\mathbf{r}) \tag{4.16}$$

$$\dot{e}_{XC}'(\mathbf{r}) = \dot{\mu}_{XC}(\mathbf{r}) n(\mathbf{r}). \tag{4.17}$$

4.1.1 Hartree current $\mathbf{J}_H$

Adding $\dot{e}_H'$ and $\dot{e}_H$ the first current, called hear *Hartree current*, is readily obtained:

$$\dot{e}_H(\mathbf{r}) = \dot{e}_H(\mathbf{r}) + \dot{e}_H'(\mathbf{r}) =$$
$$= \frac{1}{2} \left(n(\mathbf{r}) \dot{v}_H(\mathbf{r}) - \dot{n}(\mathbf{r}) v_H(\mathbf{r}) \right)$$
$$= -\frac{1}{8\pi e^2} \left(\nabla^2 v_H \dot{v}_H(\mathbf{r}) - \nabla^2 \dot{v}_H v_H(\mathbf{r}) \right) = \tag{4.18}$$
$$= -\frac{1}{8\pi e^2} \nabla \cdot \left(\nabla v_H(\mathbf{r}) \dot{v}_H(\mathbf{r}) - \nabla \dot{v}_H(\mathbf{r}) v_H(\mathbf{r}) \right) = \tag{4.19}$$
$$= -\frac{1}{8\pi e^2} \nabla \cdot \mathbf{j}_h(\mathbf{r}) \tag{4.20}$$

Where an intermediate current $\mathbf{j}_h(\mathbf{r})$ has been defined:

$$\mathbf{j}_h(\mathbf{r}) = \nabla v_H(\mathbf{r}) \dot{v}_H(\mathbf{r}) - \nabla \dot{v}_H(\mathbf{r}) v_H(\mathbf{r}) \tag{4.21}$$

From here we can get the value of the *Hartree current*:

$$\mathbf{J}_H = \int_\Omega \dot{e}_H(\mathbf{r}) r_a d\mathbf{r} = -\frac{1}{8\pi e^2} \int_\Omega \partial_b j_{h,b} r_a d\mathbf{r} = \tag{4.22}$$
$$= \frac{1}{8\pi e^2} \int_\Omega \mathbf{j}_h d\mathbf{r} \tag{4.23}$$

and therefore we end up with the final expression:

$$\mathbf{J}_H = \frac{1}{8\pi e^2} \int_\Omega \nabla v_H(\mathbf{r})\dot{v}_H(\mathbf{r}) - \nabla \dot{v}_H(\mathbf{r})v_H(\mathbf{r})d\mathbf{r} = \tag{4.24}$$

$$= \frac{1}{4\pi e^2} \int_\Omega \nabla v_H(\mathbf{r})\dot{v}_H(\mathbf{r})d\mathbf{r} \tag{4.25}$$

4.1.2 Exchange-correlation current $\mathbf{J}_{XC}$

As for the XC terms, we define:

$$\dot{\bar{e}}_{XC}(\mathbf{r}) = \dot{e}_{XC}(\mathbf{r}) + \dot{e}'_{XC}(\mathbf{r})$$
$$= (\epsilon_{XC}(\mathbf{r}) - \mu_{XC}(\mathbf{r}))\, \dot{n}(\mathbf{r}) + \dot{\epsilon}_{XC}(\mathbf{r})n(\mathbf{r}). \tag{4.26}$$

By inserting the relations:

$$\epsilon_{XC}(\mathbf{r}) - \mu_{XC}(\mathbf{r}) \;=\; -\int \frac{\delta\epsilon_{XC}(\mathbf{r}')}{\delta n(\mathbf{r})}n(\mathbf{r}')d\mathbf{r}', \tag{4.27}$$

(see eq. 4.5) and

$$\dot{\epsilon}_{XC}(\mathbf{r}) = \int \frac{\delta\epsilon_{XC}(\mathbf{r})}{\delta n(\mathbf{r}')}\dot{n}(\mathbf{r}')d\mathbf{r}' \tag{4.28}$$

into eq. (4.26), we obtain:

$$\dot{\bar{e}}_{XC}(\mathbf{r}) = n(\mathbf{r})\int \frac{\delta\epsilon_{XC}(\mathbf{r})}{\delta n(\mathbf{r}')}\dot{n}(\mathbf{r}')d\mathbf{r}' - \dot{n}(\mathbf{r})\int \frac{\delta\epsilon_{XC}(\mathbf{r}')}{\delta n(\mathbf{r})}n(\mathbf{r}')d\mathbf{r}'. \tag{4.29}$$

In the LDA, one has $\frac{\delta\epsilon_{LDA}(\mathbf{r})}{\delta n(\mathbf{r}')} = \epsilon'_{LDA}\big(n(\mathbf{r})\big)\delta(\mathbf{r} - \mathbf{r}')$, where $\epsilon'_{LDA}(n) = \frac{d\epsilon_{LDA}(n)}{dn}$. In this case one has

$$\dot{\bar{e}}_{LDA}(\mathbf{r}) \equiv 0. \tag{4.30}$$

$$\mathbf{J}_{XC}^{LDA} = 0 \tag{4.31}$$

We can perform a similar calculation also for the PBE exchange correlation functional. In order to compute the first moment of $\dot{\bar{e}}_{XC}(\mathbf{r})$ in the GGA case, let us start from eq. (4.29) and write its first moment in a form that is manifestly boundary-insensitive:

$$\bar{\mathbf{J}}_{XC} \;=\; \int \dot{\bar{e}}_{XC}(\mathbf{r})\mathbf{r}d\mathbf{r}$$
$$= \int \mathbf{r}\left[n(\mathbf{r})\frac{\delta\epsilon_{XC}(\mathbf{r})}{\delta n(\mathbf{r}')}\dot{n}(\mathbf{r}')d\mathbf{r}' - \dot{n}(\mathbf{r})\int \frac{\delta\epsilon_{XC}(\mathbf{r}')}{\delta n(\mathbf{r})}n(\mathbf{r}')\right]d\mathbf{r}d\mathbf{r}' \tag{4.32}$$
$$= \int (\mathbf{r} - \mathbf{r}')n(\mathbf{r})\dot{n}(\mathbf{r}')\frac{\delta\epsilon_{XC}(\mathbf{r})}{\delta n(\mathbf{r}')}d\mathbf{r}d\mathbf{r}'. \tag{4.33}$$

In the GGA one has:

$$
\begin{aligned}
\epsilon_{GGA}[n](\mathbf{r}) &= \epsilon_{GGA}\big(n(\mathbf{r}), \nabla n(\mathbf{r})\big) \\
\frac{\delta \epsilon_{GGA}(\mathbf{r})}{\delta n(\mathbf{r}')} &= \epsilon'_{GGA}(\mathbf{r})\delta(\mathbf{r} - \mathbf{r}') + \sum_{\beta} \epsilon^{\beta}_{GGA}(\mathbf{r})\nabla_{\beta}\delta(\mathbf{r} - \mathbf{r}'),
\end{aligned}
\tag{4.34}
$$

where

$$
\begin{aligned}
\epsilon'_{GGA}(\mathbf{r}) &= \frac{\partial \epsilon_{GGA}(n, \nabla n)}{\partial n}(\mathbf{r}) \\
\epsilon^{\beta}_{GGA}(\mathbf{r}) &= \frac{\partial \epsilon_{GGA}(n, \nabla n)}{\partial(\nabla_{\beta} n)}(\mathbf{r}) \\
\int f(\mathbf{r}')\nabla_{\beta}\delta(\mathbf{r} - \mathbf{r}')d\mathbf{r}' &= \nabla_{\beta} f(\mathbf{r}).
\end{aligned}
$$

By inserting eq. (4.34) into eq. (4.33), one sees that the term with the derivative with respect to the local density vanishes, in agreement with eq. (4.30). The gradient term gives:

$$
\begin{aligned}
\mathbf{J}^{PBE}_{XC,\alpha} &= \sum_{\beta} \int (\mathbf{r} - \mathbf{r}')_{\alpha} n(\mathbf{r})\dot{n}(\mathbf{r}')\epsilon^{\beta}_{GGA}(\mathbf{r})\nabla_{\beta}\delta(\mathbf{r} - \mathbf{r}')d\mathbf{r}d\mathbf{r}' \\
&= \sum_{\beta} \int d\mathbf{r}\, n(\mathbf{r})\epsilon^{\beta}_{GGA}(\mathbf{r})\left[\nabla'_{\beta}(\mathbf{r} - \mathbf{r}')_{\alpha}\dot{n}(\mathbf{r}')\right]_{\mathbf{r}'=\mathbf{r}} \\
&= \sum_{\beta} \int d\mathbf{r}\, n(\mathbf{r})\epsilon^{\beta}_{GGA}(\mathbf{r})(-\delta_{\alpha\beta})\dot{n}(\mathbf{r}) \\
&= -\int n(\mathbf{r})\dot{n}(\mathbf{r})\epsilon^{\alpha}_{GGA}(\mathbf{r})d\mathbf{r},
\end{aligned}
\tag{4.35}
$$

4.1.3 Kohn-Sham current $\mathbf{J}_{KS}$

The macroscopic current associated with $\dot{\bar{e}}_{KS}(\mathbf{r})$, eq. (4.14), is:

$$
\begin{aligned}
\mathbf{J}_{KS} &= \int \dot{\bar{e}}_{KS}(\mathbf{r})\mathbf{r}d\mathbf{r} \\
&= \sum_{v=1}^{N_v} \left(\langle \phi_v | \mathbf{r}H_{KS} | \dot{\phi}_v \rangle + \langle \dot{\phi}_v | \mathbf{r}H_{KS} | \phi_v \rangle\right).
\end{aligned}
\tag{4.36}
$$

This can be rewritten:

$$
\mathbf{J}_{KS} = \frac{\partial}{\partial t'} \sum_{v} \langle \phi_v(t') | \mathbf{r}H_{KS}(t) | \phi_v(t') \rangle |_{t'=t},
\tag{4.37}
$$

thus making it apparent its gauge invariance properties, thanks to the appearance of a trace over the base manifold. The only gauge invariant part of $|\dot{\phi}_v\rangle$ is its component onto the conduction manifold (the only present in the gauge of parallel transport [51]) and therefore we can replace all wavefunctions with their projections onto the conduction band. To make this point more explicit we check it in the gauge where all orbitals at time t are real and using the

connection given by first order perturbation theory [52]. Decomposing the operator into its Hermitian and anti-Hermitian part:

$$\mathbf{J}_{KS} = \frac{1}{2} \left(\frac{\partial}{\partial t'} \sum_v \langle \phi_v(t') | \{\mathbf{r}, H(t)\} | \phi_v(t') \rangle |_{t'=t} + \right.$$
(4.38)

$$\left. \frac{\partial}{\partial t'} \sum_v \langle \phi_v(t') | [\mathbf{r}, H(t)] | \phi_v(t') \rangle |_{t'=t} \right)$$
(4.39)

The expectation value of the anti-hermitian part is zero, because the wavefunctions are chosen real. Therefore:

$$\mathbf{J}_{KS} = \frac{1}{2} \left(\frac{\partial}{\partial t'} \sum_v \langle \phi_v(t') | \{\mathbf{r}, H(t)\} | \phi_v(t') \rangle |_{t'=t} \right) =$$
(4.40)

$$\mathcal{R} \sum_v \langle \phi_v(t) | \{\mathbf{r}, H(t)\} | \dot{\phi}_v(t) \rangle$$
(4.41)

Using the connection given by first order perturbation theory:

$$|\dot{\phi}_v\rangle = \sum_{k \neq v} |\phi_k\rangle \frac{\langle \phi_k | \dot{H} | \phi_v \rangle}{\epsilon_k - \epsilon_v},$$
(4.42)

we get:

$$\mathbf{J}_{KS} = \mathcal{R} \sum_v \langle \phi_v(t) | \{\mathbf{r}, H(t)\} | \dot{\phi}_v(t) \rangle =$$
(4.43)

$$= \mathcal{R} \sum_v \sum_{k \neq v} \frac{\langle \phi_v | \{\mathbf{r}, H\} | \phi_k \rangle \langle \phi_k | \dot{H} | \phi_v \rangle}{\epsilon_k - \epsilon_v} =$$
(4.44)

$$= \mathcal{R} \sum_v \sum_{k \in C} \frac{\langle \phi_v | \{\mathbf{r}, H\} | \phi_k \rangle \langle \phi_k | \dot{H} | \phi_v \rangle}{\epsilon_k - \epsilon_v}.$$
(4.45)

where the last step follows because the sum is antisymmetric under k, v exchange and therefore only the conduction band contribution survives. Indicating with P_v as the projector onto the valence band and $P_c = 1 - P_v$ the projector onto the conduction band, we can for convenience define the following vectors:

$$\bar{\phi}_v^c = P_c \mathbf{r} | \phi_v \rangle$$
(4.46)

$$\dot{\phi}_v^c = P_c | \dot{\phi}_v \rangle,$$
(4.47)

which are both well defined in PBC and whose computation may be performed using density functional perturbation theory techniques [7]. With these notations:

$$\mathbf{J}_{KS} = \mathcal{R} \sum_v \langle \phi_v(t) | \{\mathbf{r}, H(t)\} | \dot{\phi}_v^c(t) \rangle =$$
(4.48)

$$= \mathcal{R} \sum_v \langle \phi_v(t) | \mathbf{r} H(t) | \dot{\phi}_v^c(t) \rangle + \mathcal{R} \sum_v \epsilon_v \langle \phi_v(t) | \mathbf{r} | \dot{\phi}_v^c(t) \rangle.$$
(4.49)

Since H does not mix conduction and valence band:

$$\mathbf{J}_{KS} = \mathcal{R}\sum_v \langle \bar{\phi}_v^c(t)|H(t)|\dot{\phi}_v^c\rangle + \mathcal{R}\sum_v \epsilon_v \langle \bar{\phi}_v^c(t)|\dot{\phi}_v^c(t)\rangle = \tag{4.50}$$

$$= \mathcal{R}\sum_v \langle \bar{\phi}_v^c|H + \epsilon_v|\dot{\phi}_v^c\rangle, \tag{4.51}$$

which is the final expression of the Kohn-Sham current.

The current (4.51) is not manifestly invariant with respect to the arbitrary choice of the zero of the one-electron energy levels: if this zero is shifted by a quantity Δ, the current gets modified by $2\Delta \sum_v \langle \bar{\phi}_v^c|\dot{\phi}_v^c\rangle$ a term proportional to the zero component of the adiabatic electronic current, defined by the conservation equation $\partial_a J_a^{el}(\mathbf{r}) = \sum_v \phi_v^*(\mathbf{r})\phi_v(\mathbf{r})$ and introduced in reference [47]. It can be derived by the same techniques used in this chapter:

$$\mathbf{J}^{el} = \int_\Omega \dot{n}(\mathbf{r})\mathbf{r}d\mathbf{r} = \sum_v <\dot{\phi}_v|\mathbf{r}|\phi_v> + <\phi_v|\mathbf{r}|\dot{\phi}_v>, \tag{4.52}$$

and from here an analysis analogous to the one already performed leads to the desired result. The electronic current is the difference between the total charge current and its ionic component: the first is by definition non-diffusive in insulators, while the second vanishes in the center of mass of mono-atomic systems (to which we restrict our analysis for the time being), because of momentum conservation. We conclude that the electronic current is non-diffusive, thus not contributing to the heat conductivity of insulators, and that the current is independent of the reference chosen for the energy levels.

4.1.4 Zero current $\mathbf{J}_0$ and ionic current $\mathbf{J}_n$

The macroscopic current associated with $\dot{e}_0'(\mathbf{r})$ is:

$$\int_\Omega \mathbf{r}\dot{e}_0(\mathbf{r})d\mathbf{r} = \sum_n \langle \phi_n|\mathbf{r}\hat{\dot{v}}_0|\phi_n\rangle$$

$$= \sum_n \sum_I \left\langle \phi_n \left|\mathbf{r}\left(\mathbf{V}_I \cdot \frac{\partial \hat{v}_0}{\partial \mathbf{R}_I}\right)\right| \phi_n\right\rangle \tag{4.53}$$

$$= \mathbf{J}_0 + \mathbf{J}_0' \tag{4.54}$$

$$\mathbf{J}_0 = \sum_I \sum_n \left\langle \phi_n \left|(\mathbf{r}-\mathbf{R}_I)\left(\mathbf{V}_I \cdot \frac{\partial \hat{v}_0}{\partial \mathbf{R}_I}\right)\right| \phi_n\right\rangle \tag{4.55}$$

$$\mathbf{J}_0' = \sum_I \sum_n \mathbf{R}_I \left(\mathbf{V}_I \cdot \left\langle \phi_n \left|\frac{\partial \hat{v}_0}{\partial \mathbf{R}_I}\right| \phi_n\right\rangle\right)$$

$$= -\sum_I \mathbf{R}_I \left(\mathbf{V}_I \cdot \mathbf{F}_I^{el}\right), \tag{4.56}$$

where $\mathbf{F}_I^{el}$, according to the Hellmann-Feynman theorem [48][7], is the electronic contribution to the force acting on the I-th atom. According to eq. (4.55) $\mathbf{J}_0$ is well defined in PBC, whereas $\mathbf{J}_0'$ is not. The latter, however, will cancel a similar term appearing in the ionic contribution to the current.

The ionic contribution to the current can be calculated along similar lines as in the classical case [53]. Performing the computation:

$$\int \mathbf{r}\dot{e}_n(\mathbf{r})d\mathbf{r} = \tag{4.57}$$

$$\sum_I \mathbf{V}_I \left(\frac{1}{2}M_I V_I^2 + w_I \right) + \sum_I \mathbf{R}_I \left(\dot{\mathbf{V}}_I \cdot \frac{\partial}{\partial \mathbf{V}_I} \frac{1}{2}M_I V_I^2 + \sum_L \mathbf{V}_L \cdot \frac{\partial w_I}{\partial \mathbf{R}_L} \right). \tag{4.58}$$

Using the equations of motion, $M_I \dot{\mathbf{V}}_I = \mathbf{F}_I$, eq. (4.58) we can write:

$$\int \mathbf{r}\dot{e}_n(\mathbf{r})d\mathbf{r} = \mathbf{J}_n' + \mathbf{J}_n'' + \mathbf{J}_n''' \tag{4.59}$$

where:

$$\mathbf{J}_n' = \sum_I \mathbf{V}_I \left(\frac{1}{2}M_I V_I^2 + w_I \right) \tag{4.60}$$

$$\mathbf{J}_n'' = \sum_I \mathbf{R}_I (\mathbf{F}_I \cdot \mathbf{V}_I), \tag{4.61}$$

$$\mathbf{J}_n''' = \sum_I \sum_{L \neq I} \mathbf{R}_I \left(\mathbf{V}_L \cdot \frac{\partial w_I}{\partial \mathbf{R}_L} \right). \tag{4.62}$$

Using eq. (4.56), one can combine the second and third contribution with the term previously obtained $\mathbf{J}_0'$:

$$\mathbf{J}_0' + \mathbf{J}_n'' + \mathbf{J}_n''' = \sum_I \mathbf{R}_I \left[(\mathbf{F}_I - \mathbf{F}_I^{el}) \cdot \mathbf{V}_I + \sum_{L \neq I} \left(\mathbf{V}_L \cdot \frac{\partial w_I}{\partial \mathbf{R}_L} \right) \right]$$

$$= \sum_I \left[\mathbf{R}_I(\mathbf{F}_I^n \cdot \mathbf{V}_I) + \sum_{L \neq I} \mathbf{R}_I \left(\mathbf{V}_L \cdot \frac{\partial w_I}{\partial \mathbf{R}_L} \right) \right]$$

$$= \sum_I \sum_{L \neq I} \mathbf{R}_I \left(\mathbf{V}_L \cdot \frac{\partial w_I}{\partial \mathbf{R}_L} - \mathbf{V}_I \cdot \frac{\partial w_L}{\partial \mathbf{R}_I} \right). \tag{4.63}$$

where $\mathbf{F}_I^n = -\sum_L \frac{\partial w_L}{\partial \mathbf{R}_I}$ is the nuclear (ionic) contribution to the force acting on the I-th atom. By interchanging the I and L dummy indexes in the above equation, we have therefore obtained:

$$\mathbf{J}_0' + \mathbf{J}_n'' + \mathbf{J}_n''' = \sum_I \sum_{L \neq I} (\mathbf{R}_I - \mathbf{R}_L) \left(\mathbf{V}_L \cdot \frac{\partial w_I}{\partial \mathbf{R}_L} \right). \tag{4.64}$$

Summing all the contributions we define:

$$\mathbf{J}_n = \mathbf{J}_n' + \mathbf{J}_0' + \mathbf{J}_n'' + \mathbf{J}_n''', \tag{4.65}$$

which is our last current:

$$\mathbf{J}_n = \sum_I \left[\mathbf{V}_I \left(\frac{1}{2} M_I V_I^2 + w_I \right) + \sum_I \sum_{L \neq I} (\mathbf{R}_I - \mathbf{R}_L) \left(\mathbf{V}_L \cdot \frac{\partial w_I}{\partial \mathbf{R}_L} \right) \right]. \tag{4.66}$$

4.1.5 Summary

We write down here all formulas obtained:

$$\begin{cases} \mathbf{J}_H = \dfrac{1}{4\pi e^2} \displaystyle\int_\Omega \nabla v_H(\mathbf{r}) \dot{v}_H(\mathbf{r}) d\mathbf{r} \\[2mm] \mathbf{J}_0 = \displaystyle\sum_I \sum_n \left\langle \phi_n \left| (\mathbf{r} - \mathbf{R}_I) \left(\mathbf{V}_I \cdot \dfrac{\partial \hat{v}_0}{\partial \mathbf{R}_I} \right) \right| \phi_n \right\rangle \\[2mm] \mathbf{J}_{KS} = \mathcal{R} \displaystyle\sum_v \langle \bar{\phi}_v^c | H_{KS} + \epsilon_v | \dot{\phi}_v^c \rangle \\[2mm] \mathbf{J}_{XC}^{LDA} = 0 \qquad \mathbf{J}_{XC}^{PBE} = - \displaystyle\int n(\mathbf{r}) \dot{n}(\mathbf{r}) \epsilon_{GGA}^\alpha (\mathbf{r}) d\mathbf{r} \\[2mm] \mathbf{J}_n = \displaystyle\sum_I \left[\mathbf{V}_I \left(\frac{1}{2} M_I V_I^2 + w_I \right) + \sum_I \sum_{L \neq I} (\mathbf{R}_I - \mathbf{R}_L) \left(\mathbf{V}_L \cdot \frac{\partial w_I}{\partial \mathbf{R}_L} \right) \right] \end{cases} \tag{4.67}$$

4.2 Numerical implementation

We now describe the methodologies developed in order to compute at each time step of the dynamics the heat flux $\mathbf{J}(t)$ in plane wave ab-initio computer simulations codes. The use of a supercell is required in order to simulate the bulk behavior of liquid systems. This means that only wavefunctions at the Γ point are needed, thus permitting to exploit the reality of the wavefunctions through standard Gamma point tricks often used in plane wave codes [54]. Nevertheless, formulas are here written for simplicity without these tricks. It is supposed that positions and velocities at time t are available from a previous performed molecular dynamics calculation, obtained for example through the Car-Parrinello scheme.

4.2.1 Hartree current $\mathbf{J}_H$ and Exchange correlation current $\mathbf{J}_{XC}$

First of all explain how time derivatives, which are present both in $\mathbf{J}_H$ and in $\mathbf{J}_{XC}$, have been implemented (the same technique has been applied also to the derivative of the projector in the Kohn-Sham current). Time derivatives are applied always to quantities f depending only on the ions positions (for example, the time derivative of the Hartree potential) and not on ion velocities. A finite difference scheme has been used:

$$\dot{f}(t) = \frac{f(\mathbf{R}(t+dt)) - f(\mathbf{R}(t))}{dt}, \tag{4.68}$$

where $\mathbf{R}(t)$ are the ion positions at time t. The quantity f has therefore to be computed twice for each current computation at slightly different times. The time step dt required has been found to be much smaller than the frequency necessary to sample the dynamics of the heat flux. In order to avoid saving positions at a frequency much higher than required, positions at time $t + dt$ have been computed from ion velocities and positions at time t, which are supposed to be available:

$$\mathbf{R}(t+dt) = \mathbf{R}(t) + \mathbf{V}(t)dt. \tag{4.69}$$

This scheme is exact at first order in dt.

The Hartree current is then most easily computed in reciprocal space, with the formula:

$$\mathbf{J}_H = \frac{\Omega}{4\pi e^2} \sum_{\mathbf{G}} \dot{v}_H(\mathbf{G}) v_H(-\mathbf{G})(-i\mathbf{G}). \tag{4.70}$$

In a DFT calculation, where reciprocal G-vectors are distributed across different processors, this formula is easily implemented in a parallel scheme.

The exchange correlation current has to be computed in real space:

$$\mathbf{J}_{XC}^{\alpha} \sim - \sum_i n(\mathbf{r}_i)\dot{n}(\mathbf{r}_i)\epsilon_{GGA}^{\alpha}(\mathbf{r}_i), \tag{4.71}$$

where the explicit expression for ϵ_{GGA}^{α} is readily deduced from the original article [55] and is a scalar function of the local density and local gradient density. Also this sum is easily parallelizable, since different points of the real space grid are not coupled.

4.2.2 Kohn-Sham current $\mathbf{J}_{KS}$

The two main ingredients necessary to compute the Kohn-Sham current are the wavevectors $\bar{\phi}_v^c$ and $\dot{\phi}_v^c$, as defined in section 4.1.3. Using DFPT techniques, the first of the two is recognized to be the solution of the linear system:

$$(H - \epsilon_v + \alpha P_v)|\bar{\phi}_v^c\rangle = P_c[H, \mathbf{r}]|\phi_v\rangle, \tag{4.72}$$

where α is a constant different from zero, chosen to make the system non singular. The commutator is well defined in periodic boundary conditions and therefore a conjugate gradient procedure [56] can be performed to solve the linear system in an efficient way.

To compute $\dot{\phi}_v^c$ we exploit the identity [51]:

$$P_c|\dot{\phi}_v\rangle = \dot{P}_v|\phi_v\rangle = P_c\dot{P}_v|\phi_v\rangle \sim \tag{4.73}$$

$$\sim \frac{1}{\Delta t}\left[(1 - P_v(t))(P_v(t) - P_v(t - dt))\right]|\phi_v(t)\rangle, \tag{4.74}$$

which permits to avoid problematic alignment of the wavefunctions at different time steps, thanks to the fact that the derivative has been moved from the wavefunction to the projector. This is useful because the projector on the valence band is a gauge invariant quantity. When calculating finite differences in equation 4.74 we can therefore choose uncorrelated bases sets for the valence band at different times. The direct computation of $\dot{\phi}_v$ using finite differences with an expression of the type $\dot{\phi}_v = (\phi(t + dt) - \phi(t))/dt$ is problematic because it is difficult numerically to assure that $\phi(t)$ and $\phi(t - dt)$ are correctly aligned, especially in the presence of degeneracy and crossing levels.

The projector P_c has been added in the second step of equation (4.74) in order to guarantee numerically that the resulting wavefunction is orthogonal to the valence band, even when discretizing the time derivative.

4.2.3 Ionic current $\mathbf{J}_n$

The ionic current $\mathbf{J}_n$ and the zero current $\mathbf{J}_0$ are separately subject to Coulumbian divergences. In order to deal with the divergence we replace the Coulomb potential $\frac{1}{x}$ with a screened one $f(x) = e^{-\mu x}\frac{1}{x}$, a Yukawa potential. For finite μ both currents are finite, but $\mathbf{J}_n$ and $\mathbf{J}_0$ are divergent as $\mu \to 0$. Nevertheless, the divergent terms originating from the two currents sum to zero, leading to well defined limit . We notice that the introduction of a finite screen is just a formal device aimed at dealing with the divergent Coulombian behavior of the singular terms, but it does not enter into the final formulas actually implemented.

We used Ewald summation technique. This is convenient both because fast converging summations appear and the divergent terms are isolated in the zero component of the reciprocal space summation.

We consider here for the the sake of simplicity the case of a cubic cell. $\mathbf{L}$ indicates a lattice vector in real space. With the definitions:

$$S_1(\mathbf{d})_{\alpha,\beta} = \sum_{\mathbf{L}} \frac{(\mathbf{d} - \mathbf{L})_\alpha (\mathbf{d} - \mathbf{L})_\beta}{|\mathbf{d} - \mathbf{L}|} f'(|\mathbf{d} - \mathbf{L}|)$$

$$S_{1,B} = \frac{1}{3} \sum_{\mathbf{L} \neq \mathbf{0}} L f'(L)$$

$$S_2(\mathbf{d}) = \sum_{\mathbf{L}} f(|\mathbf{d} - \mathbf{L}|)$$

$$S_{2,B} = \sum_{\mathbf{L} \neq \mathbf{0}} f(L),$$

the ionic current is written as a sum of three terms:

$$\mathbf{J}_n = \mathbf{J}_{1,n} + \mathbf{J}_{2,n} + \mathbf{J}_{3,n} \tag{4.75}$$

$$\mathbf{J}_{1,n} = \sum_i \mathbf{v}_i \left(\frac{1}{2} m v_i^2 \right) \tag{4.76}$$

$$\mathbf{J}_{2,n} = \sum_i \mathbf{v}_i \left(\frac{1}{2} \sum_{j \neq i} Z_i Z_j \, e^2 \, S_2(|\mathbf{R}_i - \mathbf{R}_j|) + \frac{1}{2} e^2 \, Z_i^2 S_{2,B} \right) \tag{4.77}$$

$$\mathbf{J}_{3,n} = \sum_i \sum_{j \neq i} v_{j,b} \frac{Z_i Z_j e^2}{2} S_1(|\mathbf{R}_i - \mathbf{R}_j|) - \sum_i \mathbf{v}_i \frac{Z_i^2 e^2}{2} S_{1,B}. \tag{4.78}$$

The Ewald techniques applies with no further modifications in the case of $S_{1,B}$, $S_2(\mathbf{d})$ and $S_{2,B}$, as it is discussed in [44][57]:

$$S_2(\mathbf{d}) = \sum_{\mathbf{L}} f(|\mathbf{d} - \mathbf{L}|) erfc(\sqrt{\eta}|\mathbf{d} - \mathbf{L}|) + \tag{4.79}$$

$$+ \frac{4\pi}{\Omega} \sum_{\mathbf{G} \neq 0} \frac{\exp(\frac{-G^2}{4\eta})}{G^2} e^{i\mathbf{G}\mathbf{d}} + \frac{4\pi}{\Omega} \left(\frac{1}{\mu^2} - \frac{1}{4\eta} \right), \tag{4.80}$$

$$S_{2,B} = \sum_{\mathbf{L} \neq 0} f(L) erfc(\sqrt{\eta}L) + \tag{4.81}$$

$$+ \frac{4\pi}{\Omega} \sum_{\mathbf{G} \neq 0} \frac{\exp(\frac{-G^2}{4\eta})}{G^2} + \frac{4\pi}{\Omega} \left(\frac{1}{\mu^2} - \frac{1}{4\eta} \right) - 2\sqrt{\frac{\eta}{\pi}}, \tag{4.82}$$

$$S_{1,B} = \frac{1}{3} \sum_{\mathbf{L} \neq 0} L f'(L) erfc(\sqrt{\eta}L) - \tag{4.83}$$

$$- \frac{4\pi}{3\Omega} \sum_{\mathbf{G} \neq 0} \frac{\exp(\frac{-G^2}{4\eta})}{G^2} e^{i\mathbf{G}\mathbf{d}} - \frac{4\pi}{\Omega} \left(\frac{3}{\mu^2} - \frac{1}{4\eta} \right) + \frac{2}{3}\sqrt{\frac{\eta}{\pi}}, \tag{4.84}$$

where $erfc(x) = 1 - erf(x)$ and $erf(x)$ is the standard error function. η is the Ewald convergence factor.

In order to apply the Ewald technique to $S_1(\mathbf{d})$, it is convenient to replace first $\mathbf{d}$ with a continuous $\mathbf{x}$ and then exploit the formula:

$$\partial_b f(|\mathbf{x} - \mathbf{L}|) = \frac{(\mathbf{x} - \mathbf{L})_b}{|\mathbf{x} - \mathbf{L}|} f'(|\mathbf{x} - \mathbf{L}|). \tag{4.85}$$

Without this trick summations in reciprocal space would be convergent, but not exponentially. With this trick fast summations formulas are obtained. We obtain:

$$S_1(\mathbf{x})_{a,b} = \partial_b \sum_{\mathbf{L}} (\mathbf{x} - \mathbf{L})_a f(|\mathbf{x} - \mathbf{L}|) - \sum_{\mathbf{L}} f(|\mathbf{x} - \mathbf{L}|) \delta_{a,b} \equiv \overline{S}(\mathbf{x})_{a,b} - S_2(\mathbf{x}) \delta_{a,b}. \tag{4.86}$$

Now the Ewald technique is applied to $\overline{S}(\mathbf{x})_{a,b}$. With the definition:

$$h(x) = \frac{erfc(x)}{x} \tag{4.87}$$

and $\overline{S} = \overline{S^R} + \overline{S^K}$, one has:

$$\overline{S^R} = \sum_{\mathbf{L}} \left[\sqrt{\eta} h(\sqrt{\eta}|\mathbf{x} - \mathbf{L}|) \delta_{a,b} + \eta h'(\sqrt{\eta}|\mathbf{x} - \mathbf{L}|) \frac{(\mathbf{x} - \mathbf{L})_a (\mathbf{x} - \mathbf{L})_b}{|\mathbf{x} - \mathbf{L}|} \right] \tag{4.88}$$

$$\overline{S^K} = \sum_{\mathbf{G} \neq 0} \frac{4\pi}{\Omega} \frac{G_a G_b}{G^2} \frac{\exp(\frac{-G^2}{4\eta})}{G^2} \left[2 + \frac{G^2}{2\eta} \right] e^{i\mathbf{G}\mathbf{x}}. \tag{4.89}$$

We note that $\overline{S^K}$ has no Coulombian divergent terms. Summing all the Coulombian divergent contributions from the $\mathbf{G} = 0$ terms till now obtained we get:

$$\mathbf{J}_n^{div} = \frac{Z_{tot}}{\Omega} \frac{4\pi}{\mu^2} \sum_i \mathbf{v}_i Z_i. \tag{4.90}$$

We will find an equal, opposite Coulombian divergence, in current $\mathbf{J}_0$.

4.2.4 Zero-current $\mathbf{J}_0$

We consider here norm conserving potentiality, whose derivative with respect to the ionic positions is given by a local and a non-local contribution.

$$\frac{\partial \hat{v}_0}{\partial \mathbf{R}_I} = \frac{\partial \hat{v}_{NL}^I}{\partial \mathbf{R}_I} + \frac{\partial}{\partial \mathbf{R}_I} f^i(|\mathbf{r} - \mathbf{R}_I|), \tag{4.91}$$

where in this paragraph f^i refers to the local part of the pseudo-potential of atom i. We study first the local part , the only one divergent when the Coulomb screen goes to zero.

4.2.4.1 Local part

We call this local long range contribution $\mathbf{J}_0^{LR}$. With the definitions:

$$n(\mathbf{r}) \equiv \sum_n |\phi_n(\mathbf{r})|^2$$

$$h_{a,b}^i(\mathbf{x}) \equiv \sum_{\mathbf{L}} \frac{(\mathbf{x} - \mathbf{L})_a (\mathbf{x} - \mathbf{L})_b}{|\mathbf{x} - \mathbf{L}|} f^{i\prime}(|\mathbf{x} - \mathbf{L}|) \tag{4.92}$$

$$u(\mathbf{r}) = -\sum_i v_{i,b} h_{a,b}^i(\mathbf{r} - \mathbf{R}_i), \tag{4.93}$$

the current is rewritten:

$$\mathbf{J}_0^{LR} = \int_\Omega n(\mathbf{r}) u(\mathbf{r}) = \Omega \sum_{\mathbf{G}} n(\mathbf{G}) \overline{u(\mathbf{G})}. \tag{4.94}$$

The reciprocal components of $h_{a,b}^i(\mathbf{x})$, from which the reciprocal components of u are easily obtained, are computed through a similar procedure followed for obtaining the component of $S_1(\mathbf{d})$ in the ionic current. One writes:

$$h_{a,b}^i(\mathbf{x}) = \partial_b \left[\sum_{\mathbf{L}} (\mathbf{x} - \mathbf{L})_a f^i(|\mathbf{x} - \mathbf{L}|) \right] - \delta_{a,b} \sum_{\mathbf{L}} f^i(|\mathbf{x} - \mathbf{L}|) = \tag{4.95}$$

$$= \sum_{\mathbf{G}} \left(h1_{a,b}^i(\mathbf{G}) + h2_{a,b}^i(\mathbf{G}) \right) e^{i\mathbf{G} \cdot \mathbf{x}}. \tag{4.96}$$

Numerical integrations of the radial part of the pseudo-potential are performed adding and subtracting the asymptotic behavior of the local pseudo-potential, as it is common in plane wave computations. The resulting formulas implemented:

$$
\begin{cases}
h1^i_{a,b}(\mathbf{G}) = \mathbf{0} \quad \text{for} \quad \mathbf{G} = \mathbf{0} \\
h1^i_{a,b}(\mathbf{G}) = \dfrac{4\pi}{\Omega}\dfrac{G_a G_b}{G^2} G \displaystyle\int_0^\infty x^2[x f^i(x) + 2Z_v]J_1(Gx)dx- \\
\qquad - \dfrac{4\pi}{\Omega}(2Z_v)\dfrac{G_a G_b}{G^2}\dfrac{2}{G^2} \quad \text{for} \quad \mathbf{G} \neq \mathbf{0}
\end{cases}
\tag{4.97}
$$

and

$$
\begin{cases}
h2^i_{a,b}(\mathbf{G}) = -\delta_{a,b}\dfrac{4\pi}{\Omega}\displaystyle\int_0^\infty [x^2 f^i(x) + 2Z_v x]dx+ \\
\qquad + 2\delta_{a,b}Z_v\dfrac{4\pi}{\Omega}\dfrac{1}{\mu^2} \quad \text{for} \quad \mathbf{G} = \mathbf{0} \\
h2^i_{a,b}(\mathbf{G}) = -\delta_{a,b}\dfrac{4\pi}{\Omega}\displaystyle\int_0^\infty [x^2 f^i(x) + 2Z_v x]J_0(Gx)dx+ \\
\qquad + \delta_{a,b}\dfrac{2Z_v}{G^2}\dfrac{4\pi}{\Omega} \quad \text{for} \quad \mathbf{G} \neq \mathbf{0}
\end{cases}
\tag{4.98}
$$

We not here that only from $h2$ we get a Coulombian divergence when $\mu \to 0$. By explicit computation this is exactly equal, apart from a sign, to the one obtained in the computation of the ionic current $\mathbf{J}_n$.

4.2.4.2 Non-local part

The non-local part is inherently short range and we call it $\mathbf{J}_0^{SR}$:

$$
\mathbf{J}_0^{SR} = \sum_{I,n}\langle\phi_n|(\mathbf{r} - \mathbf{R}_I)\left(\mathbf{V}_I \cdot \dfrac{\partial \hat{v}_{NL}}{\partial \mathbf{R}_I}\right)|\phi_n\rangle,
\tag{4.99}
$$

where index I runs over all atoms, even belonging to periodic images of the supercell, whereas index n runs over the occupied electronic manifold. We consider only non conserving non local potentials:

$$
\hat{v}_{NL} = \sum_{I,k}D_{k,I}|\beta_k^I\rangle\langle\beta_k^I|_v,
\tag{4.100}
$$

where index $k = (l, m)$ is a composite index considering the angular momentum of the projector. β-functions are localized but not periodic. Explicitly the potential acts in this way on a periodic wave-function ϕ_n:

$$
(\hat{v}_{NL}\phi_n)(\mathbf{x}) = \sum_{I,k}D_{k,I}\beta_k^I(\mathbf{x} - \mathbf{R}_I)\int_{R^3}\beta_k^I(\mathbf{y} - \mathbf{R}_I)\phi_n(\mathbf{y})d\mathbf{y}
\tag{4.101}
$$

(thanks to localization, for every $\mathbf{x}$, only a finite number of atoms enter in the summation, which is therefore well defined).

We define from a localized function $\gamma(\mathbf{x})$ its periodic and translated counterpart as:

$$\overline{\gamma}(\mathbf{x} - \mathbf{a})(\mathbf{G}) = e^{-i\mathbf{G}\mathbf{a}} \frac{1}{\Omega} \int_\Omega \sum_{\mathbf{L}} \gamma(\mathbf{x} - \mathbf{L}) e^{-i\mathbf{G}\mathbf{x}} d\mathbf{x} = \tag{4.102}$$

$$= e^{-i\mathbf{G}\mathbf{a}} \frac{1}{\Omega} \int_{R^3} \gamma(\mathbf{x}) e^{-i\mathbf{G}\mathbf{x}} d\mathbf{x} = \tag{4.103}$$

$$= e^{-i\mathbf{G}\mathbf{a}} \widetilde{\gamma(\mathbf{x})}(\mathbf{G}), \tag{4.104}$$

where $\gamma(\mathbf{x})$ is a standard Fourier transform. These functions are easily computed in a plane wave code.

From two such periodic functions we define:

$$\mathbf{A}[\gamma; \delta](\mathbf{a}) = \sum_n \langle \phi_n(\mathbf{x}) | \overline{\gamma}(\mathbf{x} - \mathbf{a}) \rangle \langle \phi_n(\mathbf{x}) | \overline{\delta}(\mathbf{x} - \mathbf{a}) \rangle \tag{4.105}$$

After computation one ends up with the final expression:

$$\mathbf{J}_0^{SR} = \sum_{i,k} V_{i,b} D_{i,k} \left(\mathbf{A}[-x_a \partial_b \beta_k^i; \beta_k^i](\mathbf{R}_i) + \mathbf{A}[x_a \beta_k^i; -\partial_b \beta_k^i](\mathbf{R}_i) \right) \tag{4.106}$$

where index i runs over all atoms of the unit cell (periodic images are no more present). One needs to take care of the angular dependence of the projectors when doing Fourier transforms of needed beta functions.

Chapter 5

Implementation and benchmarks

We implemented the methodology outlined in chapter 3 in the quantum ESPRESSO suite of computer codes [54] and used norm-conserving pseudo potentials from the quantum espresso public repository. As a first preliminary test we computed with high precision the heat flux for systems at equilibrium, translating at constant speed, using different pseudo potentials and exchange correlation functionals. Then, for a real benchmark, we computed thermal conductivity of ab initio DFT Argon, following the computational procedure described in section 5.2. It was possible for this system to devise a classical pair potential reproducing faithfully the quantum Born-Oppenheimer dynamics. We therefore compared our results with the ones computed within a classical framework, finding good correspondence.

5.1 Preliminary tests: isolated systems

The result expected for the heat flux in the case of an isolated system (even interacting), translating at constant speed, is known a priori and has been derived in appendix D. Calling E the total energy of the system (including the kinetic energy component) and $\mathbf{v}$ the translational velocity, the instantaneous heat flux will not depend on time and its value must be equal to $\mathbf{J} = E\mathbf{v}$. As a consequence current and velocity point in the same direction. We will first show, for testing purposes, that our program satisfies this condition, when an isolated system is simulated with the use of a big enough supercell. We will consider first the case of an Helium atom and then of an Hydrogen chloride molecule.

5.1.1 Helium atom

Pseudo-potential datasets used for Helium computation are reported in the "He.pbe-hgh.UPF" pseudo-potential file [54]. We tested a PBE functional [55], used both for exchange and correlation contributions. The pseudo potential is of a local type, norm conserving.

The simulation cell was taken cubic, with an edge of 20 Bohr. Ion velocity was chosen equal to $0.01\frac{Bohr}{\tau_{BO}}$, where τ_{BO} is the unit of time usually used in Born-Oppenheimer dynamics, with a value of 4.8379 10^{-2} fs. The threshold for self consistency was taken very small, equal to 10^{-15} Ryd in order to obtain, for this test case, very good convergence. A time step of $0.5\tau_{BO}$ was used for performing numerical derivatives.

Table 5.1: Currents computed at convergence for the case of an Helium atom translating at constant speed, in units of $Ryd\frac{Bohr}{\tau_{BO}}$, as defined in equations (4.67). The trivial kinetic component $(\frac{1}{2}Mv^2)\mathbf{v}$ in current $\mathbf{J}_n$ has not been considered. In the same units the value of total energy multiplied by atomic velocity has been reported.

$\mathbf{J}_H$:	-2.322e-2
$\mathbf{J}_n$:	-7.566e-3
$\mathbf{J}_0$:	-4.008e-2
$\mathbf{J}_{KS}$:	1.392e-2
$\mathbf{J}_{XC}$:	8.651e-4
$\mathbf{J}_{tot}$:	-5.781e-2
$|E\mathbf{v}|$:	-5.780e-2

As expected, neglibile value of the current were observed along directions orthogonal to the atomic velocity. In figure 5.1 we report on the same graph the heat flux along the direction of the velocity (taking out the trivial kinetic component appearing $(\frac{1}{2}Mv^2)\mathbf{v}$ in the ionic current $\mathbf{J}_n$ (4.66)) as a function of the kinetic energy cutoff , and the modulus of $\mathbf{v}$ times internal energy E. The energy has been obtained of course by the same self consistent calculation by which Kohn-Sham orbitals were derived. Total energy, being a variational propriety, will tend monotonically to its asymptotic value, but we do not expect this propriety to hold for the heat flux.

In the inset of figure 5.1 the ratio of the same quantities is also plotted. We expect this value to reach unity when both total energy and current are converged and this is indeed observed. Actually even at very small cutoffs the quantities differ only by less than 10%.
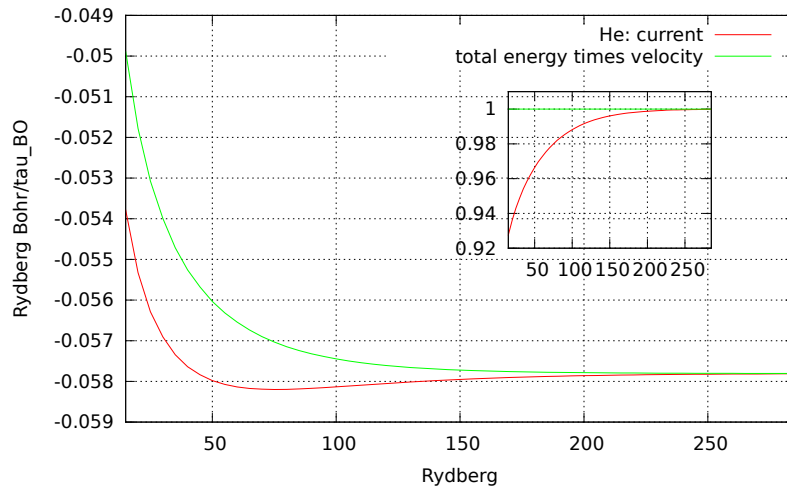
Figure 5.1: Total energy multiplied by atomic velocity and the heat flux along the direction of the velocity, as a function of the kinetic energy cutoff. The quantities refer to the case of an Helium atom translating at constant speed. In the inset the ratio of the two quantities, which must be equal under convergence, is reported.

In table 5.1 we report the values of the different components of the heat flux in this system, when converged with respect to the kinetic energy cutoff. It is observed that every current is bigger than the difference between total energy times velocity and the total current, which is given by the sum of the different components. This confirms that each current has been correctly computed, even if we do not expect such a precision to be needed in a real calculation.

5.1.2 Hydrogen chloride molecule

In this paragraph the different case of an Hydrogen chloride molecule rigidly translating is considered. This system differs from the previous one qualitatively because of two main reasons. First of all it is no more isotropic and we take the axes of the molecule to lie on the x direction. Secondly, the total force acting on each of the two atoms can be non-zero, depending on the inter-atomic distance chosen. We point out that in the derivation the time derivative of velocities in formula (4.61) was substituted by a force term. Therefore, if the total force acting on one of the molecules is different from zero, the heat flux, computed through equations (4.67), is not associated anymore to a rigidly translating system. As a practical consequence, before performing any current computation the positions of Hydrogen and Chlorine were relaxed to their equilibrium positions.

We used pseudo potentials from file "Cl.pz-bhs.UPF" for Chlorine and from "H.pz-vbc.UPF" for hydrogen. These possess LDA type exchange correlation functionals and are both norm-conserving. The pseudo potential for Chlorine is non local with two different beta functions, whereas Hydrogen pseudo-potential is local. A molecular velocity of $0.01 \frac{Bohr}{\tau_{BO}}$ was again chosen and a time step for time derivatives $0.5\tau_{BO}$ used. The simulation cell was again cubic with a length of $20 Bohr$ and a self consistency cutoff of $10^{-15} Ryd$ used.

An equilibrium distance of 2.434 Bohr was first computed. The molecule has then been given a translational velocity along each of the three cartesian directions and a heat flux equal to total energy times velocity has always been computed. As before, apart from numerical errors, the heat flux and the velocity point always in the same direction. Furthermore, y and z directions are equivalent by symmetry and this is indeed observed. In table 5.2 we report the values of the of the partial currents along the velocity, for the two inequivalent directions, as well as the total current and the total energy computed.

Table 5.2: As in table 5.1 we report the values of the currents computed in the case of an Hydrogen chloride molecule moving at constant speed. The axes of the molecule lies along the x direction. The molecule has been given a translational velocity along each of the three cartesian directions and all cases are reported.

	velocity along x	velocity along y/z
$\mathbf{J}_H$	-1.434e-1	-1.550e-1
$\mathbf{J}_n$	-5.409e-3	-6.344e-2
$\mathbf{J}_0$	-9.115e-3	5.425e-3
$\mathbf{J}_{KS}$	-1.540e-1	-9.892e-2
$\mathbf{J}_{tot}$:	-3.120e-1	-3.120e-1
$\lvert E\mathbf{v} \rvert$:	-3.120e-1	-3.120e-1

An other complication arises from the degeneracy of the highest occupied molecular horbital (HOMO). We are therefore able to check that the numerical procedures exploited (section 4.2) are indeed automatically able to deal with such situations. Interestingly, the value of the currents depends strongly on the direction chosen, but they sum always to the same value, as expected. As before, in figure 5.2 we plot on the same graph the total current and total energy times velocity, as a function of the kinetic energy cutoff. It can be seen that in this molecular
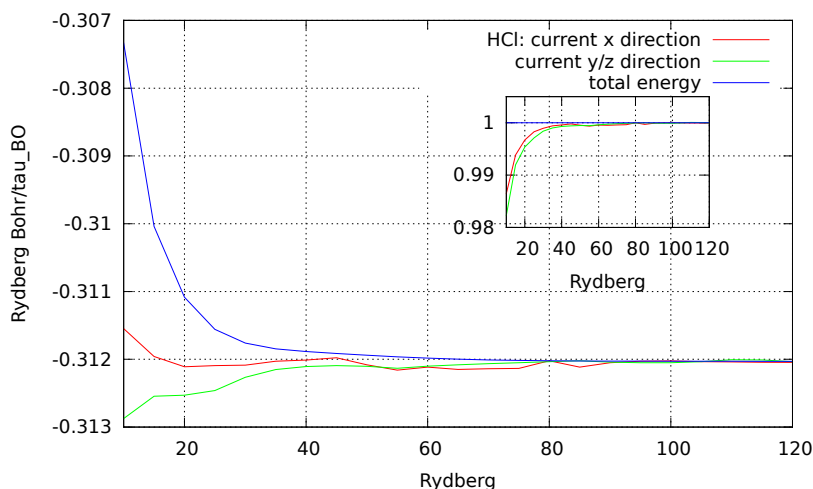
Figure 5.2: As in figure 5.1 for the case of a translating HCl molecule . Both the case when translational velocity is along the axes of the molecule, lying in the x direction, and when it is orthogonal to the axes, are reported.

system we obtain a faster convergence to the asymptotic value than in the previous Helium atom test case.

5.2 First benchmark and implementation scheme: Argon DFT

Before applying the devised technique in a predictive way and in interesting systems, we need to test it. We chose Argon as a first, non trivial test, because it is a simple system, well described by a simple pair Lennard Jones potential, and often used in classical molecular dynamics simulations for testing purposes. Unluckily, Argon is well known not to be well described by local DFT functionals, to which our formulation is for the moment restricted and dispersion forces in the exchange-correlation energy functionals must be included [58]. Therefore we do not expect to be able to compare the results with experimental ones. To circumvent this problem we fitted the DFT Born-Oppenheimer, many body potential, to an effective classical pair potential. We then used this classical potential to generate a trajectory, as closest as possible to the DFT one, and computed the heat flux in this new system. For this purpose the classical formula for the heat flux, applicable to a generic pair body potentials, equation (3.104), has been used.

The computational procedure followed for obtaining the DFT heat flux time series is qualitatively divided into four main steps:

5. Implementation and benchmarks

1. First a quantum trajectory is generated. We used for this purpose the Car Parrinello technique (CPMD) [59]. After this step, positions and velocities of the atoms are saved on disk with a chosen frequency, much bigger than the time step used for the dynamics;

2. As a first post-processing step, for every configuration two self consistent calculations are performed in order to save on disk the exact Kohn-Sham orbitals required for computing the current. As discussed in section 4.2.1, two self consistent calculations are performed, with the positions of the atoms slightly displaced according to their velocity, because of the finite difference scheme used for performing time derivatives;

3. As a third step, saved orbitals are fed into the program devoted to the current computation, applying equations (4.67) and the computational techniques described in section 4.2. After this step the heat flux current time series is at disposal;

4. Finally, exploiting ergodicity a Green-Kubo estimate for the autocorrelation function $\langle \mathbf{J}(t) \cdot \mathbf{J}(0) \rangle$ is readily obtained [60]:

$$\langle \mathbf{J}(k\Delta t) \cdot \mathbf{J}(0) \rangle_{eq} \sim \frac{1}{N-k} \sum_{n'=1}^{N-k} \mathbf{J}(n') \cdot \mathbf{J}(n'+k). \tag{5.1}$$

Using a trapezoidal rule the autocorrelation function has been integrated and inserted into formula (2.14), therefore obtaining thermal conductivity values as in section 2.3. Error bars were estimated using the block averaging technique, as described in [61];

To equilibrate the system we used a Nosè Hoover thermostat [62], as implemented in the cp.x program of the quantum espresso suite, for 8 picoseconds, selecting at least qualitatively the temperature of the system. We then switched off the thermostat and the actual production runs were computed in the micro-canonical ensemble. Four long trajectories of 100 picoseconds each were computed. Car Parrinello simulations data are reported in table 5.3. The number of atoms chosen, 108, is known to be able to describe well the thermodynamic limit in the Green-Kubo formula [16],[24].

In figure 5.3. we can see the fictitious electronic kinetic energy compared to the total kinetic energy of the ions, confirming that the simulations parameters we chose permitted to maintain the adiabatic separation between electrons and ions. Indeed, what must be observed for determining the quality of a CPMD dynamics is the absence of a drift in the fictitious electronic kinetic energy comparable with the natural fluctuations of ionic kinetic energy.

Classical trajectories were implemented in the open-source code Lammps [63], where a new pair style was implemented, thus permitting to exploit all the levels of parallelization

Table 5.3

Details for CPMD Argon computation

Simulation length:	100 ps, 8 ps of equilibration
Cell dimension (cubic):	33 Bohr
Number of atoms:	108
Density:	1.34 $\frac{g}{cm^3}$
Pseudo-potential file:	Ar.pz-rrkj.UPF
Exchange correlation functional:	LDA, Slater
Pseudo potential type:	non local, 2 beta functions
	with $l = 0$ and $l = 1$, norm conserving
Electronic mass:	1000 a.u.
Energy cutoffs:	24/96 Ryd
Time step:	10.0 a.u.
Preconditioning:	not present
Thermostat:	Nosè Hoover, not present in production

and molecular dynamics technicalities (neighbor lists, energy shifts...) implemented in this code.

In the next section we describe the fitting procedure followed in order to obtain a classical pair potential able to describe the DFT dynamics. Then we describe the details for the heat flux computation and compare classical and quantum results.

5.2.1 Generation of a classical model

We first derived a classical pair potential computing the force acting between two isolated Argon atoms in a DFT self consistent calculation. This method relies on the hypothesis that forces between argon atoms are not affected by the presence of other particles and therefore can be computed first by a simulation where only two Argon atoms are present and then used in a many particle simulation. We than took as initial condition an equilibrated configuration
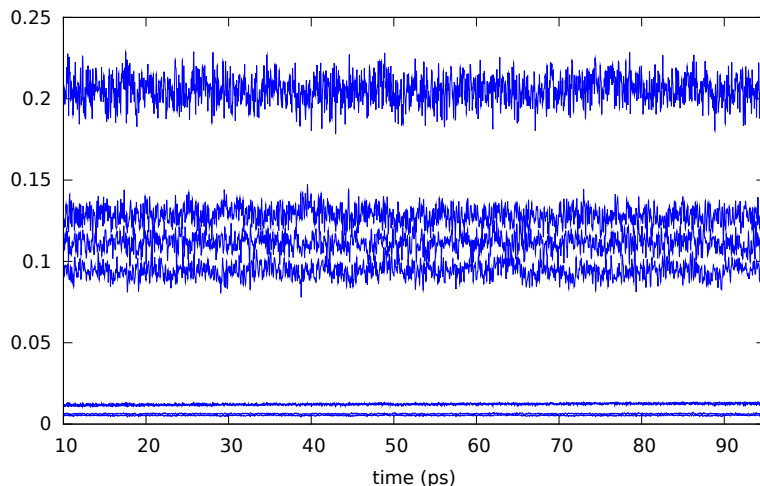
Figure 5.3: Total kinetic energy of ions and electrons for each of the liquid argon simulations after equilibration, in Hartree units. The fictitious electronic kinetic energy presents no drift comparable with the natural fluctuations of the total ionic kinetic energy.

at 184 K obtained by a previous CPMD run. In figure 5.4 we report the temperature dependence obtained. Temperature was observed to vary even more than the standard finite size fluctuations , meaning that the pair potential used did not furnish a good description of the dynamics.

Despite this failure, one can still look for better two body potentials, able to take into account many body effects in an effective way. We decided to fit a functional form for the potential $u(\alpha, x)$, depending on several parameters α and optimized them with the following scheme. This way we obtained a classical potential able to reproduce the DFT dynamics. We will refer to it as the *fitted potential*.

In particular we fixed $N = 2$ and fixed as a functional form:

$$u(x) = e^{-\alpha x} \sum_{n=0}^{N-1} c_n x^n. \tag{5.2}$$

We chose the optimized parameters α, c_0, c_1, c_2 as the ones giving the best fit of the Car-Parrinello forces computed during the dynamics. Therefore we saved the forces $f_{a,t,i}^{CP}$ acting along direction i on atom a at time t during a CPMD run. $F_{a,t,i}^{\alpha}$ are instead the forces computed using the new pair potential (but along the same CPMD trajectory) and the optimal parameters are chosen to minimize:

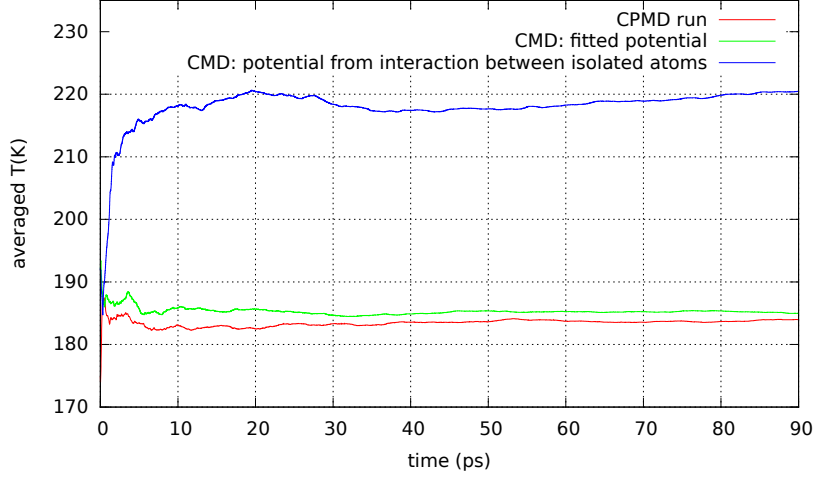$$\chi^2(\alpha, c_n) = \frac{1}{T} \sum_{a,t,i} |f_{a,t,i}^{CP} - F_{a,t,i}^{\alpha}|^2, \tag{5.3}$$

Figure 5.4: Running averaged temperature obtained for three different runs: (red) Car Par-rinello run; (green) classical molecular dynamics (CMD) starting with an equilibrated initial condition from the CMPD run and using the fitted potential from section 5.2.1; (blue) CMD starting from the same equilibrated initial condition from the CMPD run but using the potential obtained from the interaction energy between isolated atoms;

where T is the total simulation length over which the parameters are optimized (just a nor-malization factor).

Minimization of c_n at fixed α can be performed in an analytic way, since the dependence on these parameters is quadratic. One can write for convenience:

$$F_{a,t,i}^{\alpha} = \sum_{n=0}^{N-1} c_n G_{a,t,i}^{n,\alpha} \tag{5.4}$$

$$G_{a,t,i}^{n,\alpha} = -\sum_{a' \neq a} e^{-\alpha r_{aa'}} r_{aa'}^{n-2} (n - \alpha r_{aa'})(r_{a,i} - r_{a',i}), \tag{5.5}$$

where as usual $r_{a,i}$ are the i components of the atomic positions and $r_{aa'} = |\mathbf{r}_a - \mathbf{r}_{a'}|$. With these definitions:

$$\frac{\partial \chi^2}{\partial c_k} = 0 \Rightarrow \sum_n A_{k,n}^{\alpha} c_n = B_k^{\alpha}, \tag{5.6}$$

$$A_{n,k}^{\alpha} = \sum_{a,t,i} G_{a,t,i}^{n,\alpha} G_{a,t,i}^{k,\alpha}, \tag{5.7}$$

$$B_k^{\alpha} = \sum_{a,t,i} G_{a,t,i}^{k,\alpha} f_{a,t,i}^{CP}. \tag{5.8}$$

The solution to the linear system gives the best coefficients $c_k(\alpha)$ for fixed α. Minimiza-tion over α was then finally performed numerically plotting the resulting function $f(\alpha) =$
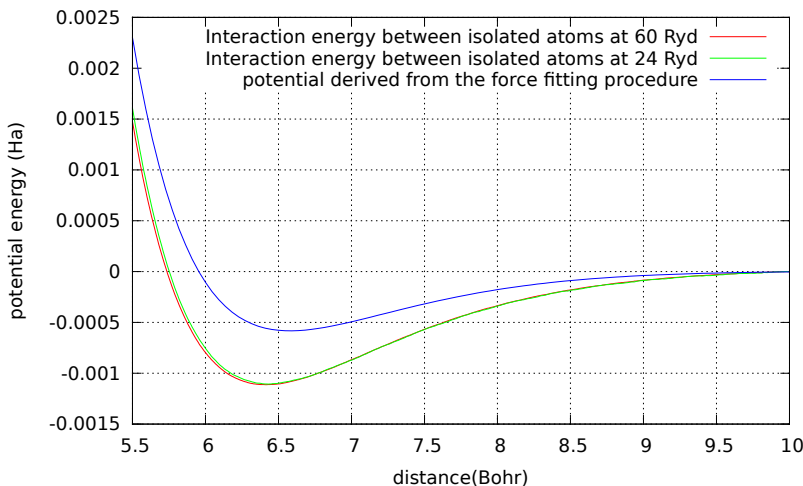
Figure 5.5: Potential derived from interaction energy between isolated atoms computed at 24 and at 60 Rydberg, compared with the one resulting from the fitting procedure. We can see that, because of the interaction with other atoms, the effective pair potential gets modified in a substantial way. The temperature dependence of the *fitted potential* (not reported) is much less than the difference with respect to the potential derived from the interaction energy.

$\chi^2(\alpha, c_k(\alpha))$ and studying its minima. The optimal values of α and of c_n were found to be stable with respect to the choice of different trajectories in the temperature range of interest. This means that dynamics of DFT Argon is effectively well described by a pair potential. One can see the difference between this fitted potential and the one derived from the interaction energy between two isolated atoms in figure 5.5.

In figure 5.6 we plot the computed radial distribution functions using the fitted potential and the ones obtained by the CPMD runs at the extreme temperatures of 184*K* and 400*K*. The agreement is excellent across the whole temperature range. To compare a dynamical quantity, we report in table 5.4 the measured diffusion coefficients.

5.2.2   Comparison of classical and quantum heat fluxes

If the fitted potential reproduces well DTF dynamics, we expect the thermal conductivities of the two systems, the quantum and the classical one, to agree with a degree of accuracy depending on the quality of the fit.

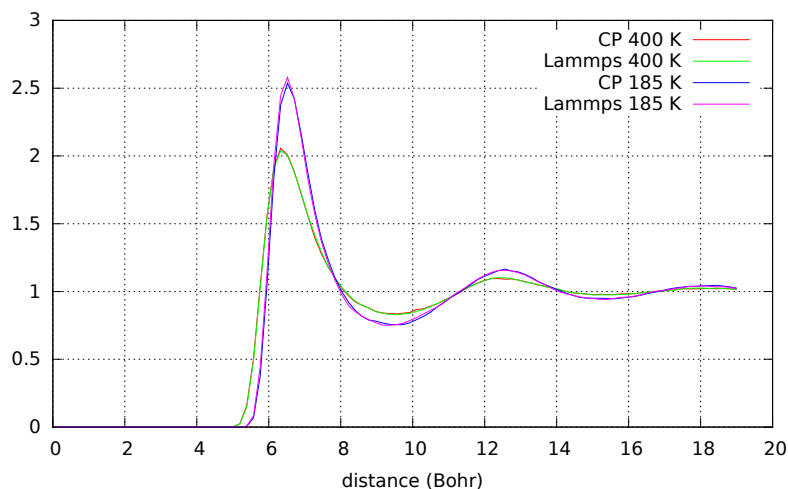We do not instead expect to find an agreement between the following quantities, computed in

Figure 5.6: Computed radial distribution functions at the temperature of 184*K* and 400*K*, resulting from the fitted potential and the CPMD runs. The Agreement is excellent across the whole temperature range of interest.

the quantum and classical case:

1. The heat fluxes computed for a fixed ionic configuration;

2. The autocorrelation function of the heat fluxes before being integrated;

This is clear from the discussion of the previous chapter. Even if the systems were exactly equivalent, the heat fluxes would be related to different local "unpacking" of the total energy density. As a consequence, the head flux autocorrelation functions can differ, but their integrals, which are the measurable physical quantities, should be comparable. This is exactly what we find from our calculations.

We chose to compute the current every 50 CPMD steps, which means that the current is computed every 12.09 fs. As it can be seen in figure 5.7 this is enough for following precisely all time frequencies describing the evolution of the total current. In the same figure the time series is reported both at 24 Ryd and at 40 Ryd, thus confirming that 40 Ryd is enough for obtaining convergence. We choose 2.0 a.u. as the time step for time derivatives, which was verified to be small enough. It is essential to choose a small enough energy convergence factor for obtaining well converged wavefunctions: $10^{-13} Ryd$ was found to be small enough.

In figures from 5.8,5.9,5.10 and 5.11 we report the autocorrelation function $\langle \mathbf{J}(t)\mathbf{J}(0)\rangle$ of the heat flux, for the four temperatures considered. For each temperature a classical molecular

Table 5.4: Temperatures measured in the CPMD run and in the restart, from equilibrated configuration, with the fitted potential. Also reported are the diffusion coefficients in the two cases. An error for the temperatures in the last significant digit is intended.

Temperature measured (K)		Diffusion coefficient ($10^{-5} cm^2/s$)	
cp.x	Lammps	cp.x	Lammps
184	185	7.8 ± 0.1	8.3 ± 0.1
217	219	9.6 ± 0.1	9.3 ± 0.1
250	252	10.8 ± 0.1	10.3 ± 0.1
400	407	15.6 ± 0.2	15.8 ± 0.2

dynamics run, using the fitted potential and starting from an equilibrated Car Parrinello configuration, was performed for one nanosecond. The first 100 picoseconds of these CMD runs were used to compare classical and quantum autocorrelation functions with the same statistics. The values obtained by the whole one nanosecond run are also computed and effectively considered as converged values. We can see from the figures that 100 picoseconds of dynamics are sufficient for obtaining a good autocorrelation function, since the converged classical functions are much similar to the ones obtained from the first 100 ps of dynamics. When $T = 184K$ there is a certain discrepancy, which does not affect the qualitative behavior, but does not permit to integrate the autocorrelation function with the required precision. At the higher temperatures this problem is not present.

As expected the classical and the quantum adiabatic autocorrelation function differ much more than statistical errors, even if they retain the same order of magnitude. In figures 5.12 and 5.13 we report instead the values of $\frac{1}{3} \int_0^t \langle \mathbf{J}(t')\mathbf{J}(0)\rangle dt'$, as a function of t: a quantitatively compatible value for large t, for the quantum and the classical computation, is obtained, apart from statistical errors. Only when $T = 184$ the classical converged value is not contained in the error estimated and this means that the 100 picoseconds of dynamics were not sufficient at this low temperature. This is clear because also the first 100 picoseconds of classical dynamics suffer of the same problem, as it can be seen in figure 5.12. In figure 5.14 we therefore plotted the thermal conductivities for the three higher temperatures, computed using the Green-Kubo formula. The conductivities are of the same order of magnitude of the ones reported in ref. [24], where a classical molecular dynamics of liquid Argon was performed,
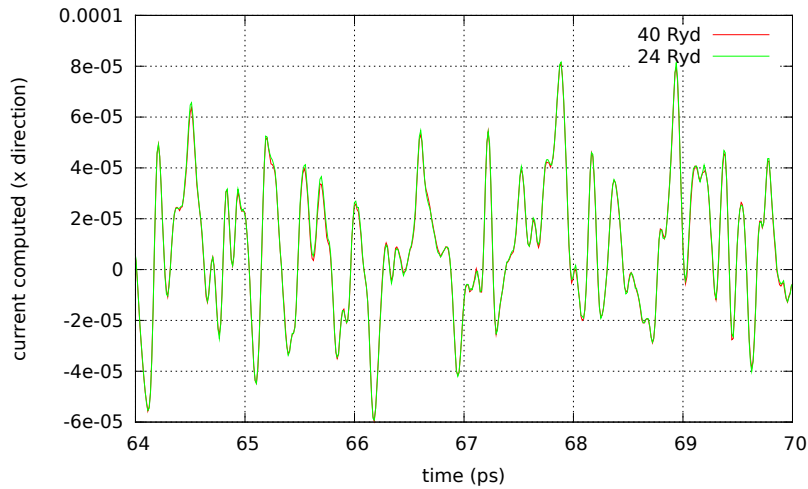
Figure 5.7: Example of the time series of the total current in Argon simulation, along x direction, computed with a kinetic energy cutoff of 24 and of 40 Ryd

using the well known Lennard Jones potential. In particular we estimate thermal conductivities of $(94 \pm 5)\frac{mW}{mK}$ for $T = 217$, $(104 \pm 5)\frac{mW}{mK}$ for $T = 250$ and $(118 \pm 8)\frac{mW}{mK}$ for $T = 400$, to be compared with classical converged values of $93, 103$ and 110 respectively. These results confirm that the methodology is working and can be used in more realistic systems. We present in the next section such an application.
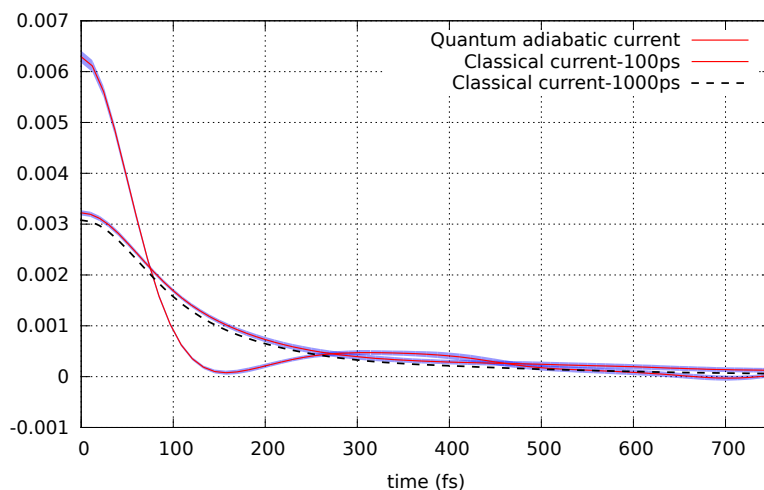
Figure 5.8: Quantum and classical auto-correlation functions $\frac{1}{3}\langle \mathbf{J}(t)\mathbf{J}(0)\rangle$, in units of $\left(\frac{Kcal}{mol}\frac{}{fs}\right)^2$, for $T = 184K$. The classical autocorrelation function is computed both with the same statistics of the quantum case and with a nanosecond of dynamics, thus permitting to compare with a well converged value. Statistical error bars are shaded. At this temperature the converged value and the classical autocorrelation function differ more than statistical errors. This means that the sampling was not good enough.
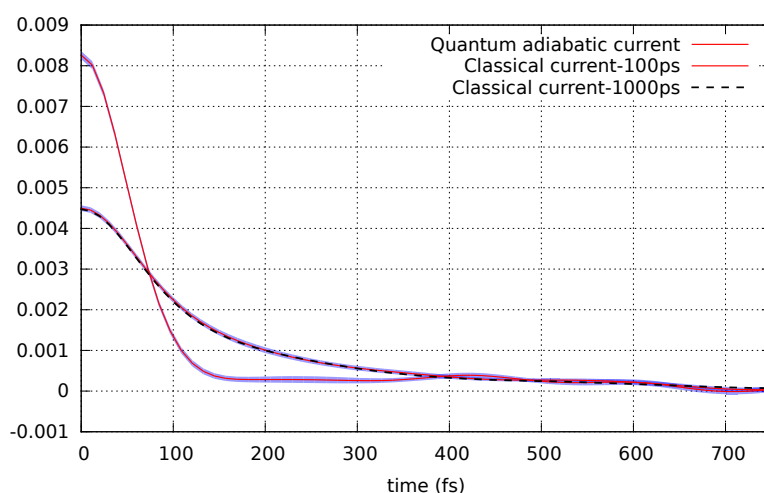
Figure 5.9: As in figure 5.8, for $T = 217K$.
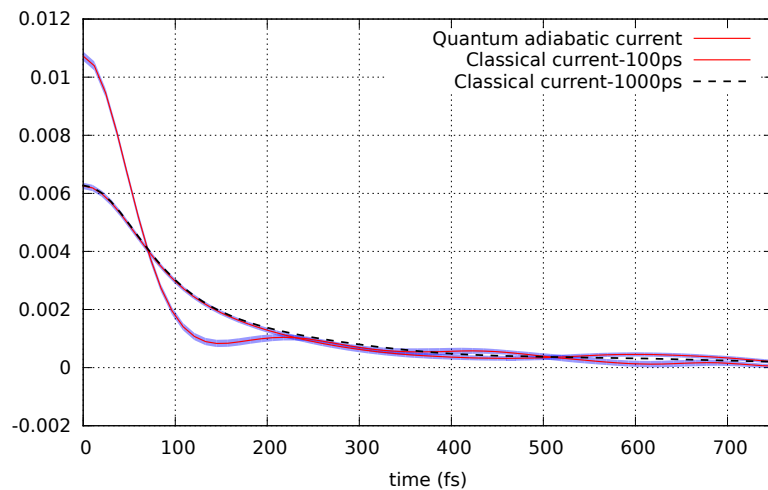
Figure 5.10: As in figure 5.8, for $T = 250K$.
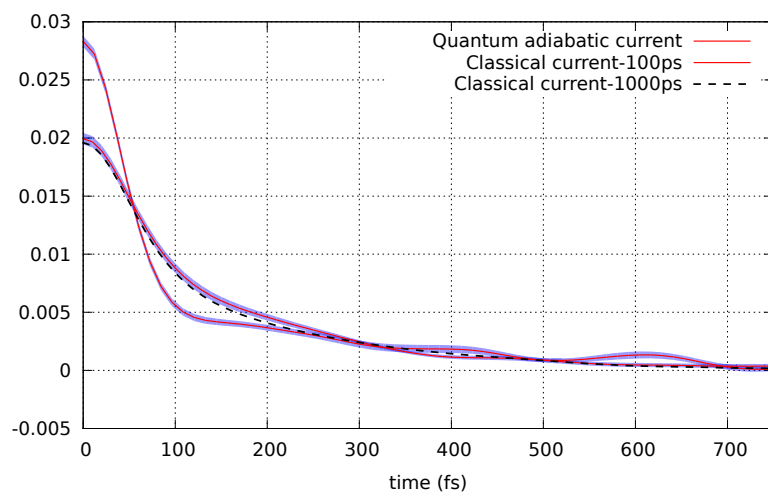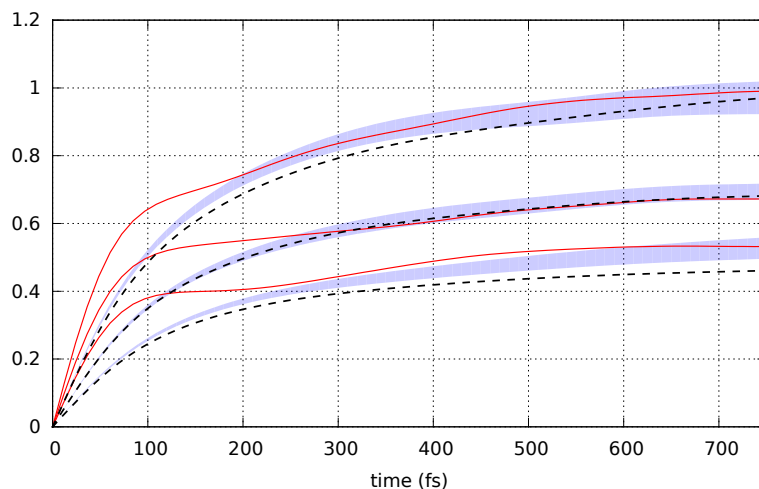

Figure 5.11: As in figure 5.8, for $T = 400K$.

Figure 5.12: In red continuous line $\int_0^t \frac{1}{3} \langle \mathbf{J}(t')\mathbf{J}(0) \rangle dt'$ as a function of t, for the quantum adiabatic head flux with a statistics of 100 picoseconds. The integral is reported in units of $(\frac{Kcal}{mol\ fs})^2 fs$ and the trapezoidal rule used for integration. The converged classical value is reported in black dotted lines. The shaded blue region corresponds to the value with uncertainty obtained using only the first 100 picoseconds of the classical molecular dynamics run with the fitted potential. The integrals refer to the temperatures $T = 184, 217, 400$, with a value increasing with temperature.
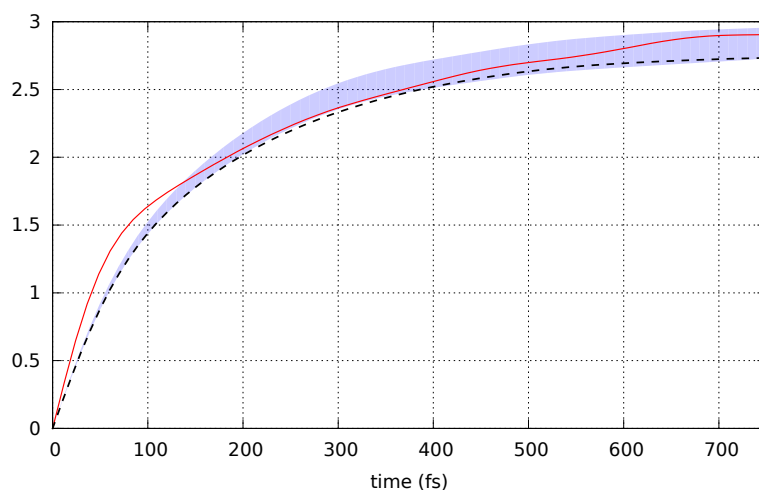

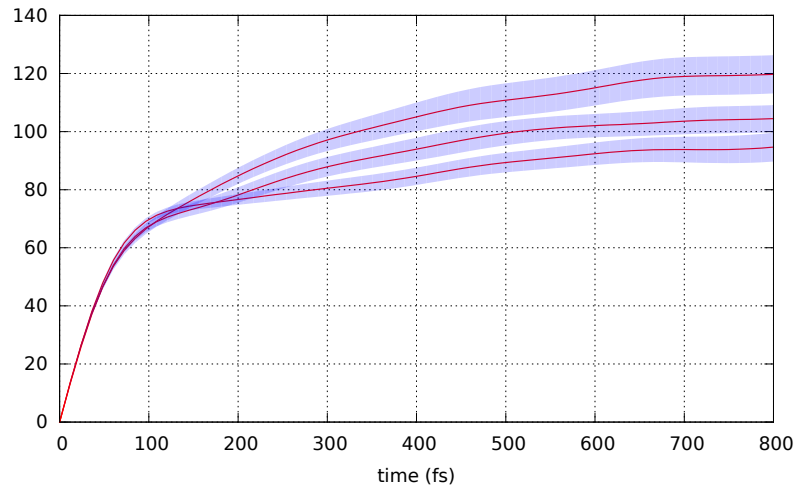Figure 5.13: As in figure 5.12, for $T = 400K$

Figure 5.14: Thermal conductivities obtained for $T = 217, 250$ and 400 K, as a function of the upper integration interval, in $\frac{mJ}{mKs}$ units. It can be seen that, even considering statistical errors, shaded in blue, three statistically different values for the thermal conductivities are obtained. Thermal conductivity increases with increasing temperature.

5.3   Thermal conductivity of heavy water at ambient conditions

We can now apply the tested methodology to analyze thermal conductivity of water at ambient conditions. At the moment, water properties are still not well replicated by classical simulations. A large number of classical model potentials have been proposed, trying to mimic the physics of the system in different ways, but all of them overestimate the value of thermal conductivity at ambient conditions by approximately 30% [18] , as we reported at the end of section 2.3. We do not aim for the moment at a realistic description of water as well, because dispersion forces have not been implemented yet in the heat transport equations, but we will show that reasonable results can be obtained in an ab-initio framework, thus motivating future research.

Heavy water differs from standard light water because in all molecules hydrogen is replaced by one of its isotopes, deuterium. Deuterium differs from hydrogen mainly because its atomic mass has a value of 2 a.m.u. instead of one and this explains the name heavy water attached to this water flavor. The two types have equivalent equilibrium structural properties, at a classical level, since the kinetic contribution in the Boltzmann distribution trivially factors out in both cases. On the other hand, simulating heavy water is more convenient because ions move slowlier and a longer time step can be used. When computing structural properties like

77

e.g. radial distribution functions, the mass of hydrogen and of oxygen can even be considered equal, in order to achieve optimal performance. Dynamical properties, like self diffusion and thermal conductivity are expected to differ, but numerical results for particle diffusion [64] and experimental results for thermal conductivity [65] confirm that the values obtained for the two water flavors are rather similar.

Following the same scheme developed for liquid Argon computations, we first generated a quantum trajectory using the cp.x code of the QUANTUM-ESPRESSO distribution, starting from a previously equilibrated trajectory, and the simulation parameters reported in table 5.5. We note here that only for a ionic temperature around 400 Kelvin the choice of PBE exchange correlation energy functionals is known to replicate qualitatively the self diffusion coefficient of water at ambient conditions, i.e. around 300 K [64]. We therefore imposed this condition in our simulation.

We report in figure 5.15 the total kinetic energy of ions and the fictitious kinetic energy of

Table 5.5

Details for CPMD water computation

|	
Simulation length:	90 ps
Cell dimension (cubic):	23.46 Bohr
Number of molecules:	64
Density:	1.11 $\frac{g}{cm^3}$, the experimental one
Pseudopotential files:	O.pbe-hgh.UPF, H.pbe-vbc.UPF
Exchange correlation functional:	PBE
Pseudopotential types:	Norm conserving. Oxygen non local,
	1 beta function. Hydrogen local.
Electronic mass:	340 a.u.
Energy cutoffs:	80/320 Ryd
Time step:	3.0 a.u.
Preconditioning:	not present
Thermostat:	not present
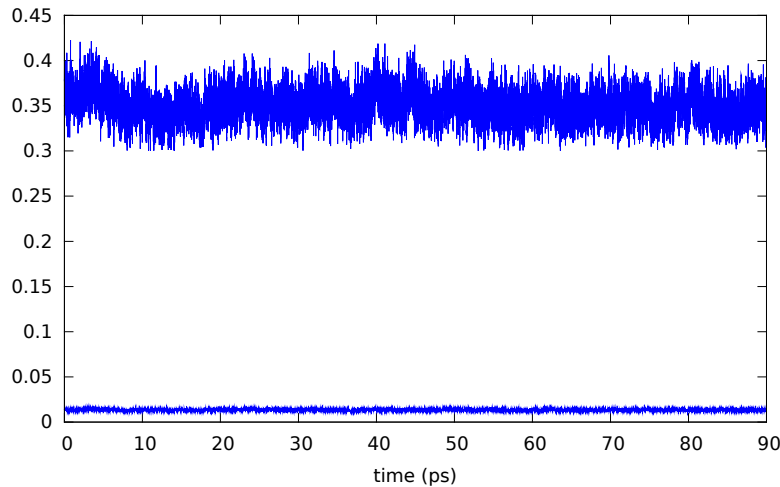
Figure 5.15: Total kinetic energy of ions and electrons for the heavy water simulation, in Hartree units.

electrons, confirming the absence of energy exchange between electrons and ions during the CPMD run. An average temperature of $385K$ was computed. As an other index of the quality of the dynamics we computed a diffusion coefficient of $(2.6 \pm 0.2) \times 10^{-5} \frac{cm^2}{s}$, to be compared with the experimental value at ambient conditions of $2.0 \times 10^{-5} \frac{cm^2}{s}$. In figure 5.16 we report the integral of the velocity autocorrelation functions of oxygens and of hydrogens. They must be equal in the limit of large t, within statistical errors, because the dynamics is too short to observe proton transfers between molecules and this is indeed confirmed.

 The analysis of the energy current in this system is different from the case of Argon, because of two main factors:

- The energy current is highly correlated with a different signal, called here $\mathbf{J}^n \equiv \sum_i \mathbf{v}_i$, where the sum is over all molecules. This signal in the case of a mono-atomic system is zero because proportional to the total momentum, whereas in molecular systems it is proven to be non diffusive (see Appendix E) but can spoil the data because of its very slow decay and high amplitude;

- It is difficult to integrate directly long-lived high frequency intra-molecular modes, even if they contribute very little to the thermal conductivity;

The first problem can be tackled replacing the computed heat flux $\mathbf{J}$ with a modified one $\mathbf{J}' = \mathbf{J} - \lambda \mathbf{J}^n$ and choosing λ such as to force the new signal to be uncorrelated from $\mathbf{J}^n$, that is $Corr(\mathbf{J} - \lambda \mathbf{J}^n, \mathbf{J}^n) = 0$. This approach can be generalized uncorrelating the signal also with
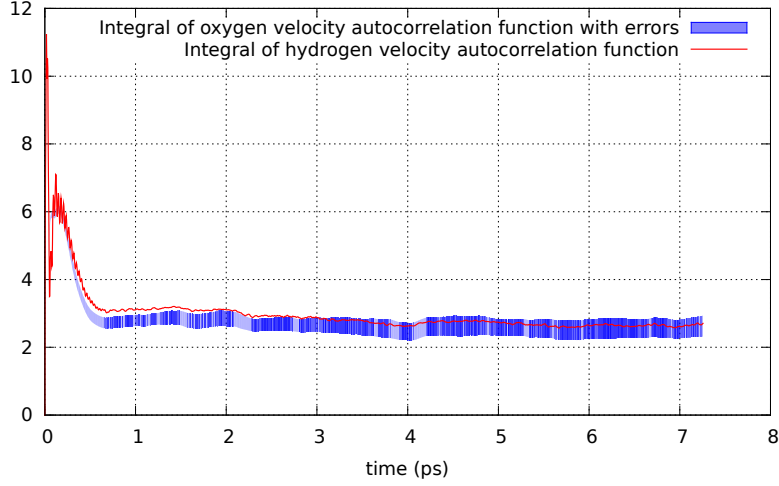
79

Figure 5.16: Diffusion coefficient of water, as obtained from the integrated velocity autocorrelation function, in units of $10^{-5}\frac{cm^2}{s}$. The values obtained from oxygens (shaded in blue, with error bars) and from hydrogens are reported. Within statistical uncertainty the two values obtained are equal, as expected.

respect to the electronic current $\mathbf{J}^{el}$, which is not diffusive as well, and fixing two constants λ_n, λ_{el} imposing the new current $\mathbf{J}' = \mathbf{J} - \lambda_n\mathbf{J}^n - \lambda_{el}\mathbf{J}^{el}$ to be uncorrelated both from $\mathbf{J}^{el}$ and $\mathbf{J}^n$. Similar results were obtained from the two approaches and the coefficients λ_n and λ_{el} could be estimated with high precision from the time series, thus leading to a well defined scheme. As far as the second problem is concerned, the high frequency intra-molecular modes not only make the tail of the autocorrelation function noisy, but also force to use a very high sample frequency for the heat flux, which is a problem for ab-initio computations. In figure 5.17 we report the autocorrelation function $\langle \mathbf{J}'(t)\mathbf{J}'(0)\rangle$ computed with a sample interval of $3.628fs$ from the whole trajectory and with a sample interval of $0.725fs$, using only 15 ps of dynamics. To get rid of these oscillations we use the equivalent Einstein relation which automatically wipes out, thanks to the convolution with a Kernel, these contributions:

$$\frac{\langle|\int_0^t \mathbf{J}(t')dt'|^2\rangle}{2t} = \int_0^t dt'\langle \mathbf{J}(t') \cdot \mathbf{J}(0)\rangle \left(1 - \frac{t'}{t}\right) \tag{5.9}$$

Furthermore, computing the slope obtained plotting $\frac{\langle|\int_0^t \mathbf{J}(t')dt'|^2\rangle}{2}$ versus t, rather then simply dividing by $2t$ and making the limit for $t \to \infty$, reduces further the simulation time necessary to compute the thermal conductivity. Inserting the necessary factors, the final plot of $\frac{1}{6Vk_BT^2}\langle|\int_0^t \mathbf{J}(t')dt'|^2\rangle$ vs t is reported in figure 5.18, with superposed the estimated linear
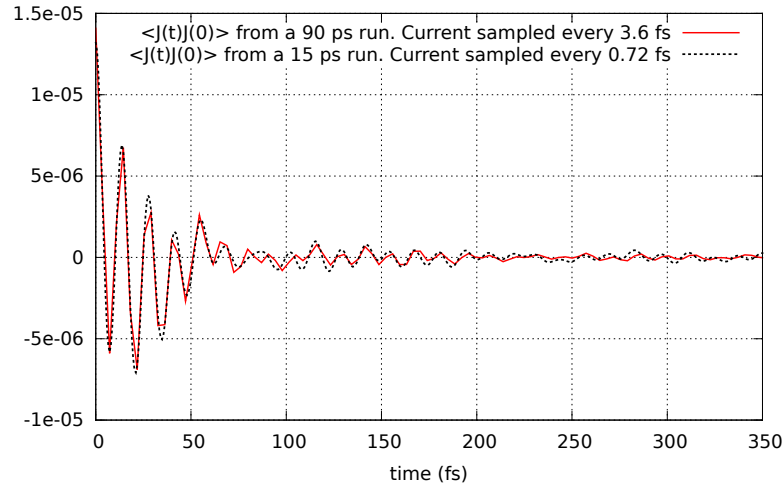
Figure 5.17: Autocorrelation function $\langle \mathbf{J}'(t)\mathbf{J}'(0) \rangle$ in units of $(Ryd\frac{Bohr}{\tau_{BO}})^2$, where τ_{BO} was defined in section 5.1.1

behavior. A thermal conductivity of $(0.74 \pm 0.12)\frac{W}{mK}$ was finally computed, which must be compared with the experimental one of $0.06096\frac{W}{mK}$ [18] for light water at ambient conditions. Within statistical errors, the agreement we found is very good.
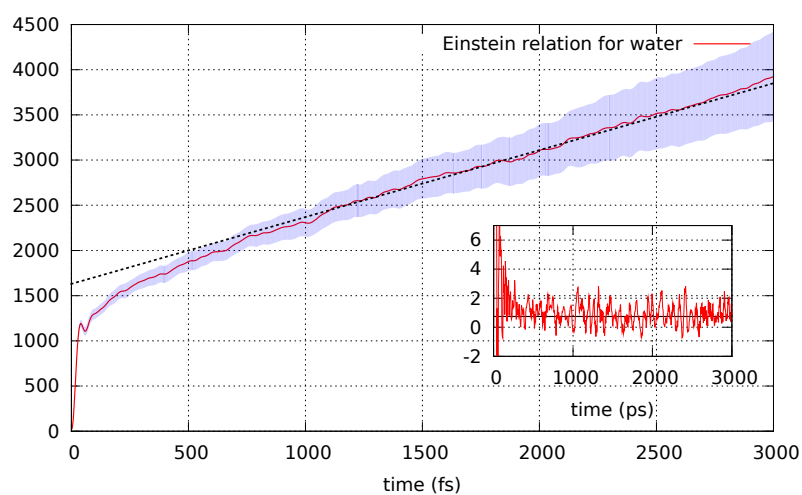
Figure 5.18: We plot here $\frac{1}{6Vk_BT^2}\langle|\int_0^t \mathbf{J}(t')dt'|^2\rangle$ vs t, in units of $10^{-15}\frac{J}{mK}$. Errors are shaded in blue. In the inset the integral of the autocorrelation function is reported. The estimated conductivity oscillates wildly about the value (reported for comparison) obtained fitting a straight line in the Einstein relation.

Fourier transforms of response functions

We fix notations and state, as a summary, some general results that are needed for following the calculations in sections 2.1, 2.2 and 2.3. A more detailed description can be found in [66],[34]. We will deal in this appendix only with Fourier transforms in the time domain.

The Fourier-Laplace transform of a function of real argument $f(t)$ is a function with complex argument $f(z)$ defined by the relation:

$$f(z) = \int_0^\infty f(t)e^{izt}dt \tag{A.1}$$

If the function $f(t)$ goes to zero faster than $e^{-\gamma t}$ for a certain $\gamma > 0$, than the function $f(z)$ is analytic in the semi-plane $\mathcal{I}z > -\gamma$ (and in particular at $z = 0$). For the plain Fourier transform we use the convention:

$$\tilde{f}(\omega) = \int_{-\infty}^\infty f(t)e^{i\omega t}dt \tag{A.2}$$

and will use the tilde only for referring to this standard Fourier transform. It can well happen that the Fourier-Laplace transform is well defined but not the Fourier transform. When both are defined (as it is usually the case in the functions that we consider) one can prove a useful relation between the two:

$$f(z) = \int_{-\infty}^{+\infty} \frac{d\omega}{2\pi i} \frac{\tilde{f}(\omega)}{\omega - z}, \quad \mathcal{I}z > 0 \tag{A.3}$$

This equality holds only in the upper complex plane, since the right member defines a function with a branch cut on the real axes. It is clear that $f(z)$ depends only on the values of $f(t)$ for $t > 0$, whereas the Fourier transform depends also on values for $t < 0$.

These transforms are routinely applied to the response function formalism. The Fourier-Laplace transform of the response function is called *dynamical susceptibility* and is often de-

A. Fourier transforms of response functions

noted with the greek letter χ:

$$\chi_{ij}(z) \equiv \int_0^{+\infty} \Phi_{A_i A_j}(t) e^{izt} dt, \tag{A.4}$$

where A_i is a set of observables of the system. In case the Fourier-Laplace transform were not defined in the real axes but the limit from the upper complex plane is, we will use the standard notation:

$$\chi_{ij}(\omega) \equiv \lim_{\epsilon \to 0^+} \int_0^{+\infty} \Phi_{A_i A_j}(t) e^{i\omega t - \epsilon t} dt \tag{A.5}$$

Taking real and imaginary parts of the above one defines χ' and χ'':

$$\chi_{ij}(\omega) = \chi'_{ij}(\omega) + i\chi''_{ij}(\omega) \tag{A.6}$$

Making explicit sine and cosines one recognizes that this is equivalent to performing two one-sided Fourier transforms:

$$\chi'_{ij}(\omega) = \lim_{\epsilon \to 0} \int_0^{+\infty} \Phi_{A_i A_j}(t) \cos(\omega t) e^{-\epsilon t} dt \tag{A.7}$$

$$\chi''_{ij}(\omega) = \lim_{\epsilon \to 0} \int_0^{+\infty} \Phi_{A_i A_j}(t) \sin(\omega t) e^{-\epsilon t} dt \tag{A.8}$$

which make it explicit that $\chi'_{ij}(\omega)$ is even and $\chi''_{ij}(\omega)$ is odd. The one sided cosine and sine transforms are not independent but are linked by the celebrated Kramers-Kronig relations:

$$\chi'_{ij}(\omega) = \frac{1}{\pi} \mathcal{P} \int_{-\infty}^{+\infty} \frac{\chi''(\omega)}{\omega' - \omega} d\omega' \qquad\qquad \chi''_{ij}(\omega) = -\frac{1}{\pi} \mathcal{P} \int_{-\infty}^{+\infty} \frac{\chi'(\omega)}{\omega' - \omega} d\omega' \tag{A.9}$$

Since the diagonal elements $\Phi_{ii}(t)$ are odd in t only $\chi''_{ii}(\omega)$ suffices to determine the Fourier transform of the response function:

$$\tilde{\Phi}_{ii}(\omega) = 2i\tilde{\chi}''_{ii}(\omega) \tag{A.10}$$

Static response functions are the $\omega \to 0$ limit of $\chi_{ij}(\omega)$:

$$\chi_{ij} \equiv \lim_{\omega \to 0} \chi_{ij}(\omega) \tag{A.11}$$

Only $\chi'(\omega)$ determines the static response functions, since $\chi''(\omega)$, being an odd function, does not contribute to the limit. Inserting the linear response result (3.25) into the definitions and integrating by parts one understands that the χ_{ij} are equal time commutators:

$$\chi_{ij} = \chi'_{ij}(\omega = 0) = \lim_{\epsilon \to 0} \int_0^{+\infty} \Phi_{A_i A_j}(t) e^{-\epsilon t} dt = -\beta C_{ij}(0) \tag{A.12}$$

Other two results are used in the the text, which link the Fourier-Laplace transform of the correlation function and the dynamical susceptibility. The first one is:

$$\frac{\chi_{ij} - \chi_{ij}(z)}{\beta i z} = C_{ij}(z), \tag{A.13}$$

which follows from the identity:

$$\chi_{ij}(z) = \beta \int_0^{+\infty} dt \frac{\partial}{\partial t} C_{ij}(t) e^{izt} = -\beta C_{ij}(0) - \beta i z C_{ij}(z). \tag{A.14}$$

Whereas the second relation:

$$\chi_{ii}''(\omega) = \beta \omega \mathcal{R} C_{ii}(\omega + i\epsilon) \tag{A.15}$$

is a consequence of the parity of C and of equation (A.10).

B | Appendix

The hydrodynamic matrix

We summarize here the main steps necessary to derive the hydrodynamic matrix M starting from the system of equations (3.54). The manipulations can be summarized into three main points:

1. We replace the momentum density $\langle \delta g_a(\mathbf{r}, t) \rangle$ with its longitudinal and transverse components: $\langle \delta g_a(\mathbf{r}, t) \rangle = \langle \delta g_a^l(\mathbf{r}, t) \rangle + \langle \delta g_a^t(\mathbf{r}, t) \rangle$. Looking at the second equation in (3.54), since the gradient of pressure is a purely longitudinal function, we can conclude that the evolution of the transverse momentum density is decoupled from the other modes. The evolution equation for the longitudinal part is still coupled because of the pressure term, but it simplifies thanks to the identity:

$$\partial_b \partial_b \langle \delta g_a^l(\mathbf{r}, t) \rangle = \partial_a \partial_b \langle \delta g_b^l(\mathbf{r}, t) \rangle \tag{B.1}$$

which holds actually for every longitudinal field;

2. We replace the energy density $\epsilon(\mathbf{r}, t)$ with the hydrodynamic variable $q(\mathbf{r}, t)$:

$$q(\mathbf{r}, t) = \epsilon(\mathbf{r}, t) - \frac{\epsilon + p}{n} n(\mathbf{r}, t) \tag{B.2}$$

This is convenient because combining the first and the third equation in (3.54) we obtain:

$$\partial_t \langle \delta q(\mathbf{r}, t) \rangle = \lambda \partial_b \partial_b \delta T(\mathbf{r}) \tag{B.3}$$

and this relation will replace the energy continuity equation for the energy;

3. The third manipulation consists in replacing pressure and temperature as a function

of the chosen thermodynamic variables, $\langle \delta n(\mathbf{r}) \rangle$ and $\langle \delta q(\mathbf{r}) \rangle$ [1]. Formally, from the hypothesis of local thermodynamic equilibrium and the fact that p and T are intensive thermodynamic quantities it follows:

$$\delta p(\mathbf{r}, t) = \left(\frac{\partial p}{\partial n} \right)_q \delta n(\mathbf{r}, t) + \left(\frac{\partial p}{\partial q} \right)_n \delta q(\mathbf{r}, t) \tag{B.4}$$

$$\delta T(\mathbf{r}, t) = \left(\frac{\partial T}{\partial n} \right)_q \delta n(\mathbf{r}, t) + \left(\frac{\partial T}{\partial q} \right)_n \delta q(\mathbf{r}, t) \tag{B.5}$$

In order to link these derivatives with more common thermodynamic quantities it is useful to characterize dq for constant number of particle transformations, that is when $dN = 0$. In this case:

$$T \frac{dS}{V} = d\epsilon - \frac{\epsilon + p}{n} dn = dq \tag{B.6}$$

When considering an intensive variable $\alpha = P, T$, we can therefore write:

$$\left(\frac{\partial \alpha}{\partial n} \right)_q = \left(\frac{\partial \alpha}{\partial n} \right)_{q,N} = \left(\frac{\partial \alpha}{\partial n} \right)_{S,N} \tag{B.7}$$

where the first identity follows from the fact that α is intensive and therefore the derivative can be performed at constant N, thus permitting to exploit relation (B.6). Analogously:

$$\left(\frac{\partial \alpha}{\partial q} \right)_n = \left(\frac{\partial \alpha}{\partial q} \right)_{n,N} = \frac{V}{T} \left(\frac{\partial \alpha}{\partial S} \right)_{n,N} \tag{B.8}$$

We have therefore succeeded, as a first step, in rewriting everything in terms of thermodynamic derivatives where q is no longer present. It is instructive to verify explicitly the previous relations, without taking the detour of constant number of particle transformations. We write as an example the first one, which is the most cumbersome:

$$\left(\frac{\partial \alpha}{\partial n} \right)_{S,N} = \left(\frac{\partial \alpha}{\partial n} \right)_s + \left(\frac{\partial \alpha}{\partial s} \right)_n \left(\frac{\partial s}{\partial n} \right)_{S,N} = \tag{B.9}$$

$$= \left(\frac{\partial \alpha}{\partial \epsilon} \right)_n \left(\frac{\partial \epsilon}{\partial n} \right)_s + \left(\frac{\partial \alpha}{\partial n} \right)_\epsilon + \frac{Ts}{n} \left(\frac{\partial \alpha}{\partial \epsilon} \right)_n = \tag{B.10}$$

$$= \left(\frac{\partial \alpha}{\partial \epsilon} \right)_n \left(\mu + \frac{Ts}{n} \right) + \left(\frac{\partial \alpha}{\partial n} \right)_\epsilon = \tag{B.11}$$

$$= \left(\frac{\epsilon + p}{n} \right) \left(\frac{\partial \alpha}{\partial \epsilon} \right)_n + \left(\frac{\partial \alpha}{\partial n} \right)_\epsilon = \left(\frac{\partial \alpha}{\partial n} \right)_q \tag{B.12}$$

---

[1] Other choices are possible for the independent hydrodynamic variables. One could decide for example to consider the local temperature in addition to number and momentum density and obtain an equally good description of the dynamics [35]. The normal modes of the system would not change but will be merely expressed in a different base. On the other hand, since here we want to link the energy density correlation function with the thermal conduction coefficient, this choice is not the best one

, where $s = \frac{S}{V}$ is the entropy density. The relations $d\epsilon = Tds + \mu dn$, $\mu = \frac{\epsilon+p-Ts}{n}$ and the chain rule have been exploited.

Now standard thermodynamic manipulations lead to expressions where only the specific heat per particle c_v, the isothermal compressibility β_V and the adiabatic speed of sound c^2 appear:

$$\left(\frac{\partial p}{\partial n}\right)_{S,N} = mc^2 \qquad \left(\frac{\partial p}{\partial S}\right)_{n,N} = \frac{\beta_V T}{nc_v V} \tag{B.13}$$

$$\left(\frac{\partial T}{\partial n}\right)_{S,N} = \frac{\beta_V T}{n^2 c_v} \qquad \left(\frac{\partial T}{\partial S}\right)_{n,N} = \frac{T}{c_v V} \tag{B.14}$$

It is also useful to define $D_l = \frac{\frac{4}{3}\eta+\zeta}{mn}$ as the longitudinal diffusion coefficient.

Performing the three previous steps we can rewrite the system in the following way:

$$\begin{cases} \partial_t \langle \delta n(\mathbf{r},t) \rangle + \frac{1}{m}\partial_a \langle \delta g_a^l(\mathbf{r},t) \rangle = 0 \\ \\ \\ \partial_t \langle \delta g_a(\mathbf{r},t) \rangle + D_l \partial_b \partial_b \langle \delta g_a^l(\mathbf{r},t) \rangle + \\ + mc^2 \partial_a \langle \delta n(\mathbf{r},t) \rangle + \frac{\beta_V}{nc_v}\partial_a \langle \delta q(\mathbf{r},t) \rangle = 0 \\ \\ \\ \partial_t \langle \delta q(\mathbf{r},t) \rangle - \lambda \frac{\beta_V T}{n^2 c_v}\partial_b \partial_b \langle \delta n(\mathbf{r}) \rangle - \frac{\lambda}{c_v}\partial_b \partial_b \langle \delta q(\mathbf{r},t) \rangle = 0 \end{cases}$$

This is almost the final form [2]. In order to be able to compare with the results from LRT and obtain the matrix used in the text it is necessary to rewrite these linearized Navier Stokes equations in reciprocal space and to introduce the Fourier-Laplace transform of appendix A but this step is quite mechanical.

In the text we need also the eigenvalues of the hydrodynamic matrix $M(k)$ up to the second order in k, to perform the matrix inversion. These can be found by perturbation theory, dividing the matrix M into an unperturbed part M_0, proportional to q and a perturbation M_1, proportional to q^2, such that $M = M_0 + M_1$. M_0 has the form:

$$M_0 = \begin{pmatrix} 0 & A & 0 \\ B & 0 & C \\ 0 & 0 & 0 \end{pmatrix} \tag{B.15}$$

---

[2]We can observe that the dependence on the volume V of the subsystem is not present anymore and only intensive quantities remained.

B. The hydrodynamic matrix

with A,B and C parameters linear in k and:

$$M_1 = \begin{pmatrix} 0 & 0 & 0 \\ 0 & D & 0 \\ E & 0 & F \end{pmatrix} \tag{B.16}$$

where D, E and F are quadratic in k. The eigenvalues, right and left eigenvector of M_0 are simple to compute:

$$\lambda_0 = 0 \quad e_0^R = \begin{pmatrix} -\frac{C}{B} \\ 0 \\ 1 \end{pmatrix} \quad e_0^L = \begin{pmatrix} 0 \\ 0 \\ 1 \end{pmatrix} \tag{B.17}$$

$$\lambda_+ = \sqrt{AB} \quad e_+^R = \begin{pmatrix} 1 \\ \sqrt{\frac{B}{A}} \\ 0 \end{pmatrix} \quad e_+^L = \frac{1}{2} \begin{pmatrix} 1 \\ \sqrt{\frac{B}{A}} \\ \frac{C}{B} \end{pmatrix} \tag{B.18}$$

$$\lambda_- = -\sqrt{AB} \quad e_-^R = \begin{pmatrix} 1 \\ -\sqrt{\frac{B}{A}} \\ 0 \end{pmatrix} \quad e_-^L = \begin{pmatrix} 1 \\ -\sqrt{\frac{B}{A}} \\ \frac{C}{B} \end{pmatrix} \tag{B.19}$$

Using these results one can compute $\Delta\lambda_i = (e_i^L)^+ M_1(e_i^R)$. Extensive use must be made of the relations:

$$\gamma = \frac{c_p}{c_v} \tag{B.20}$$

$$mc^2 = \frac{\gamma}{n\chi_T} \tag{B.21}$$

$$\gamma - 1 = \frac{T\chi_T\beta_V^2}{nc_v} \tag{B.22}$$

Inserting the explicit expression of the coefficients one obtains $\lambda_0 = 0$, $\lambda_+ = ck$, $\lambda_- = -ck$ and:

$$\Delta\lambda_0 = F - \frac{EC}{B} = iq^2 \frac{\lambda}{nc_v}\left(1 - \frac{T\beta_V^2}{n^2 c_v mc^2}\right) = iq^2 \frac{\lambda}{nc_p} = iq^2 D_T \tag{B.23}$$

where $D_T = \frac{\lambda}{nc_p}$ is the thermal diffusivity. The correction for the second eigenvalue:

$$\Delta\lambda_+ = \frac{1}{2}\left(D + \frac{EC}{B}\right) = iq^2\left(D_l - \frac{T\beta_V^2\lambda}{n^3 c_v^2 mc^2}\right) = \tag{B.24}$$

$$= iq^2\left(D_l - \frac{\lambda}{nc_p}(\gamma - 1)\right) = iq^2\left(D_l + D_T(\gamma - 1)\right) = iq^2\Gamma \tag{B.25}$$

where Γ, defined as $D_l + D_T(\gamma - 1)$, is called the sound attenuation constant. Along similar lines the result $\Delta\lambda_+ = \Delta\lambda_-$ is obtained.

C

Equal time correlators

We show here how the results:

$$\frac{1}{V}\lim_{k\to 0}\langle \delta n(\mathbf{k},0)\delta q(-\mathbf{k},0)\rangle = k_B T^2 \left(\frac{\partial n}{\partial T}\right)_p, \tag{C.1}$$

$$\frac{1}{V}\lim_{k\to 0}\langle \delta q(\mathbf{k},0)\delta q(-\mathbf{k},0)\rangle = nc_p, \tag{C.2}$$

$$\frac{1}{V}\lim_{k\to 0}\langle \delta g^l(\mathbf{k},0)\delta q(-\mathbf{k},0)\rangle = 0, \tag{C.3}$$

reported in section 2.3.1 can be obtained from macroscopic fluctuation theory, as it is developed in [67], chap. XII, to which we refer for several formulas. [1].

Equation (C.3) is obvious because $g(r)$ and $q(t)$ have opposite signs under time reversal. We can compute the first limit as:

$$\lim_{k\to 0}\langle \delta n(\mathbf{k},0)\delta q(-\mathbf{k},0)\rangle = \langle \delta N\delta Q\rangle_V, \tag{C.4}$$

where Q is the volume integral of density $q(r)$ and N the total number of particles. We put a subscript V to point out the fact that statistical fluctuations are computed in a constant volume ensemble, thus permitting the total number of particles and of Q to fluctuate. It is possible to rewrite equation (C.4) in terms of a correlation function computed in a constant particle ensemble. This can be performed exploiting the relation respected by macroscopic fluctuations [67] $\langle \delta n\delta Q\rangle_V = \langle \delta n\delta Q\rangle_N$, where $n = \frac{N}{V}$ is the density as usual. As a consequence:

$$\langle \delta N\delta Q\rangle_V = -n\langle \delta V\delta Q\rangle_N = -nT\langle \delta V\delta S\rangle_N, \tag{C.5}$$

---

[1] We remember that, as in the text, specific heats per particle are always intended.

C. Equal time correlators

The last equality holds because $T\delta S = \delta Q$, when $\delta N = 0$, as shown in appendix B.

The probability w of a fluctuation in a constant particle ensemble is known to be:

$$w \sim Exp\left[-\frac{N^2 c_v}{2T^2}(\delta T)^2 + \frac{1}{2T}\left(\frac{\partial p}{\partial V}\right)_T (\delta V)^2\right]. \tag{C.6}$$

To proceed we need to express δS as a function of δV and δT:

$$\delta S = \left(\frac{\partial S}{\partial T}\right)_V \delta T + \left(\frac{\partial S}{\partial V}\right)_T \delta V \tag{C.7}$$

and the result follows:

$$\langle \delta V \delta S\rangle_N = \left(\frac{\partial S}{\partial V}\right)_T \langle(\delta V)^2\rangle = -T\left(\frac{\partial S}{\partial V}\right)_T \left(\frac{\partial V}{\partial P}\right)_T = -T\left(\frac{\partial S}{\partial P}\right)_T. \tag{C.8}$$

Using then the Maxwell identity derived from the Gibbs potential $dG = -SdT + Vdp$ we obtain:

$$\langle \delta V \delta S\rangle_N = -T\left(\frac{\partial V}{\partial T}\right)_p, \tag{C.9}$$

which is the last needed result to obtain the first equation (C.1).

The second equation (C.2) is proved along similar lines considering P and S as independent variables. In this case the probability, always in the constant particle ensemble, reads:

$$w \sim Exp\left[-\frac{1}{2T}\left(\frac{\partial V}{\partial p}\right)_S (\delta P)^2 - \frac{1}{2N c_p}(\delta S)^2\right] \tag{C.10}$$

Green Kubo current for isolated systems, moving at constant speed

In these particular systems the Green Kubo current is known a priori. The analysis of this section will be very useful for preliminary tests of correct code implementation.

An isolated system is characterized by a localized energy density. Formula (4.9) therefore reads:

$$\mathbf{J} = \int_V \dot{\epsilon}(\mathbf{r})\mathbf{r}d\mathbf{r} = \frac{\partial}{\partial t}\mathbf{P}_O$$

$$\mathbf{P}_O = \int_V \epsilon(\mathbf{r})\mathbf{r}d\mathbf{r}, \tag{D.1}$$

where the first momentum of the energy density is not affected by boundary problems because the energy density is localized. Subscript O means that we are computing the momentum with respect to the origin O. If we compute it with respect to a point O' the usual relation is satisfied:

$$\mathbf{P}_{O'} = \mathbf{P}_O + E(\mathbf{R}_O - \mathbf{R}_{O'}), \tag{D.2}$$

where E is the conserved total energy of the system. Choosing the origin O' moving together with the system and deriving with respect to time:

$$\frac{\partial}{\partial t}\mathbf{P}_{O'} = \frac{\partial}{\partial t}\mathbf{P}_O - E\mathbf{v}, \tag{D.3}$$

where $\mathbf{v} = \dot{\mathbf{R}}_O$. If the system is at internal equilibrium the energy density is rigidly translating. Therefore we have $\frac{\partial}{\partial t}\mathbf{P}_{O'} = 0$ and $\mathbf{J} = E\mathbf{v}$. This is the result we wanted to prove.

We want now here to see explicitly that the procedure followed in the text, applied to an

D. Green Kubo current for isolated systems, moving at constant speed

isolated, non interacting quantum system leads to the same result: $\mathbf{J} = E\mathbf{v}$. We start by the definitions, equivalent to (4.8):

$$e(\mathbf{r},t) = \sum_v \varphi_v(\mathbf{r} - \mathbf{v}t) \left(\hat{H}(t)\varphi_v(\mathbf{r} - \mathbf{v}t) \right)$$

$$\dot{e}(\mathbf{r},t) = \sum_v \left[\dot{\varphi}_v(\mathbf{r},t) \left(\hat{H}(t)\varphi_v(\mathbf{r},t) \right) + \varphi_v(\mathbf{r},t) \left(\dot{\hat{H}}(t)\varphi_v(\mathbf{r},t) \right) \right.$$

$$\left. + \varphi_v(\mathbf{r} - \mathbf{v}t) \left(\hat{H}(t)\dot{\varphi}_v(\mathbf{r},t) \right) \right]. \qquad (D.4)$$

And one has:

$$\hat{H}(t)\varphi_v(t) = \epsilon_v \varphi_v(t) \qquad (D.5)$$

$$\dot{\hat{H}}(t)\varphi_v(t) + \hat{H}(t)\dot{\varphi}_v(t) = \epsilon_v \dot{\varphi}_v(t). \qquad (D.6)$$

By substituting Eqs. (D.5) and (D.6)into Eq. (D.4), we obtain:

$$\dot{e}(\mathbf{r},t) = 2\sum_v \epsilon_v \dot{\varphi}_v(\mathbf{r} - \mathbf{v}t)\varphi_v(\mathbf{r} - \mathbf{v}t)$$

$$= -2\sum_v \epsilon_v \varphi_v(\mathbf{r} - \mathbf{v}t)\mathbf{v} \cdot \nabla \varphi_v(\mathbf{r} - \mathbf{v}t).$$

The corresponding current is:

$$J_\alpha = \int x_\alpha \dot{e}(\mathbf{r},t)d\mathbf{r}$$

$$= -2\sum_v \epsilon_v v_\beta \int \varphi_v(\mathbf{r} - \mathbf{v}t)(x_\alpha - v_\alpha t)\partial_\beta \varphi_v(\mathbf{r} - \mathbf{v}t)d\mathbf{r}$$

$$- 2tv_\alpha v_\beta \int \varphi_v(\mathbf{r} - \mathbf{v}t)\partial_\beta \varphi_v(\mathbf{r} - \mathbf{v}t)d\mathbf{r}.$$

The second term in the above equation vanishes, while the first reads:

$$
\begin{aligned}
J_\alpha \quad &= \quad -2i\sum_v \epsilon_v \langle \varphi_v | x_\alpha p_\beta | \varphi_v \rangle \\
&= - \quad i\sum_v \epsilon_v v_\beta \left(\langle \varphi_v | x_\alpha p_\beta | \varphi_v \rangle - \langle \varphi_v | p_\beta x_\alpha | \varphi_v \rangle \right) \\
&= - \quad i\sum_v \epsilon_v v_\beta \langle \varphi_v | [x_\alpha, p_\beta] | \varphi_v \rangle \\
&= \quad v_\alpha \sum_v \epsilon_v,
\end{aligned}
$$

where use has been made of the canonical commutation rules: $[x_\alpha, p_\beta] = i\delta_{\alpha\beta}$.

Non diffusivity of particle current in molecular systems

We fix first some notation. We number the species of the atoms in the molecule with an index $i = 1, n$ and call m_i their masses. Molecules will be referred instead with an index a running from 1 to N_m. n_i indicates the stechiometric number associated to species i and N_i the total number of particles of type i in the system. Therefore $N_i = n_i N_M$ and the total number of atoms is $N = \sum_i N_i$. We indicate with $\{\mathbf{v}_j^i(t), i = 1, n, j = 1, N_i\}$ the velocity at time t of the $j - esime$ particle of type i and with V the volume of the system.

We want here to prove that, in the center of mass reference frame, the signal:

$$\mathbf{J}^n(t) = \sum_i \sum_{j=1}^{N_i} \mathbf{v}_j^i(t), \tag{E.1}$$

, is non diffusive. With this we mean that:

$$\lim_{t \to \infty} \frac{\langle | \int_0^t \mathbf{J}^n(t')dt' |^2 \rangle}{2tV} = \frac{1}{V} \int_0^\infty dt \langle \mathbf{J}^n(t)\mathbf{J}^n(0) \rangle = 0 \tag{E.2}$$

It is convenient for this purpose to define a partial signal for every species:

$$\mathbf{w}_i(t) = \frac{N}{N_i} \sum_{j=1}^{N_i} \mathbf{v}_j^i(t) \tag{E.3}$$

and the quantity $\Delta_a^{ij}(t)$ as the variation after time t of the position of the centre of atoms of type i and atoms of type j beloning the $a-$molecule. Explicitely:

$$\Delta_a^{ij}(t) = \int_0^t \frac{1}{n_i} \sum_{k \in a} \mathbf{v}_k^i - \int_0^t \frac{1}{n_j} \sum_{k \in a} \mathbf{v}_k^j \tag{E.4}$$

E. Non diffusivity of particle current in molecular systems

Since molecular covalent bonds do not break during the dynamics $\Delta_a^{ij}(t)$ can assume only limited values. As a consequence the signal $\mathbf{w}_i - \mathbf{w}_j$ is non diffusive for every i, j. In fact its time integral $\int_0^t dt' (\mathbf{w}_i(t') - \mathbf{w}_j(t'))$ is equal to $\frac{N}{N_m} \sum_{a=1}^{N_m} \Delta_a^{ij}(t)$ and inserting this expression into the Einstein relation, the numerator remains limited as t grows, whereas the denominator increases linearly, thus confirming the non diffusivity of the signal $\mathbf{w}_i - \mathbf{w}_j$.

The total momentum $\mathbf{P}$, equal to zero in the center of masse referance frame, can be written in terms of the $\mathbf{w}_i$:

$$\mathbf{P} = \sum_{i=1}^n \frac{m_i N_i}{N} \mathbf{w}_i(t) \tag{E.5}$$

It is easily seen that the n vectors:

$$\left\{ (\mathbf{w_1} - \mathbf{w_2}), (\mathbf{w_2} - \mathbf{w_3}), ..., (\mathbf{w_{n-1}} - \mathbf{w_n}), \sum_{i=1}^n (m_i N_i) \mathbf{w}_i \right\} \tag{E.6}$$

form a linear indipendent set and every quantity has been proven to be non diffusive. Since linear combinations of non diffusive quantities are non diffusive as well (sec. 3.4), we can conclude that $\mathbf{J}^n$ ($\sum_{i=1}^n \frac{N_i}{N} \mathbf{w}_i = \mathbf{J}^n$) and actually every $\mathbf{w}_i$ is non diffusive.

Bibliography

[1] J. Ziman, *Electrons and phonons: The theory of transport phenomena in solids*. Clarendon, 1960. 5, 7, 8

[2] D. Broido and al., "Intrinsic lattice thermal conductivity of semiconductors from first principles," *Appl. Phys. Lett.*, vol. 98, p. 113114, 2011. 6, 7, 8

[3] D. Broido and al., "Lattice thermal conductivity of silicon from empirical interatomic potentials," *Phys. Rev. B*, vol. 72, p. 014308, 2006. 7, 8

[4] M. Omini and A. Sparavigna, "Beyond the isotropic-model approximation in the theory of thermal conductivity," *Physica B*, vol. 212, p. 101, 1995. 7

[5] N. Ashcroft and N. Mermin, *Solid State Physics*. Saunders, 1976. 7, 8

[6] M. B. Nardelli, "First-principles analysis of lattice thermal conductivity in monolayer and bilayer graphene," *Phys. Rev. B*, vol. 80, p. 033406, 2009. 7

[7] S. Baroni, "Phonons and related crystal properties from density functional perturbation theory," *Rev. Mod. Phys. B*, vol. 73, p. 515, 2001. 7, 50, 52

[8] G. Kresse and al., "Ab initio force constant approach to phonon dispersion relations of diamond and graphite," *Europhys. Lett.*, vol. 32, p. 729, 1995. 7

[9] K. Esfarajani and al, "Heat transport in silicon from first-principles calculations," *Phys. Rev. B*, vol. 84, p. 085204, 2011. 7

[10] N. Koker, "Thermal conductivity of mgo periclase from equilibrium first principles molecular dynamics," *Phys. Rev. Lett*, vol. 103, p. 125902, 1995. 8

[11] F. Muller-Plathe, "A simple nonequilibrium molecular dynamics method for calculating the thermal conductivity," *J. Chem. Phys.*, vol. 106, p. 6082, 1997. 9

[12] T. Tritt, *Thermal conductivity. Theory, proprierties and applications*. Springer, 2004. 9

[13] P. Jund, "Molecular-dynamics calculation of the thermal conductivity of vitreous silica," *Phys. Rev. B*, vol. 59, p. 13707, 1999. 9

[14] S. Stackhouse and L. Stixrude, "Theoretical methods for calculating the lattice thermal conductivity of minerals," *Rev. Min. and. Geoc.*, vol. 71, p. 253, 2010. 9

[15] P. Schelling, "Comparison of atomic-level simulation methods for computing thermal conductivity," *Phys. Rev. B*, vol. 65, p. 144306, 2002. 11

[16] K. V. Tretiakov and S. Scandolo, "Thermal conductivity of solid argon from molecular dynamics simulations," *J. Chem. Phys. 120*, vol. 120, p. 3765, 2004. 12, 66

[17] K. V. Tretiakov and S. Scandolo, "Thermal conductivity of solid argon at high pressure and high temperature: A molecular dynamics study," *J. Chem. Phys. 120*, vol. 121, p. 11177, 2004. 12

[18] T. W. Sirk and al., "Characteristics of thermal conductivity in classical water models," *J. Chem. Phys.*, vol. 138, p. 064505, 2013. 12, 13, 77, 81

[19] G. D. Samolyuk and al., "Molecular dynamics study of influence of vacancy types defects on thermal conductivity of b-sic," *J. of Nuc. Mat.*, vol. 418, p. 174, 2011. 12

[20] A. J. H. McGaughey and M. Kaviany, "Thermal conductivity decomposition and analysis using molecular dynamics simulations," *Int. Jour. of heat and mass transfer*, vol. 47, p. 1799, 2004. 12

[21] D. Sellan, "Size effects in molecular dynamics thermal conductivity predictions," *Phys. Rev. B*, vol. 81, p. 214305, 1998. 13

[22] G. Ciccotti and al., "Nonlinear thermal response of a lennard jones fluid near the triple point," *Phys. Rev. A*, vol. 34,2, p. 1355, 1986. 14

[23] D. Evans and M. G.P., *Statistical Mechanics of Nonequilibrium Fluids*. New York: Academic Press, 1990. 14, 15, 27, 28

[24] G. Ciccotti and al., "Thermal conductivity of the lennard jones liquid by molecular dynamics calculations," *J. Chem. Phys.*, vol. 86, p. 6371, 1987. 15, 66, 72

[25] F. Romer and al, "Nonequilibrium molecular dynamics simulations of the thermal conductivity of water: A systematic investigation of the spc/e and tip4p/2005 models," *J. Chem. Phys.*, vol. 137, p. 074503, 2012. 16

[26] S. Stackhouse and al., "Thermal conductivity of periclase (mgo) from first principles," *Phys. Rev. Lett*, vol. 104, p. 208501, 2010. 16

[27] M. S. Green, "Markoff random processes and the statistical mechanics of time dependent phenomena," *J. Chem. Phys.*, vol. 20, p. 1281, 1952. 17

[28] M. S. Green, "Markoff random processes and the statistical mechanics of time dependent phenomena. ii irreversible processes in fluids.," *J. Chem. Phys.*, vol. 22, p. 398, 1954. 17

[29] R. Kubo, "Statistical mechanical theory of irreversible processes," *J.Phys.Soc. of Japan*, vol. 12, p. 6, 1957. 17

[30] R. Zwanzig, "Time correlation functions and transport coefficients in statistical mechanics," *Ann. Rev. Phys. Chem.*, vol. 16, p. 1965, 67. 17

[31] H. Goldstein, *Classical mechanics*. Addison-Wesley, 1965. 20

[32] G. Vignale and G. Giuliani, *Quantum theory of the electron liquid*. Cambridge University Press, 2005. 21

[33] a. M. P. Kadanoff L.P., "Hydrodynamic equations and correlation functions," *Ann. Phys.*, vol. 24, p. 419, 1963. 23

[34] D. Forster, *Fluctuations, Broken Symmetry, and Correlation Functions*. Addison-Wesley, Advanced Book Program, 1975. 23, 41, 42, 83

[35] J. Hansen, *Theory of simple liquids*. Academic Press, 1976. 23, 88

[36] P. M. Chaikin and T. C. Lubensky, *Principles of Condensed Matter Physics*. Cambridge University Press, 2000. 23

[37] D. A. McQuarrie, *Statistical Mechanics*. University Science Books, 2000. 23

[38] L. Onsager, "Reciprocal relations in irreversible processes. i," *Phys. Rev.*, vol. 37, p. 405, 1931. 26

BIBLIOGRAPHY

[39] L. Onsager, "Reciprocal relations in irreversible processes. ii," *Phys. Rev.*, vol. 38, p. 2265, 1931. 26

[40] J. P. Boon and S. Yip, *Molecular hydronamics*. Courier Dover Publications, 1980. 27, 41

[41] D. Schepper and al., "Hydrodynamic time correlation functions for a lennard jones fluid," *Phys. Rev. A*, vol. 38, p. 271, 1988. 29

[42] J. Hardy, "Energy-flux operator for a lattice," *Phys. Rev.*, vol. 132,1, p. 168, 1963. 32

[43] E. Helfand, "Transport coefficients from dissipation in a canonical ensemble," *Phys. Rev.*, vol. 119, p. 1, 1960. 34

[44] G. Grosso and G. P. Parravicini, *Solid State Physics*. Academic Press, 2000. 43, 57

[45] P. Hohenberg and W. Kohn, "Inhomogeneous electron gas," *Phys. Rev.*, vol. 136, p. B 864, 1964. 43

[46] W. Kohn and L. J. Sham, "Self consistent equations including exchange and correlation effects," *Phys. Rev.*, vol. 140, A, p. 1133, 1965. 43

[47] D. Thouless, "Quantization of particle transport," *Phys. Rev. B*, vol. 27, p. 6083, 1983. 43, 51

[48] R. M. Martin, *Electronic Structure*. Cambridge University Press, 2008. 44, 52

[49] N. Chetty and R. M. Martin, "First-principles energy density and its applications to selected polar surfaces," *Phys. Rev. B*, vol. 45, p. 6074, 1992. 44

[50] R. Resta, "Theory of the electric polarization in crystals," *Ferroelectric*, vol. 136, p. 51, 1992. 45

[51] C. A. Mead, "The geometric phase in molecular systems," *Rev. Mod. Phys.*, vol. 64, p. 51, 1992. 49, 55

[52] A. Messiah, *Quantum-Mechanics*. Elsevier, 1981. 50

[53] Y. H. Lee and al., "Molecular-dynamics simulation of thermal conductivity in amorphous silicon," *Phys. Rev. B*, vol. 43, p. 6573, 1991. 52

[54] P. Giannozzi and al., "Quantum espresso: a modular and open-source software project for quantum simulations of materials; http://www.quantum-espresso.org," *Journal of Physics: Condensed Matter*, vol. 21, no. 39, p. 395502, 2009. 54, 61, 62

[55] J. P. Perdew and al., "Generalized gradient approximation made simple," *Phys. Rev. Lett*, vol. 77, p. 3864, 1996. 55, 62

[56] W. H. Press and al., *Numerical Recipes. The Art of Scientific Computing*. Cambridge University Press, 2007, III edition. 55

[57] D. Frenkel and S. Berend, *Understanding Molecular Simulation*. Academic Press, 2002. 57

[58] P. L. Silvestrelli, "Van der waals interactions in dft made easy by wannier functions," *Phys. Rev. Lett.*, vol. 100, p. 053002, 2008. 65

[59] R. Car and M. Parrinello, "Unified approach for molecular dynamics and density-functional theory," *Phys. Rev. Lett.*, vol. 55, p. 2471, 1985. 66

[60] M. P. Allen and D. Tildesley, *Computer simulation of liquids*. Clarendon Press, 1987. 66

[61] E. Reese and K. Kranthi, "Adaptive green-kubo estimates of transport coefficients from molecular dynamics based on robust error analysis," *J. Chem. Phys.*, vol. 136, p. 154102, 2012. 66

[62] S. Nosè, "A molecular dynamics method for simulations in the canonical ensemble," *Mol. Phys.*, vol. 52, p. 255, 1984. 66

[63] S. Plimpton, "Fast parallel algorithms for short-range molecular dynamics, http://lammps.sandia.gov," *J. Comp. Phys., 117, 1-19 (1995)*, vol. 21, p. 1, 1995. 66

[64] H.-L. P. Sit and N. Marzari, "Static and dynamical properties of heavy water at ambient conditions from first-principles molecular dynamics," *Phys. Rev. Lett.*, vol. 100, p. 053002, 2008. 78

[65] B. Neindre and al., "Thermal conductivity coefficients of water and heavy water in the liquid state up to 370 °c," *Journal of Chemical and Engineering Data*, vol. 21, p. 265, 1976. 78

[66] B. Berne and G. Harp, "On the calculation of time correlation functions," *Advan. Chem. Phys.*, vol. 17, p. 63, 1970. 83

[67] L. Landau and E. M. Lifshitz, *Statistical Physics*. Elsevier, 1980,III edition. 91